N O T I C E

THIS DOCUMENT HAS BEEN REPRODUCED FROM
MICROFICHE. ALTHOUGH IT IS RECOGNIZED THAT
CERTAIN PORTIONS ARE ILLEGIBLE, IT IS BEING RELEASED
IN THE INTEREST OF MAKING AVAILABLE AS MUCH
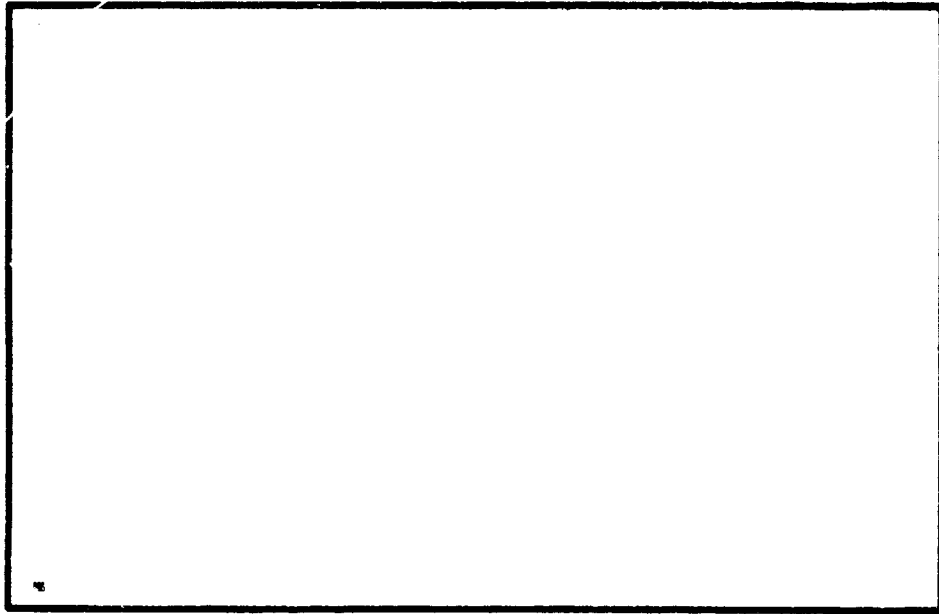INFORMATION AS POSSIBLE

COLLEGE
OF
ENGINEERING

VIRGINIA
POLYTECHNIC
INSTITUTE AND
STATE
UNIVERSITY
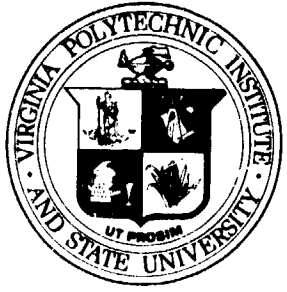
BLACKSBURG,
VIRGINIA

College of Engineering
Virginia Polytechnic Institute and State University
Blacksburg, Virginia 24061

VPI-E-80-28   November, 1980

THREE DIMENSIONAL INELASTIC FINITE ELEMENT
ANALYSIS OF LAMINATED COMPOSITES

Odis H. Griffin, Jr.[1]

Manohar P. Kamat[2]

Carl T. Herakovich[3]

Department of Engineering Science and Mechanics

[1]Former Graduate Student now with B. F. Goodrich

[2]Associate Professor of Engineering Science and Mechanics - Virginia Tech

[3]Professor of Engineering Science and Mechanics - Virginia Tech

BIBLIOGRAPHIC DATA SHEET	1. Report No. VPI-E-80-28	2.	3. Recipient's Accession No.

4. Title and Subtitle	5. Report Date
THREE DIMENSIONAL INELASTIC FINITE ELEMENT ANALYSIS OF LAMINATED COMPOSITES.	
	6.

7. Author(s)	8. Performing Organization Rept.
O. H. Griffin, Jr., M. P. Kamat, C. T. Herakovich	No. VPI-E-80-28

9. Performing Organization Name and Address	10. Project/Task/Work Unit No.
Virginia Polytechnic Institute and State University Engineering Science and Mechanics Blacksburg, Virginia 24061	
	11. Contract/Grant No. NGR 47-004-129 & CA NCCI-15

12. Sponsoring Organization Name and Address	13. Type of Report & Period Covered
National Aeronautics and Space Administration Langley Research Center Hampton, Virgnina 23665 (see page iii)	
	14.

15. Supplementary Notes

16. Abstracts

see page iv

17. Key Words and Document Analysis. 17a. Descriptors

Composite materials, nonlinear, inelastic, plasticity, three dimensional finite element analysis, temperature, moisture, curing stress

17b. Identifiers/Open-Ended Terms

17c. COSATI Field/Group

18. Availability Statement	19. Security Class (This Report) UNCLASSIFIED	21. No. of Pages
Distribution Unlimited	20. Security Class (This Page) UNCLASSIFIED	22. Price

ACKNOWLEDGEMENT

ABSTRACT

Three dimensional inelastic response of laminated composites to thermal and mechanical loading is formulated and analyzed using the finite element method. Individual laminae are modeled as homogeneous and transversely isotropic, with material nonlinearities introduced via a Hill-type yield criterion and an incremental plasticity approach. Nonlinear isotropic hardening is described by Ramberg-Osgood representations of uniaxial stress-strain data. A nonlinear hardening coefficient is derived based on extrapolation of plastic straining during the incremental loading process. Constitutive equations for thermal effects include either constant or temperature dependent expansion coefficients.

The formulations are used as the basis for development of a computer program designated NALCOM (Nonlinear Analysis of Laminated COMposites). The program uses a fully three-dimensional isoparametric finite element with 24 nodes and 72 degrees of freedom. An incremental solution is performed with nonlinearities introduced as pseudoloads computed from initial strains. Equilibrium iteration may be performed at every step. Elastic and elastic-plastic response of boron/epoxy and graphite/epoxy and problems of curing $[0/90]_s$ Gr/Ep laminates with and without circular holes are analyzed. Mechanical loading of $[\pm 45]_s$ Gr/Ep laminates is modeled and symmetry conditions which exist in angle-ply laminates are discussed. Results are compared to experiments and other analytical models when possible. All models are seen to agree reasonably well with experimental results for off-axis tensile coupons. The laminate analyses show the three-dimensional effects which are present near holes and free corners. Symmetry conditions often used for

angle-ply laminates are shown to be substantially in error for thick laminates, becoming better approximations as the thickness decreases.

An appendix discusses the computer implementation of the model and includes storage allocations, a flow chart, and a user's guide.

TABLE OF CONTENTS

LIST OF FIGURES

LIST OF TABLES

Chapter 1

INTRODUCTION

Since the initial work of Smith [1] for plywood, considerable
research has been conducted in the area of stress analysis of laminated
orthotropic materials. With the introduction of fiberglass and the
advanced (e.g. boron and graphite) and intermediate (e.g. Kevlar)
composites, efforts were accelerated due to their potential in aero-
space applications. Composite materials exhibit higher stiffness to
weight ratios than their isotropic counterparts. They can be made
highly corrosion resistant. Composite materials are not, however,
free of problems. Due to the stiffness mismatch of the orthotropic
layers bonded together with different fiber orientations, internal
stresses, known as interlaminar stresses, may be developed in the
vicinity of free edges. For certain stacking sequences and loading
conditions interlaminar effects may be the dominant factor in
structural design.

Analyses of varying degrees of complexity have been applied to
laminated composites. The simplest techniques have limited areas of
applicability, but perform well when properly applied. The more
complex techniques are computer based, often allowing for detailed
material models, geometry, and loading conditions. They also are
accurate when properly applied. The increased complexity is expensive,
both in terms of machine time and man time for setup and later for
interpretation of results.

Considerable progress has been made since Smith's efforts, but

several areas in the analysis of composites seem to be lacking. Composites are known to exhibit significant nonlinearity in stress-strain behavior, even at relatively low strains. The nonlinearity is not isotropic, but varies with direction, as do the elastic properties. Models for such elastic-plastic behavior of orthotropic materials are not well developed. Two dimensional models for nonlinear material behavior have been developed, as have three dimensional linear elastic models. Time dependent straining (creep) phenomena have been modeled to a limited extent, but more research is needed.

The present study presents a model for the three dimensional elastic-plastic stress analysis of layered orthotropic materials. Varying degrees of thermal nonlinearity are considered. A computer program developed for implementation of the model is validated on problems involving nonlinear stress analysis of laminated composites including finite width laminates with and without central holes subjected to a variety of thermal and mechanical loads. Particular attention is given to the interlaminar stresses near free edges.

Chapter 2

COMPOSITE MATERIALS LITERATURE REVIEW

The early work in the analysis of composite laminates was prompted
by the need to design optimal plywood structures. In 1953, Smith [1]
presented a means of computing the effective shear modulus for plywood.
A state of plane stress was assumed. Reissner and Stavsky [2]
presented a means of including coupling between in-plane stretching
and transverse bending. This work presents the basis of the so-called
"lamination theory" for analysis of materials composed of laminated
orthotropic plies. Ashton and Whitney [3] present a detailed
description of lamination theory and its extension to dynamic and
stability regimes. Jones [4] also discusses lamination theory in
detail.

Considerable effort has gone into prediction of failure of
laminated composites. Failure models range from very simple maximum
stress or strain models to sophisticated models which allow progressive
failure of individual plies and concurrent assumption of load by
unfailed plies. Failure prediction is beyond the scope of this study,
and will not be discussed further. For more information on failure
criteria of laminates, the reader is directed to the book edited by
Herakovich [5].

The basic areas of composites discussed herein are divided between
lamination theory studies and a more detailed group of solutions
referred to here as full-field solutions. The nature of the two

areas and rationale for the nomenclature will be evident as the areas are discussed.

As previously mentioned, the initial work on lamination theory was presented by Reissner and Stavsky [2]. The basic assumptions of classical lamination theory (CLT) are that the laminate is in a state of plane stress, and the individual laminae act independently. Thus, integrals through the thickness of a laminate are replaced by integrals over the individual laminae with a summation over the laminate. Two significant effects arise from this procedure. First, all interlaminar effects are omitted. That is, all forces which exist between the laminae are ignored. Such forces may be shown by more sophisticated numerical analyses to be significant. Second, the effects of stacking sequence on stress distributions are lost. These effects have also been shown to be significant near free edges.

In defense of CLT, it should be noted that away from free edges the CLT solutions are recovered exactly even by the most sophisticated techniques. The area of non-applicability of CLT is confined to a region which extends inward from the edge to a distance approximately equal to the laminate thickness. This region is normally referred to as the boundary layer. Pagano [6,7] has used a modified lamination theory to model the boundary layer. Stresses are shown to change rapidly with spatial position and grow very large near free edges. Several investigators [8,9] have postulated the existence of stress singularities in the boundary layer for linear elastic material behavior. In reality, singular stresses do not exist, but are

relieved by plasticity or failure. Thus, accurate modeling of free edge effects requires an inelastic capability, and possibly the inclusion of failure mechanisms.

The early lamination theory work was presented for linear elastic materials with no thermal effects. Tsai [10] presented a means of including thermal loading based on room temperature thermal coefficients. Petit and Waddoups [11] developed a method of nonlinear analysis to failure. Symmetric laminates subject to biaxial loads were modeled. Loads were applied incrementally, and nonlinearities were introduced using stress-strain curves obtained from uniaxial tests. Good agreement was shown between theory and experiment for limited load conditions. Hashin, Bagchi and Rosen [12] and later Hashin, Rosen, and Pipes [13] used Ramberg-Osgood representations of unidirectional stress-strain data to model the nonlinear response of laminates. The deformation theory of plasticity was used, and interaction of stresses for multiaxial stress states was accomplished via arguments based on isotropic J_2 theory [13].

Sandhu [14] used a method of fitting nonlinear lamina stress-strain data by cubic spline functions to predict nonlinear laminate response to failure. Loads were applied incrementally, and a flow rule of sorts was used to model stress interactions by introduction of an equivalent strain function. Compliances for successive steps were assumed to be functions of total equivalent strains.

Hahn and Pagano [15] developed a method of including what might be referred to as second order thermal effects. They included the effects

of stress-temperature coupling using an instantaneous coupling coefficient. The consequences of omitting this effect were shown to be significant.

In his modified lamination theory, Pagano [6,7] has extended Reissner's variational principle to laminated bodies. Using an assumption of stresses varying linearly with the through-thickness coordinate, he developed a set of differential equations along with the appropriate boundary conditions. His results compare well with the generalized plane strain finite element results of Wang and Crossman [16]. Linear elastic material properties were assumed, and no thermal effects were included.

More recently, Hashin, Rosen, and Pipes [13] developed a method of nonlinear laminate analysis including thermal effects. Simultaneous heating and loading were considered. As in the previous work of Hashin, et al [12], deformation theory was used. The results are startling in that they report experimental data that show that in the case of [0/90]$_s$ Graphite/Epoxy laminates the thermal expansion coefficients c ⁊ affected by time dependent (creep) characteristics and response. Results such as these appear to parallel works such as Mauri, et al [17], who report that moisture expansion coefficients are not only a function of temperature, but of the temperature at which the moisture was absorbed.

The solutions referred to here as full field are so called because the problem is not limited by assumptions such as those for laminate analysis. Thus, the full set of stresses may be solved for, as well as the displacements for the complete mathematical model. These

solutions have been dominated by finite element work, but some early
finite difference models are noteworthy.

Pipes and Pagano [18] and Pipes [19] utilized a finite difference
technique to solve the quasi-three dimensional elasticity equations
for laminates. Interlaminar stresses were evaluated, and the capability
for thermal effects was included. Two mechanisms of interlaminar load
transfer were discussed. More recently, Hsu and Herakovich [8]
reported a perturbation solution to the quasi-three dimensional
elasticity problem. The perturbation solution permits a better
treatment near the "singularity" at the free edge than was previously
available. The results of Hsu and Herakovich [8] are based on a
stretching transformation of the boundary layer and are therefore
dependent on an undetermined parameter of the transformation. They
are thus qualitative in nature, but are valuable in that they place
bounds on the region of applicability of the standard finite
difference solution, as well as showing relative shapes of stress
profiles in the boundary layer. Thermal effects were not included.

Isakson and Levy [20] used the finite element method (FEM) to
model a laminate in a state of plane stress. The plies were modeled
as orthotropic layers separated by isotropic shear layers. Inter-
laminar normal stress was omitted. The technique of using isotropic
shear layers had been previously used by Puppo and Evensen [21], but
not in conjunction with the FEM. Subsequently, Levy, Armen, and
Whiteside [22] extended the work of Isakson and Levy for plastic
deformation of the shear layer. A Ramberg-Osgood representation for

boron/epoxy was used as a model for the nonlinearity of the shear
layer. Results were presented for interlaminar stresses around holes,
and the effects of stacking sequence were discussed. No thermal effects
were considered.

Herakovich and Brooks [23] used the FEM to examine stress distribu-
tions in uniaxial and cross-plied laminates subjected to thermal and
uniaxial strain loading. Material models were linear elastic. Inter-
laminar stresses were shown to be significant near free edges.
Herakovich [24] later showed the effects of stacking sequence on inter-
laminar thermal stress. His analysis indicated an effect on the overall
strength of the laminate. The analysis was again linear elastic. Lin
[25], and later Dana [26], and Dana and Barker [27] used a 72 degree
of freedom, three dimensional orthotropic isoparametric finite element
element to model laminates. All results were linear elastic, and
thermal effects were not included. Stresses were computed near holes
and free edges. Comparisons of hole shape and size were made with
regard to interlaminar stresses.

Rybicki has used several variants of the FEM to examine the
behavior of composites. Complementary energy methods [28], stress
function methods [29], and standard displacement techniques [30,31]
have been used. More recently, Rybicki and Schmuesser [32] used the
three dimensional finite element program SAP IV to predict stress
distributions near holes in linear elastic laminates. Stanton has used
a parametric cubic modeling system [33,34] to analyze nonlinear material
behavior in laminates. His analysis is three dimensional, its basic
drawback being that the complexity of the element and resulting large

bandwidth dictate the use of a minimization technique for solution.

Foye [35] has used a micromechanics approach based on the FEM to model nonlinear behavior of composites, including both nonlinear time independent and time dependent effects. By using a micromechanics approach and thus introducing fiber and matrix properties independently, the difficulty of orthotropic plasticity as noted by Hill [36] is avoided. Effects of differences in cure cycle are examined. The cure cycle for these analyses was approximated by a series of finite steps of temperature followed by a constant temperature until the next step.

Pifko, Levine and Armen [37] have developed a method of three dimensional stress analysis of composites. Their work is based on the FEM displacement formulation. Plasticity is included via the normal flow rule (Drucker's postulate) and an incremental analysis. Hardening is either nonlinear or linear, with nonlinear hardening introduced via Ramberg-Osgood approximations. Kinematic hardening [38] is used. Unfortunately, the kinematic hardening coefficients are based on heuristic arguments, and are not fully checked out [39].

Renieri and Herakovich [40] used a quasi-three dimensional finite element analysis to model the response of laminates to thermal and mechanical laoding. Nonlinear material properties were introduced via one-dimensional Ramberg-Osgood representations. Interaction of stresses was not considered, and loading and unloading were along the same path. Hence the analysis may be called nonlinear elastic. Differing properties in tension and compression were included.

Various non-displacement finite element formulations have also

been used for stress analysis of composites. Lee [41] and Wang, et al [42,43] have used the hybrid stress formulation of Pian [44] to perform finite element analyses of composites. Several problems exist with this approach. In the boundary layer, steep gradients of stress are known to exist. Thus, in the hybrid stress approach one must include significant numbers of higher order terms in the assumed stress polynomials. The analysis is thereby complicated by a large number of unknowns per element. Kathiresan [45] and Atluri and Kathiresan [46] have used the hybrid displacement formulation for modeling of composites. Such an approach appears to have favorable qualities for investigation of fracture mechanics and laminates containing initial flaws, although treatment of nonlinearities may be difficult.

In summary, considerable work has been done in lamination theory studies and finite element studies. In lamination theory, the work of Pagano [6,7] stands out as the only one capable of inclusion of inter- laminar effects. Problems will undoubtedly arise, however, if extension to nonlinear material behavior and/or thermal effects is attempted. The finite element method has been used in all forms to solve laminate problems. The current state-of-the-art appears to be two dimensional (quasi-three dimensional) analysis with nonlinear elastic material properties (different in tension and compression) with first order thermal effects or three dimensional analysis with nonlinear material behavior. The nonlinear three-dimensional analysis of Stanton [33,34] apparently has not been widely accepted by the composites community. The areas which seem to be lacking are two

dimensional (quasi-three dimensional) analysis with time dependent material properties and three dimensional analysis with a full plasticity treatment and moisture and creep effects included. No finite element analysis to date appears to have included second order thermal effects as described by Hahn and Pagano [15], even though the formulations have been made by Ueda and Yamakawa [47].

When considering the modeling of a material system, one must always survey the availability of material property data. For composites, the data package is far from complete. Quasi-static stress-strain data at room temperature is relatively abundant. The most effective means of implementing temperature dependence seems to be the percent retention at temperature curves as used by Renieri and Herakovich [40], even though their validity is only for certain strain ranges. Time dependent properties such as viscoelastic moduli and creep compliances are only now being generated [48] for even the most common composites. Temperature dependence of these properties is only known as far as tests at a very limited number of temperatures. Effects such as the stress dependence of thermal expansion coefficient noted by Hashin, et al [13] and the absorption temperature dependence of moisture coefficients noted by Mauri, et al [17] are only pointed out as anomalies. These effects are likely the result of the complex polymerization characteristic of resin matrix composites. Understanding, and ultimately intelligent and accurate modeling, must await more knowledge of the physical processes of the materials involved.

Chapter 3

NONLINEAR FINITE ELEMENT FORMULATION

3.1 Introduction

The finite element used for the nonlinear studies is the 24 node isoparametric element described in Appendix A. The basis for an incremental solution of the nonlinear load-deflection equations is also presented in Appendix A. This chapter details the pseudoloads used for implementation of plasticity using the method of initial strains, as well as the nonlinear thermal and plasticity modifications to the elastic constitutive relationships. It should be emphasized that the thermal and moisture effects are <u>uncoupled</u>. That is, the temperature and moisture distributions are known <u>a priori</u> by means of some also uncoupled thermal or moisture diffusion analysis. Furthermore, the plasticity developed here is time independent. No viscoelastic or creep effects are considered. However, using the initial strain method for time dependent effects proposed by Zienkiewicz and Cormeau [49], their inclusion is straightforward. Several additional assumptions are necessary in the developments to follow. These will be stated as they are introduced.

Several types of nonlinearities exist for laminated composites. The constitutive parameters are temperature and moisture dependent, history dependent (plasticity) and time dependent (creep). The thermal expansion coefficients are temperature and moisture dependent. Moisture expansion coefficients are temperature dependent.

Various "coupling" of these effects may be shown to exist. Hahn and Pagano [15] have used a lamination theory model to show the significance of the so-called "coupling" terms which exist between temperature effects and stress. In the present work, these have been termed "second order" thermal effects and are included in the constitutive relationships.

In the developments of this chapter, contracted tensor notation for strain (ϵ_i) will imply engineering shear strains, while full strain tensor notation (ϵ_{ij}) implies tensor shear strain. Conversion from tensor to engineering shear strain is assumed to have been performed as required.

3.2 Incremental Solution of Nonlinear Equations

The method chosen for the incremental solution of the nonlinear load-deflection equations is referred to by Desai and Abel [50] as the direct incremental initial strain method. All nonlinearities are introduced as pseudoloads, with corresponding initial strain modifications to the constitutive relationships. One of the benefits of the initial strain method is that the global stiffness matrix need only be assembled once. Furthermore, unless a change of specified displacement boundary conditions occurs, the solution requires only one triangularization. The utility and computational efficiency of the initial strain method is widely recognized. Pifko, et al [37] used an initial strain method in the development of the PLANS system. The following paragraphs contain a description of the initial strain method as implemented for the present study.

3.2.1 Direct Incremental Initial Strain Method

The starting point for the method is the incremental load-deflection solution of Appendix A,

$$K_{ij}(\Delta q_j)^{k+1} = (\Delta Q_i)^{k+1} + (\Delta Q_i^{0,T})^{k+1} + (\Delta Q_i^{0,P})^k + (R_i)^k \quad (3.1)$$

$$i = 1,2,\ldots,N$$

where

k	= previous load increment
$k+1$	= current load increment
$(\Delta q_i)^{k+1}$	= current incremental nodal displacement vector
$(\Delta Q_i)^{k+1}$	= mechanical load increment
$(\Delta Q_i^{0,T})^{k+1}$	= incremental pseudoload due to temperature effects
$(\Delta Q_i^{0,P})^k$	= incremental pseudoload due to plastic flow during previous load step
$(R_i)^k$	= residual from total equilibrium at end of previous load step
K_{ij}	= global elastic stiffness matrix.
N	= total number of degrees of freedom.

Note that the method is directly applicable to linear elastic problems, where only one load step to full load results in a purely linear analysis, using the linear elastic constitutive relationships.

The basic procedure is a direct stepping technique, where, given the state variables and material properties at the beginning of a step, the increments are found by solution of Equ's. (3.1) and the appropriate constitutive relationships. Total quantities are computed by

addition of increments to previous totals. This procedure is repeated until the full load is applied.

3.2.2 Computation of Incrementai Initial Strain Pseudoloads

For the initial strain effects, the incremental pseudoload is given by

$$\Delta Q_i^0 = \iiint_\Omega B_{ji} D_{j1} \Delta \epsilon_1^0 d\Omega \tag{3.2}$$

where B_{ij}, D_{ij}, and Ω are the same as described in Appendix A, and $\Delta \epsilon_1^0$ is the increment of initial strain. For plasticity, $\Delta \epsilon_1^0$ is the plastic strain increment for the previous load step. For temperature effects, $\Delta \epsilon_1^0$ is the increment of thermal expansion for the current load step. The computation of these terms will be discussed later. The volume integral of (3.2) is computed by Gaussian quadrature, as described in Appendix A. The elasticity matrix D_{ij} is evaluated at the same temperature as the qlobal stiffness matrix.

3.2.3 Additional Assumptions

Several additional assumptions are made for implementation of the direct incremental initial strain method. All strains and displacements are assumed to be small. Furthermore, the anisotropy (transverse isotropy for the present study) is assumed constant for the entire analysis. That is, angular orientations do not change during the analysis, nor is the anisotropy altered by plastic flow. As previously stated, all thermo-elastic, thermo-plastic, hygrothermal, etc., effects are actually uncoupled, the present analysis computing the elasto-

plastic effects of thermal and moisture fields known a priori from some other analysis, also uncoupled. It is also assumed that the total strain can be written as the sum

$$\epsilon_i^T = \epsilon_i^e + \epsilon_i^\theta + \epsilon_i^M + \epsilon_i^P \, , \quad i = 1,6 \qquad (3.3)$$

where contracted tensor notation is used and ϵ_i, $i = 4,5,6$, are engineering shear strains, and

ϵ_i^T = total strain

ϵ_i^e = elastic (or mechanical) strain

ϵ_i^θ = thermal expansion strain

ϵ_i^M = moisture expansion strain

ϵ_i^P = plastic strain.

This assumption is standard in continuum analysis, and is necessary to facilitate the computation of the mechanical strain.

3.3 Incremental Nonlinear Constitutive Relationships

The derivation of nonlinear constitutive relationships which accurately represent the physical behavior of laminated composites and which are consistent with pseudoloads to be applied to a finite element model is the crux of the present study. Efforts have been made to utilize parameters which are common within composites terminology, such as the Ramberg-Osgood technique for representation of nonlinear stress-strain relationships. Certain of the assumptions made in the present study are commonly used. The method of including second order thermal effects in the finite element context is due to Ueda and Yamakawa [47],

with orthotropy modifications as suggested by Yamada [51]. Second order thermal effects, although rarely considered, were shown to be significant by Hahn ₁₁ Pagano [15].

3.3.1 Nonlinear Thermal Effects

As previously stated, thermal nonlinearities are cf two types. The instantaneous thermal expansion coefficient, α_i, defined by

$$\alpha_i = \frac{\partial \epsilon_i}{\partial T} \tag{3.4}$$

is dependent on temperature. Also, the "elastic" coefficients of the material are temperature dependent. In the present study, the first effect has been termed "first order", while the effects of the latter on thermal stress have been termed "second order". The following paragraphs describe the first and second order thermal effects and the corresponding elastic constitutive relationships.

3.3.1.1 First Order Thermal Effects

The incremental form of Equ's. (3.3) is

$$\Delta \epsilon_i^T = \Delta \epsilon_i^e + \Delta \epsilon_i^\theta + \Delta \epsilon_i^M + \Delta \epsilon_i^P. \tag{3.5}$$

In the absence of moisture and plastic flow, Equ's. (3.5) (after rearranging) become

$$\Delta \epsilon_i^e = \Delta \epsilon_i^T - \Delta \epsilon_i^\theta. \tag{3.6}$$

For first order nonlinear thermal effects, the incremental thermal strain is approximated by

$$\Delta\epsilon_i^\theta = \alpha_i\Delta T \tag{3.7}$$

where ΔT is the temperature change over the increment and α_i is an average coefficient of thermal expansion over ΔT. Note that if the α_i are not functions of temperature, Equ's. (3.7) reduce to the familiar constant property relationship of Appendix A. The incremental constitutive relationships are

$$\Delta\sigma_i = D_{ij}\Delta\epsilon_j^e \tag{3.8}$$

where $\Delta\sigma_i$ is the stress increment, and D_{ij} is the elasticity matrix (rotated to account for orthotropy if required) for the material, and is evaluated at the mean temperature over ΔT. Combining (3.6), (3.7), and (3.8), we obtain the constitutive relationship for first order thermal effects:

$$\Delta\sigma_i = D_{ij}(\Delta\epsilon_j^T - \alpha_j\Delta T). \tag{3.9}$$

The first order incremental thermal pseudoload, ΔQ_i^0, is, using Equ's. (3.2) and (3.7),

$$\Delta Q_i^0 = \iiint_\Omega B_{ji}D_{jk}\,\alpha_k\Delta T\;d\Omega. \tag{3.10}$$

Equ's. (3.9) and (3.10), along with the strain-displacement relationships

$$\Delta\epsilon_i = B_{ij}\Delta q_j \tag{3.11}$$

form the basis for the first order nonlinear thermal analysis of the present study.

3.3.1.2 Second Order Thermal Effects

An effect shown by Hahn and Pagano [15] to be significant for composites, where material properties may change rapidly with temperature, and by Ueda and Yamakawa [47] for welding problems where large temperature gradients exist, is the "coupling" between total stress and thermal stress. Note that the analysis is not truly coupled thermo-structural, but that mutual influence of effects is being considered. Suppose that the mechanical strain, ϵ_i^e, is a function of temperature and total stress, or

$$\epsilon_i^e = \epsilon_i^e(\sigma_j, T). \tag{3.12}$$

From the constitutive relationships,

$$\epsilon_i^e = S_{ij}\sigma_j \tag{3.13}$$

where S_{ij} is the elastic compliance matrix, or

$$S_{ij} = (D_{ij})^{-1}. \tag{3.14}$$

Now, realizing that the S_{ij} are functions of temperature, the differential elastic strain becomes, from Equ's. (3.13)

$$d\epsilon_i^e = S_{ij}d\sigma_j + \frac{\partial S_{ij}}{\partial T} \sigma_j dT, \tag{3.15}$$

or, in incremental form

$$\Delta\epsilon_i^e = S_{ij}\Delta\sigma_j + \frac{\partial S_{ij}}{\partial T} \sigma_j \Delta T. \tag{3.16}$$

The second term in (3.16) is what Hahn and Pagano [15] refer to as the "coupling" term. Note that S_{ij} is evaluated at the mean temperature over ΔT, as is $\frac{\partial S_{ij}}{\partial T}$. The incremental constitutive relationship becomes

$$\Delta\sigma_i = D_{ij}\Delta\varepsilon_j^T - D_{ij}\left(\alpha_j + \frac{\partial S_{jk}}{\partial T}\sigma_k\right)\Delta T. \qquad (3.17)$$

Note that in Equ's. (3.17) the incremental stress $\Delta\sigma_i$ is a function of total stress σ_k. For accuracy, σ_k should be evaluated at the midpoint of the load (temperature) step, but it is only known at the beginning of the step. The incremental solution thus is implicit, and an iteration or some additional approximation is required. In addition, the initial strain necessary for computation of the incremental thermal pseudoload is

$$\Delta\varepsilon_j^0 = \left(\alpha_j + \frac{\partial S_{jk}}{\partial T}\sigma_k\right)\Delta T, \qquad (3.18)$$

and the incremental pseudoload becomes

$$\Delta Q_i^0 = \iiint_\Omega B_{ji}D_{jk}\left(\alpha_k + \frac{\partial S_{k\ell}}{\partial T}\sigma_\ell\right)\Delta T d\Omega. \qquad (3.19)$$

Equ's. (3.17) and (3.19) are the constitutive relationship and thermal pseudoload, respectively, for the second order nonlinear thermal analysis.

3.3.1.3 Comments on Thermal Nonlinear Analysis

Several assumptions have been made in the thermal nonlinear formulations. They include the assumption of constant instantaneous thermal expansion coefficients and changes of S_{ij} with temperature over

an entire temperature step. The accuracy of these assumptions in
practice is dependent on the rates of change of the coefficients of
concern and the size of the temperature step. Where steep gradients
exist, small temperature steps may be required, as opposed to large
steps being acceptable where property behavior is less temperature
dependent. When including second order nonlinear thermal effects, the
magnitude of total stress is also of concern. As with all nonlinear
solutions, considerable care must be taken in choosing load steps, or
the software used must do considerable checking to assure that the
assumptions are not violated. Such checking is computationally
expensive and seems to be done rarely if at all.

3.3.2 Plasticity

The plasticity used in the present study is based on the yield
function, equivalent stress, and equivalent plastic strain increment
derived for anisotropic materials by Hill [36]. It should be noted
that for isotropic materials Hill's relationships reduce to the familiar
von Mises (distortion energy) theory. Inherent in this formulation
is the incompressibility of plastic strains and the assumption that
hydrostatic (spherical) stress states result in no yielding or plastic
deformation. It has been noted [52] that this is not the case for all
composite materials. Hill's yield function, or some variant, is
nevertheless widely used. Once yielding is detected, a mathematical
relationship for progression of plastic flow is required. The most
commonly used relationship is Drucker's postulate [53], which states:
"Suppose an external agency to produce a non-zero displacement by

adding a set of loads to a time-independent system in static equilibrium. The system is stable if the work done by the external agency is positive for all permissible added loads." Mathematically, Drucker's postulate is commonly combined with the so-called "normality" principle and written as

$$d\epsilon_{ij}^P = \lambda \frac{\partial f(\sigma_{ij})}{\partial \sigma_{ij}} \qquad (3.20)$$

where

$d\epsilon_{ij}^P$ = plastic strain increment

$f(\sigma_{ij})$ = yield function (associated plasticity)

σ_{ij} = stress

λ = nonnegative proportionality constant.

When Drucker's postulate is used in a numerical scheme, such as an incremental solution, several assumptions are made. The numerical value of λ is assumed to be constant over the entire step. Equations (3.20) are often referred to as the "normal flow rule". If we consider $f(\sigma_{ij})$ to be a yield hypersurface in nine-dimensional stress space, then Equ's. (3.20) require that the vector $d\epsilon_{ij}^P$ be "normal" to the hyper-surface. The assumption is thus also made that $\frac{\partial f(\sigma_{ij})}{\partial \sigma_{ij}}$, or the dir-ection of the $d\epsilon_{ij}^P$ vector, is also constant over the increment. As with all incremental schemes, plasticity for the case of nonpropor-tional loading is at best convergent in the limiting case of infinitesimally small increments.

It should be emphasized that Drucker's postulate is only a postulate, not derivable from first principles. It is a tool which

facilitates computation of plastic strains based on stress state. The
proportionality constant, λ, is usually derived from plastic work
considerations [36,38]. Other investigators [54,55,56] have chosen
approaches in which Drucker's postulate is not used, often with good
results. Drucker's postulate is used in the present study, with the
full realization that it is purely an assumption, and that other
means could be utilized.

3.3.2.1 Incremental Plastic Pseudoload

The incremental pseudoload for use in the $(k + 1)^{th}$ step is com-
puted using the plastic strain increment, $\Delta\varepsilon_i^P$ derived from the kth
step. Using the standard pseudoload form of Equ's. (3.2) in the nota-
tion of Equ's. (3.1),

$$(\Delta Q_i^{0,P})^{k+1} = \iiint_\Omega B_{ji}D_{j1}(\Delta\varepsilon_1^P)^k d\Omega. \tag{3.21}$$

The volume integral is computed, as before, using Gaussian quadrature.
Thus, the incremental pseudoload is computed using the prior step
plastic strain increment, which, as shall be shown, is derived using
some values from the $(k - 1)^{th}$ increment. The scheme is seen to be
increasingly dependent on the choice of load increment, the smaller
the load increment the better until round-off and discretization error
become of the same order as the error due to linearization.

3.3.2.2 Nonlinear Thermoplastic Constitutive Relationships

Once the total, plastic, and thermal strain increments are computed
for a given load step, a constitutive relationship is required to compute
the stress increment. The following developments follow those in the

text by Hill [36], and are restated here for completeness. It should be noted that all stresses, strains, yield conditions, etc., must be rotated to the principal material axes. The notation adopted is s_i and e_i for stress and strain, respectively, in material coordinates. The 1-direction will be assumed to be parallel to the fibers, the 2-direction to be transverse, in the plane of the thin laminae, and the 3-direction normal to the plane of the lamina, as shown in Figure B.3.

The yield function of Hill [36] for initial yield is

$$f(s_i) = F(s_2 - s_3)^2 + G(s_3 - s_1)^2 + H(s_1 - s_2)^2 + 2Ls_{23}^2$$

$$+ 2Ms_{13}^2 + 2Ns_{12}^2 = 1, \tag{3.22}$$

where

$$2F = \frac{1}{Y^2} + \frac{1}{Z^2} - \frac{1}{X^2} \tag{3.23a}$$

$$2G = \frac{1}{X^2} + \frac{1}{Z^2} - \frac{1}{Y^2} \tag{3.23b}$$

$$2H = \frac{1}{X^2} + \frac{1}{Y^2} - \frac{1}{Z^2} \tag{3.23c}$$

$$2L = \frac{1}{R^2} \tag{3.23d}$$

$$2M = \frac{1}{S^2} \tag{3.23e}$$

$$2N = \frac{1}{T^2} \tag{3.23f}$$

and

X, Y, Z, R, S and T are yield strengths in the principal material
coordinate system directions 1, 2, 3, 23, 13, and 12, respectively.
Equ. (3.22) is valid, for a hardening material, only for initial yield.
As yielding progresses, so does the numerical value of $f(s_i)$.

The model used in the present study is known as isotropic hardening.
The basic premise of isotropic hardening is that as the yield hyper-
surface grows in stress space, it grows uniformly in all directions.
As an example, consider the von Mises ellipse in two dimensional stress
space for an initially isotropic material (Figure 3.1). The solid
ellipse represents $f(\sigma_i)$ for initial yield, and the dashed ellipse
represents $f(\sigma_i)$ after some plastic flow has occurred. In either case,
a stress state in or on the ellipse is elastic, while stress states
outside the ellipse are governed by the normal flow rule. Cyclic
loading might result in loading into the plastic range, followed
by elastic unloading and reloading to subsequent yield followed by
additional plastic deformation.

Isotropic hardening has two serious shortcomings. The plastic flow
governed by the normal flow rule expands uniformly (or isotropically) in
stress space. Thus, an initially isotropic material remains isotropic,
and an initially anisotropic material undergoes no change in its
anisotropy. Experimentally, this has been shown to be inaccurate. An
example is cold rolled sheet which is initially isotropic, but exhibits
anisotropy following the plastic flow of the rolling process. The other
deficiency of isotropic hardening is that it allows for no Bauschinger
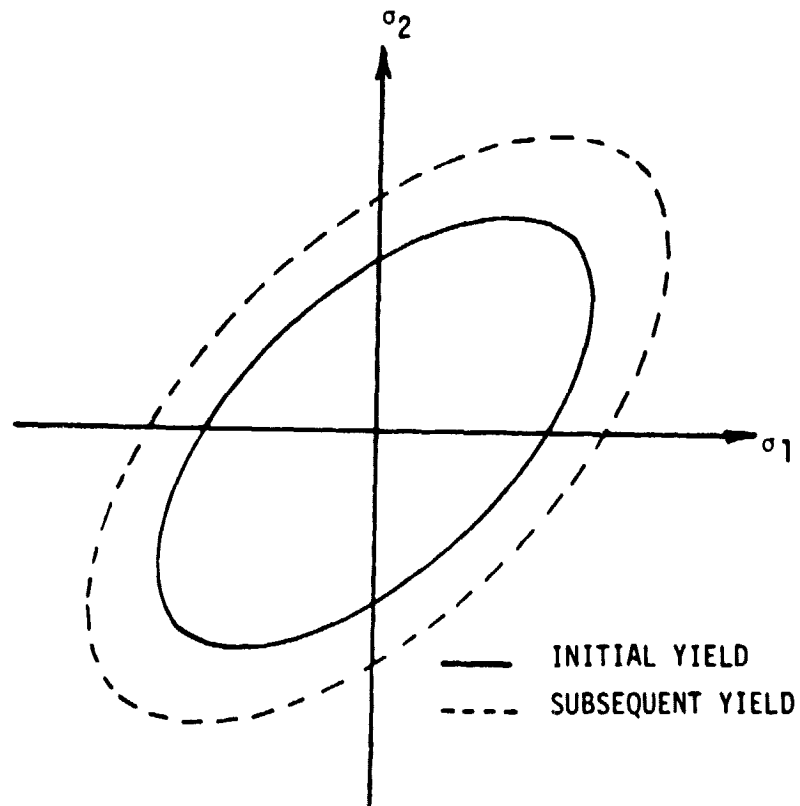
FIGURE 3.1 VON MISES ELLIPSE FOR INITIAL AND SUBSEQUENT YIELD

effect, a commonly observed phenomenon. When using the flow rule, the alternatives to isotropic hardening are kinematic hardening [37], in which the yield surface translates, but does not grow, in stress space, or some mixed model [57] which is some mixture of isotropic and kinematic hardening. Both models exhibit computational difficulties, especially for anisotropic materials.

Also used in the elastoplastic analysis is the equivalent stress, $\bar{s}$, as given by Hill [36],

$$\bar{s}^2 = \frac{3}{2(F+G+H)} [F(s_2 - s_3)^2 + G(s_3 - s_1)^2 + H(s_1 - s_2)^2$$

$$+2Ls_{23}^2 + 2Ms_{13}^2 + 2Ns_{12}^2]. \tag{3.24}$$

Note the difference in the definition of $\bar{s}$ in Equ. (3.24) and $f(s_i)$ in Equ. (3.23). Realizing the basic similarity in the definitions, it is assumed that yielding begins when

$$\bar{s}(s_i) = \hat{s}(\bar{e}^P, T) \tag{3.25}$$

where the functional notation indicates that $\bar{s}$ is a function of the current stress state, and $\hat{s}$ is a function of the equivalent plastic strain (history) and temperature. Taking the differentials of both sides, and realizing that $\bar{s}$ and $\hat{s}$ have the same functional form,

$$\frac{\partial \bar{s}}{\partial s_{ij}} ds_{ij} = \frac{\partial \bar{s}}{\partial \bar{e}^P} d\bar{e}^P + \frac{\partial \bar{s}}{\partial T} dT \tag{3.26}$$

where the equivalent plastic strain is related to the equivalent plastic strain increment as defined by Hill [36],

$$d\bar{e}^P = \sqrt{\frac{2}{3}}\,(F+G+H)\,[\frac{F(Gde_{22}^P - Hde_{33}^P)^2 + G(Hde_{33}^P - Fde_{11}^P)^2}{(FG+GH+HF)^2}$$

$$+ \frac{H(Fde_{11}^P - Gde_{22}^P)^2}{(FG+GH+HF)^2} + \frac{(de_{23}^P)^2}{2L} + \frac{(de_{13}^P)^2}{2M} + \frac{(de_{12}^P)^2}{2N}\,]^{\frac{1}{2}} \qquad (3.27)$$

where e_{ij}^P, $i \neq j$, are tensor shear strains, or

$$e_{ij} = \frac{1}{2}\,(\frac{\partial u_i}{\partial x_j} + \frac{\partial u_j}{\partial x_i}) \qquad i,j=1,2,3,4,5,6. \qquad (3.28)$$

where u_i and x_i are the standard displacement and position vectors of continuum mechanics, respectively.

It should be noted that Hill's equivalent plastic strain increment (Equ. 3.27) is, in general, only defined as an increment. It cannot be directly integrated unless some assumption is made of the loading history. The often used deformation theory of plasticity utilizes the assumption of proportional loading, in which loads and stresses increase in proportion, to facilitate integration of the equivalent plastic strain increment and the flow rule over the entire load history. The assumption of proportional loading is unacceptable for cyclic loading. Indeed, for a composite material cured at an elevated temperature, cooled to room temperature (resulting in some compressive residual stress), and then loaded in tension, any load history is cyclic to some extent. It therefore appears that deformation theory is unacceptable, unless applied in some quasi-incremental fashion, to problems involving curing and subsequent loading of composites. The incremental

or flow theory of plasticity will be used in the present study.

Several comments are necessary concerning Equ. (3.26). The functional form of the effective stress, $\bar{s}$, is given by Equ. (3.24). The terms $\frac{\partial \bar{s}}{\partial s_i}$ are computed using the closed-form partial derivative. The anisotropy coeffcients F, G, H, L, M, and N are functions of temperature which may be determined experimentally, although not without difficulty. Thus $\frac{\partial \bar{s}}{\partial T}$ reduces to terms of the form $\frac{\partial F}{\partial T}$, etc. The terms remaining are $\frac{\partial \bar{s}}{\partial \bar{e}^P}$ and $d\bar{e}^P$. The term $d\bar{e}^P$ is Hill's equivalent plastic strain increment, Equ. (3.27). The term $\frac{\partial \bar{s}}{\partial \bar{e}^P}$ will be referred to as the hardening coefficient. Hill [36] and later Pifko, et al [37] have commented on the difficulty of its determination. Mathematically, $\frac{\partial \bar{s}}{\partial \bar{e}^P}$ may be thought of as the slope of a plot of $\bar{s}$ vs $\bar{\epsilon}^P$. Unfortunately, for anisotropic materials it is not uniquely determined for a given stress-strain state, but is a function of the complete history of the material.

The first term of Equ. (3.26) determined is the equivalent plastic strain increment, $d\bar{e}^P$. The increment of plastic work, dW^P, done by a plastic strain increment de_i^P at stress s_{ij} is

$$dW^P = S_{ij} de_{ij}^P. \qquad (3.29)$$

Similarly, as shown by Hill [36],

$$dW^P = \bar{s} d\bar{e}^P. \qquad (3.30)$$

Multiplying both sides of the normal flow rule (Equ's. 3.20) by s_{ij},

$$s_{ij} de_{ij}^P = s_{ij} \lambda \frac{\partial f(s_{ij})}{\partial s_{ij}}. \qquad (3.31)$$

Using (3.29) and (3.30) in (3.31),

$$\bar{s} \, d\bar{e}^P = s_{ij} \lambda \frac{\partial f(s_{ij})}{\partial s_{ij}} \qquad (3.32)$$

or

$$d\bar{e}^P = \lambda \frac{s_{ij}}{\bar{s}} \frac{\partial f(s_{ij})}{\partial s_{ij}} . \qquad (3.33)$$

Using Equ. (3.3) in Equ. (3.26),

$$\frac{\partial \bar{s}}{\partial s_{ij}} ds_{ij} = \frac{\partial \bar{s}}{\partial \bar{e}^P} \frac{s_{ij}}{\bar{s}} \frac{\partial f(s_{ij})}{\partial s_{ij}} + \frac{\partial \bar{s}}{\partial T} dT. \qquad (3.34)$$

Writing the separation of total strain (in material coordinates) into components of Equ's. (3.3) in incremental form results in

$$\Delta e_i^T = \Delta e_i^e + \Delta e_i^\theta + \Delta e_i^P, \qquad (3.35)$$

where all strains are engineering strains.

Realizing that

$$\Delta s_i = D_{ij}^e \, \Delta e_j^e, \qquad (3.36)$$

where D_{ij}^e is the elasticity matrix, Equ's. (3.35) result in the incremental constitutive relationship

$$\Delta s_i = D_{ij}^e \, (\Delta e_j^T - \Delta e_j^\theta - \Delta e_j^P), \qquad (3.37)$$

where Δe_i^θ is given by Equ's. (3.18) as

$$\Delta e_i^\theta = (\alpha_i + \frac{\partial S_{ij}}{\partial T} s_j) \Delta T, \qquad (3.38)$$

where S_{ij} is the compliance matrix, s_j is the current stress, T the temperature, and α_i the instantaneous thermal expansion coefficient. The plastic strain increment, Δe_i^P, is given by the flow rule, Equ's. (3.20) to be, in incremental form,

$$\Delta e_i^P = \lambda \frac{\partial f(s_i)}{\partial s_i} .$$

(3.39)

Writing Equ's. (3.34) in incremental form and noting conversion to engineering shear strains,

$$\frac{\partial \bar{s}}{\partial s_i} \Delta s_i = \lambda \frac{\partial \bar{s}}{\partial \bar{e}^P} \frac{s_i}{\bar{s}} \frac{\partial f(s_i)}{\partial s_i} + \frac{\partial \bar{s}}{\partial T} \Delta T .$$

(3.40)

Substituting (3.37), (3.38), and (3.39) into (3.40)

$$\frac{\partial \bar{s}}{\partial s_i} D_{ij}^e \Delta e_j - \frac{\partial \bar{s}}{\partial s_i} D_{ij}^e (\alpha_j + \frac{\partial S_{jk}}{\partial T} s_k) \Delta T - \frac{\partial \bar{s}}{\partial T} \Delta T$$

$$= \frac{\partial \bar{s}}{\partial s_i} D_{ij}^e \lambda \frac{\partial f(s_i)}{\partial s_j} + \lambda \frac{\partial \bar{s}}{\partial \bar{e}^P} \frac{s_i}{\bar{s}} \frac{\partial f(s_i)}{\partial s_i}$$

(3.41)

where Δe_i has been used to represent the total strain increment. Solving (3.41) for λ,

$$\lambda = \frac{\frac{\partial \bar{s}}{\partial s_i} D_{ij} \Delta e_j - \frac{\partial \bar{s}}{\partial s_i} D_{ij}^e (\alpha_j + \frac{\partial S_{jk}}{\partial T} s_k) \Delta T - \frac{\partial \bar{s}}{\partial T} \Delta T}{\frac{\partial \bar{s}}{\partial \bar{e}^P} \frac{s_i}{\bar{s}} \frac{\partial f(s_i)}{\partial s_i} + \frac{\partial \bar{s}}{\partial s_i} D_{ij}^e \frac{\partial f(s_i)}{\partial s_j}}$$

(3.42)

where D_{ij}^e and S_{ij} are evaluated at the current temperature. Note that aside from being the proportionality constant in the flow rule, λ serves as a loading indicator. The three conditions are

$$\lambda < 0 \qquad\qquad (3.42a)$$

$$\lambda = 0 \qquad\qquad (3.42b)$$

$$\lambda > 0, \qquad\qquad (3.42c)$$

which are denoted as unloading, neutral loading, and loading, respectively. Unloading ($\lambda<0$) implies that no plastic flow is occurring, the stress state being inside the yield hypersurface, and the elastic constitutive relations are used. Neutral loading ($\lambda=0$) implies that no additional plastic flow is occurring, but the stress state is moving along the yield hypersurface, and the elastic constitutive relations are used. Loading ($\lambda>0$) implies that additional plastic flow is occurring, and the yield hypersurface is growing in stress space. The plastic constitutive relations are used.

In the present study, the numerical value of Hill's yield condition (Equ. 3.22) is computed at the end of each load step for each Gauss point. If unloading is detected, the elastic constitutive relations are used until the maximum value of Hill's yield condition for that Gauss point is reattained. Thus, cyclic loads may be treated.

The incremental plastic constitutive relationship becomes

$$\Delta s_i = D^e_{ij}\Delta e_j - D^e_{ij}(\alpha_j + \frac{\partial S_{jk}}{\partial T} s_k)\Delta T - \lambda D^e_{ij} \frac{\partial f(s_i)}{\partial s_j} \qquad (3.43)$$

where λ is given by Equ. (3.42). In the case where a transition from elastic to plastic is made during a load step, some adjustment to Equ's. (3.43) is required. This region has been termed the transition region. Marcal [58] gives a computationally efficient procedure for its treatment. Suppose that a fraction, denoted by m, of the load

step was elastic. Then the substitution of

$$\lambda = (1 - m)\lambda \qquad (3.44)$$

into Equ's. (3.43) reduces the plastic strain, and thus corrects the transition region stress increment.

3.3.2.3 Nonlinear Orthotropic Hardening Coefficient

The remaining term occurring in the plasticity developments is the hardening coefficient, $\frac{\partial \bar{s}}{\partial \bar{e}^p}$. As previously stated, this quantity has been pointed out as being difficult to determine for anisotropic materials. Biffle [59] used an assumption of equal plastic work in all directions. Pifko, et al [37] used heuristic arguments based on the method of weighted averages. Such approximations are necessary, but are obviously postulates. The technique developed for use in the present study utilizes assumptions which are also heuristic but will be shown to yield reasonably accurate results for both isotropic and orthotropic materials.

Suppose, in an incremental analysis, that the state variables are known at the end of an increment designated as k. For initial yielding, the step k will have been elastic. For continuing plasticity, the state will have been computed using the plastic constitutive relationships. Also suppose that the uniaxial stress-strain relations, in principal material directions for orthotropic media, are given in Ramberg-Osgood [60] form,

$$e_i = \frac{s_i}{E_i} + \beta_i (s_i)^{n_i} \qquad i=1,6 \qquad (3.45)$$

where the summation convention has been suspended for the entireity of
this development, E_i is Young's modulus for the i direction, and β_i and
n_i are known as the Ramberg-Osgood coefficients for the i direction. Let
the stress increment for the kth step be represented by $(\Delta s_i)^k$. We
define the max norm [61] of the stress increment as

$$||(\Delta s_i)^k|| = \max_{1 \le i \le 6} |(\Delta s_i)^k|. \tag{3.46}$$

The normalized stress increment, $(\Delta \tilde{s}_i)^k$, is defined by

$$(\Delta \tilde{s}_i)^k = \frac{(\Delta s_i)^k}{||(\Delta s)^k||}. \tag{3.47}$$

The model developed in this study for computation of $\frac{\partial \tilde{s}}{\partial \tilde{e}^p}$ utilizes
the normalized stress increment for the kth step and the total stresses
at the end of the kth step. For the purposes of computing the hardening
coefficient only, proportional loading is assumed during the $(k+1)^{th}$
step. Hashin, et al [12] have used proportional loading for the entire
loading history, and have discussed its accuracy for loading paths
which are "neighbors" of proportional loading. Hence, the assumption
of proportionality from step to step is reasonable unless steps are
large or contain load reversals. Note that step-to-step proportionality
is used only for computation of the hardening coefficient. Once it is
computed, the previously developed plastic constitutive relations are
used to compute the stress state at the end of the $(k+1)^{th}$ step.

As done by previous investigators [37,40], the nonlinear, or plastic,

uniaxial strain is assumed to be the power law portion of the Ramberg-Osgood approximation, or

$$e_i^P = \beta_i (s_i)^{n_i}. \tag{3.48}$$

Differentiating,

$$de_i^P = \beta_i n_i (s_i)^{n_i - 1} ds_i, \tag{3.49}$$

where the assumption is made that plastic strains are related to changes in stress. Inherent in the use of a Hill-type criterion is the incompressibility of plastic strains, or

$$\sum_{i=1}^{3} e_i^P = 0. \tag{3.50}$$

This condition must be strictly enforced for consistency.

Consider the case of a prismatical bar of an isotropic elastic-plastic material subjected to an axial load. When loaded in tension into the plastic region, the axial plastic strain is related to the stress through some relation such as Equ. 3.49, where β and n are the appropriate Ramberg-Osgood parameters. Transverse plastic strains occur such that the incompressibility condition (3.50) is satisfied, but stress changes are small, such that (3.49) are not satisfied in the transverse directions. We therefore speak of the axial direction as being the "dominant" direction of plastic flow, and use the axial Ramberg-Osgood parameters. In this manner, we obtain de_{axial}^P. From the flow rule,

$$de_{ij}^P = \lambda \, \frac{\partial f(s_{ij})}{\partial s_{ij}} \tag{3.51}$$

indicating the existence of the ratios $de_2^P : de_1^P$ and $de_3^P : de_1^P$. Therefore, de_2^P and de_3^P may be computed given $\dfrac{\partial f(s_{ij})}{\partial s_{ij}}$ and de_1^P. Note that no such conditions exist on plastic shearing strain. It is therefore assumed that the shear stress-shear strain relations follow the Ramberg-Osgood curves determined for pure shear.

Now consider the generalization of the previous arguments to an orthotropic material. The "dominant" direction is determined as the direction corresponding to the maximum absolute value of $\dfrac{\partial f(s_{ij})}{\partial s_{ij}}$. Ramberg-Osgood coefficients govern the flow in the dominant direction, and transverse flow is determined by the relative values in $\dfrac{\partial \bar{s}}{\partial s_{ij}}$ and the incompressibility condition. Plastic shearing strain follows the Ramberg-Osgood approximations determined by pure shear tests.

For purposes of illustration, consider the case where the 1-direction has been determined to be dominant. Then

$$de_1^P = \beta_1 n_1 s_1^{n_1 - 1} ds_1, \tag{3.52}$$

and

$$de_2^P = c_2 \beta_1 n_1 s_1^{n_1 - 1} ds_1 \tag{3.53a}$$

$$de_3^P = c_3 \beta_1 n_1 s_1^{n_1 - 1} ds_1 \tag{3.53b}$$

where c_2 and c_3 are determined from $\dfrac{\partial f(s_{ij})}{\partial s_{ij}}$. Furthermore, assume that the stress increment, stress, and plastic strain increment are known

at the end of the kth step, and that the loading is proportional from the kth step to the $k+1^{th}$ step. The projected stress increment for the $k+1^{th}$ step is thus

$$(\Delta s)^{k+1} = \phi^k (\Delta s)^k \tag{3.54}$$

where ϕ^k is the proportionality constant for the step k to $k+1$. Since the effective stress is a function of the individual stresses, the differential change in the effective stress is

$$d\bar{s} = \frac{\partial \bar{s}}{\partial s_1} ds_1 + \frac{\partial \bar{s}}{\partial s_2} ds_2 + \frac{\partial \bar{s}}{\partial s_3} ds_3 + \frac{\partial \bar{s}}{\partial s_4} ds_4 + \frac{\partial \bar{s}}{\partial s_5} ds_5 + \frac{\partial \bar{s}}{\partial s_6} ds_6. \tag{3.55}$$

Since the stresses and increments for the kth step are known, using the proportionality assumption, the increment of the effective stress for the $k+1^{th}$ step may be estimated as

$$(\Delta s)^{k+1} = \phi^k \{\frac{\partial \bar{s}}{\partial s_1} \Delta s_1 + \frac{\partial \bar{s}}{\partial s_2} \Delta s_2 + \frac{\partial \bar{s}}{\partial s_3} \Delta s_3 + \frac{\partial \bar{s}}{\partial s_4} \Delta s_4 + \frac{\partial \bar{s}}{\partial s_5} \Delta s_5 + \frac{\partial \bar{s}}{\partial s_6} \Delta s_6\}^k$$

$$\tag{3.56}$$

where incremental changes have been substituted for infinitesimals.

The next operation is to project the effective plastic strain increment of Equ. (3.27) from known quantities for the kth step to the $k+1^{th}$ step. Using (3.52), (3.53), the differential shear stress-shear strain relations similar to (3.52), and the proportionality assumption, the effective plastic strain increment becomes

$$(d\bar{e}^P)^{k+1} = \phi^k \sqrt{\frac{2}{3} (F+G+H)} \ \{[\beta_1 n_1 s_1^{n_1-1} (\Delta s_1)^k]^2 [\frac{F(GC_2-HC_3)^2}{(FG+GH+HF)^2}$$

$$+ \frac{G(HC_3 - F)^2 + H(F - GC_2)^2}{(FG + GH + HF)^2}] + \frac{1}{8L} [\beta_4 n_4 s_4^{n_4 - 1} (\Delta s_4)^k]^2 \qquad (3.57)$$

$$+ \frac{1}{8M} [\beta_5 n_5 s_5^{n_5 - 1} (\Delta s_5)^k]^2 + \frac{1}{8N} [\beta_6 n_6 s_6^{n_6 - 1} (\Delta s_6)^k]^2 \}^{\frac{1}{2}}$$

where the difference in tensor and engineering shear strains has been accounted for. Using the normalized stress increment of Equ. 3.47 and realizing that the hardening coefficient $(\frac{\partial \bar{s}}{\partial \bar{e}^p})^{k+1}$ may be approximated by $(\frac{\Delta \bar{s}}{\Delta \bar{e}^p})^{k+1}$, we find that the proportionality constant ϕ^k and the max norm of the prior step stress increment cancel out, leaving

$$(\frac{\partial \bar{s}}{\partial \bar{e}^p})^{k+1} = (\frac{\Delta \bar{s}}{\Delta \bar{e}^p})^{k+1} \qquad (3.58)$$

where

$$(\Delta s)^{k+1} = \frac{\partial \bar{s}}{\partial s_1} (\Delta \tilde{s}_1)^k + \frac{\partial \bar{s}}{\partial s_2} (\Delta \tilde{s}_2)^k + \frac{\partial \bar{s}}{\partial s_3} (\Delta \tilde{s}_3)^k$$

$$+ \frac{\partial \bar{s}}{\partial s_4} (\Delta \tilde{s}_4)^k + \frac{\partial \bar{s}}{\partial s_5} (\Delta \tilde{s}_5) + \frac{\partial \bar{s}}{\partial s_6} (\Delta \tilde{s}_6) \qquad (3.59)$$

and

$$(\Delta \bar{e}^p)^{k+1} = \sqrt{\frac{2}{3} (F + G + H)} \{ [\beta_1 n_1 s_1^{n_1 - 1} (\Delta \tilde{s}_1)^k]^2 [\frac{F(GC_2 - HC_3)^2}{(FG + GH + HF)^2}$$

$$+ \frac{G(HC_3 - F)^2 + H(F - GC_3)^2}{(FG + GH + HF)^2}] + \frac{1}{8L} [\beta_4 n_4 s_4^{n_4 - 1} (\Delta \tilde{s}_4)^k]^2 \qquad (3.60)$$

$$+ \frac{1}{8M} [\beta_5 n_5 s_5^{n_5 - 1} (\Delta \tilde{s}_5)^k]^2 + \frac{1}{8N} [\beta_6 n_6 s_6^{n_6 - 1} (\Delta \tilde{s}_6)^k]^2 \}^{\frac{1}{2}} .$$

Note that in Equ's. (3.58) and (3.59) the stresses, s_i and effective stress gradients, $\frac{\partial \bar{s}}{\partial s_i}$ are computed at the end of the kth load step.

Several observations may be made concerning the nonlinear orthotropic hardening coefficient. First, since the computations must be carried out at the Gauss point level, the computation of plastic material behavior will be expensive. The value of the coefficient is dependent on the anisotropy parameters, stresses and effective stress gradients at the end of the previous step, and the normalized stress increment for the previous step. Note that it is _not_ a function of the magnitude of the prior step stress increment, but of the relative values of the stress increment components. In defense of the computational efficiency, the effective stress gradients $\frac{\partial \bar{s}}{\partial s_i}$ are needed for later use in the flow rule. The method is valid for orthotropic as well as isotropic materials. For isotropic media, the method reduces to a von Mises criterion with hardening coefficients piecewise extrapolated along the $\bar{s}$ - $\bar{e}^p$ curve. The mechanics of implementation of the algorithm are presented in Appendix B. Appendix C shows the reduction of Hill's criterion to Mises' criterion for isotropic materials.

Chapter 4

APPLICATION TO COMPOSITES

Application of the finite element technique discussed in Appendix A to laminated composites was previously discussed by Lin [25], Dana [26], and Dana and Barker [27]. Some of their conclusions will be repeated here for completeness. As discussed in Appendix A, the approach of the present study follows what has been termed the "macroscopic" approach. The approximations and implications of this technique are discussed in the following paragraphs.

4.1 Microscopic Versus Macroscopic Approaches

The microscopic approach to the analysis of composite materials considers the fiber and matrix materials to be separate, each having the properties of the bulk fiber and matrix materials, respectively. Material properties are experimentally determined or assumed for the constituents, which may be isotropic or anisotropic. Some degree of bonding between the fiber and matrix is assumed. The degree of bonding is chosen based on the subject of the investigation. The microscopic approach appears to be useful for the study of fiber/matrix interactions and failure mechanisms. However, it is apparent that the computer cost for micromechanical analysis of laminates with even a small number of plies would be prohibitive. Indeed, Foye [35] used a large number of finite elements to perform a two-dimensional analysis of one fiber and its surrounding matrix, even after a significant degree of symmetry was assumed.

40

The macroscopic approach used in the present study assumes that the fiber reinforced material is, on the individual ply level, a continuous, homogeneous, orthotropic material. Properties used are generally determined by tests on unidirectional materials. A description of the tests necessary to determine the elastic (and inelastic) properties of an orthotropic material is given in the report by Brinson and Yeow [62]. When using the macroscopic approach, the analyst should realize that all fiber/matrix interactions actually occur at the microscopic (actually molecular) level, and have not been considered. Possible failure mechanisms such as fiber/matrix shearing, matrix cracking, and fiber fracture cannot readily be studied. However, important effects such as interlaminar stresses, stress concentrations near holes, free edges, and corners are well treated.

In summary, one must conclude that the microscopic approach is a more accurate model of what really occurs in a composite material, but has computational complexity which renders it impractical for all but those problems involving single fibers and the surrounding matrix. The macroscopic approach yields considerable valuable information, and is computationally efficient for many laminates. Problem size and complexity are limited by core storage and cost. The indicated approach is to use the microscopic model for matrix/fiber interaction studies and the macroscopic model for problems involving stress concentrations, end and edge effects, and interlaminar stresses. As pointed out by various investigators [6,8,9], end and edge effects

are manifested in a region known as the "boundary layer" which extends inward from the free edge of a laminate to a distance approximately equal to the thickness of the laminate. Away from the boundary layer, the computationally simple lamination theory solution is recovered by finite difference and finite element techniques.

The present study uses the macroscopic approach and its primary topic is the determination of interlaminar stresses near holes and free edges. Several material models have been considered. Linear and nonlinear thermal expansions, as well as temperature dependent plasticity, have been treated.

4.2 Modeling Considerations

Care must be taken when using the finite element method that the assumptions of the method are not violated. In addition, the analyst must insure that the finite element model (or grid) used is an accurate model of the real structure. Boundary conditions must match, and the finite element model must be capable of undergoing any deformation which is possible in the real structure. The former requirement involves the use of sufficient nodal points on the boundary for adequate modeling. The latter condition involves placing sufficient elements in the region away from the boundary layer. When the number of elements is increased, care must be taken that element aspect ratios are in the proper range. Poor aspect ratios can lead to erroneous results. In addition, the analyst must be sure that finite elements which are large in one direction do not join finite elements which are small in the same direction.

Such a condition, involving flexible (large) element connected to stiff (small) elements, may result in the assembled stiffness matrix being ill-conditioned or even quasi-singular.

The properties of the element used in the present study have been fairly well documented by previous investigators [25,26,27]. Lin [25] determined that the best shape for the element for modeling isotropic materials was a rectangular parallelpiped, square (a=b) in the 12 node plane, (see Fig. 4.1) and with an aspect ratio of three (3c=a) in the eight node plane. Acceptable stiffness matrices were generated for width to thickness (a/c) ratios up to 12. Dana and Barker [27] reported that three elements were needed through the thickness of each ply of a laminated composite for adequate determination of the through-the-thickness stress gradients. This finding is consistent with that of Wang and Crossman [16], who used a large number of elements through the thickness in order to see the gradients. Consideration of the boundary layer dictates the size of the elements near boundaries, since large gradients exist in the boundary layer. The need for three elements through each ply plus acceptable aspect ratios provides another guide for element size.

The requirements noted above are for very accurate elements. In regions where gradients are low (i.e. the lamination theory region), or where accuracy of stress is not critical (i.e. the region away from a hole being studied), elements with less than optimum size and aspect ratio may be used. This is common practice in finite element analysis. Although this practice is questionable from a theoretical
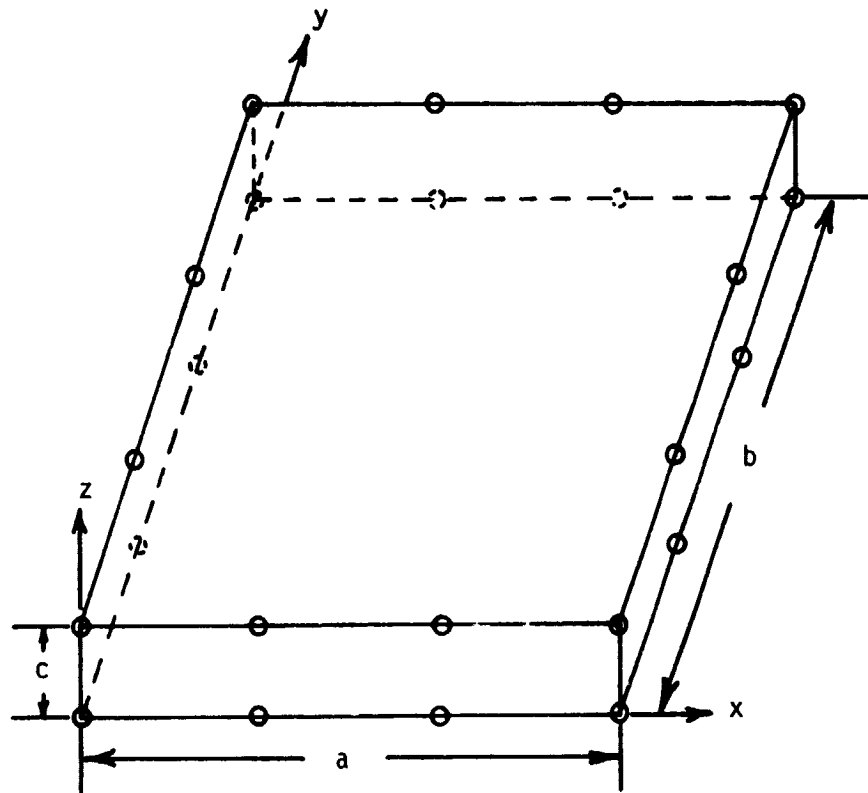
FIGURE 4.1 DIMENSIONS FOR ASPECT RATIO CALCULATIONS

standpoint, it is often the only way a problem can be run due to computer cost or storage limitations. As long as the analyst realizes the regions of accuracy and inaccuracy, the technique is viable.

4.3 Grid numbering and bandwidth considerations

As mentioned in Appendix B, the bandwidth of the global stiffness matrix is very important. But it is only the mean and not the maximum bandwidth that is crucial when using the skyline column storage scheme [63]. In this scheme, the upper triangular portion of the global stiffness matrix is stored, column by column, as a vector. Only the terms up to and including the upper nonzero entry in a column are stored. Larger mean bandwidth thus has the double effect of increasing the core required to store the matrix as well as the number of operations required for triangularization and back substitution. For example, consider the grid and numbering of Figures 4.2 and 4.3. The grids shown are similar to those used for simulation of the off-axis tensile specimens reported in the next chapter. The loading is uniform extension in the X-direction. The boundary conditions are that the ends of the specimen retain the same size as the deformation proceeds. The number of degrees of freedom of the grid is 168. Thus, the full upper triangular portion of the matrix would require 14196 core locations for its storage. The grid, numbered as shown in Figure 4.2, has 168 degrees of freedom, a maximum half bandwidth of 150, and required 12900 core locations for its storage (not counting the diagonal pointer array). The same grid, numbered
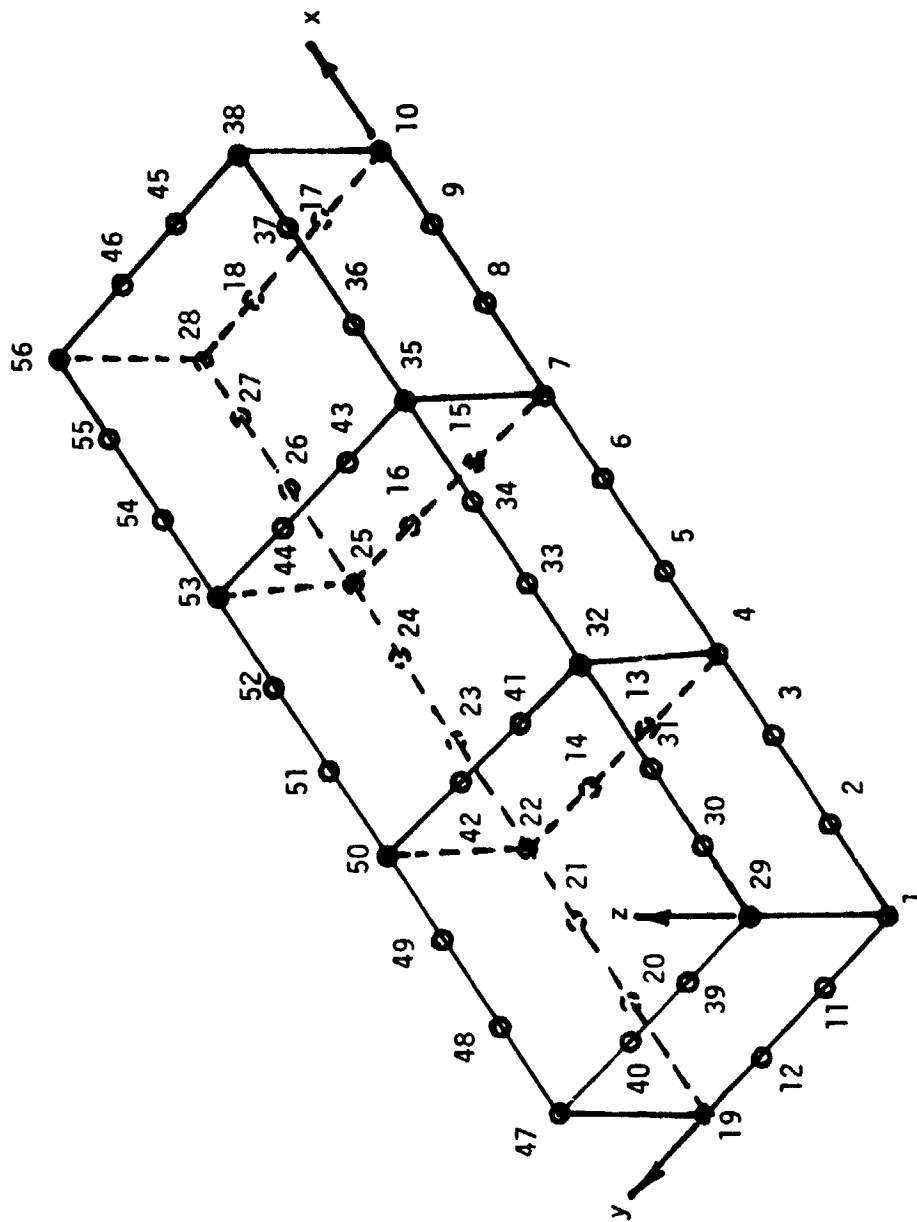
FIGURE 4.2 GRID BEFORE BANDWIDTH MINIMIZATION
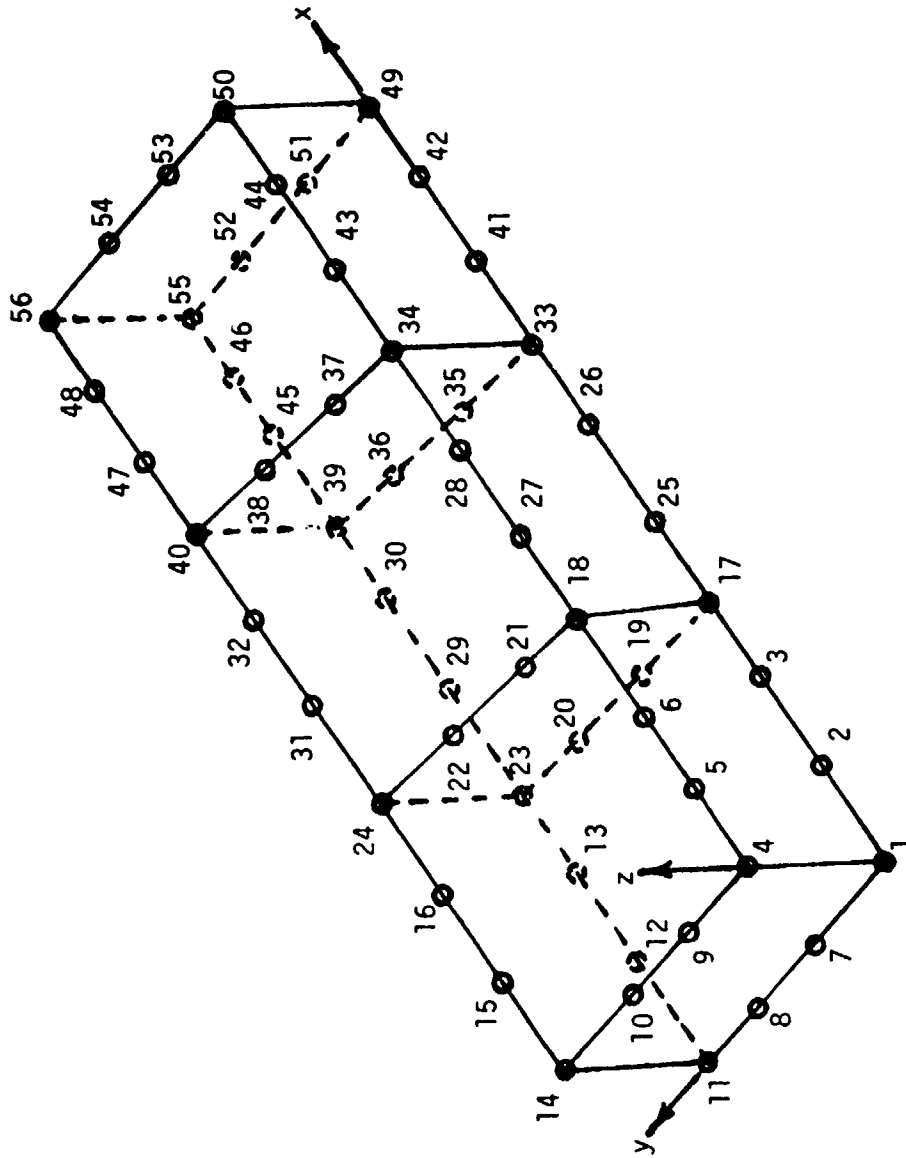
FIGURE 4.3 GRID AFTER BANDWIDTH MINIMIZATION

as shown in Figure 4.3, also has 168 degrees of freedom, but has a maximum half bandwidth of 72, and requires only 7284 storage locations. It is apparent that minimization of bandwidth should always be done before any attempt is made to run problems.

The bandwidth of all finite element grids used in this study was minimized using a modification of the computer program BANDIT [64] and the Gibbs-Poole-Stockmeyer [65] minimization algorithm. Other algorithms [66,67] are also available for bandwidth minimization. The experience of the author in using BANDIT indicates that the Gibbs-Poole-Stockmeyer method is generally cheaper and yields better results than the Cuthill-McKee [66] method.

Chapter 5

RESULTS AND DISCUSSION

This chapter details the results of a series of problems, dealing primarily with laminated composites, which were solved using the techniques derived in the previous chapters. Comparisons are made to experimental data as well as the predictions of other models. Some of the problems were solved using the CDC 6700 computer system at the U. S. Naval Surface Weapons Center, Dahlgren, Virginia, and the remainder were solved on the IBM S370/3033 at VPI&SU. The computer program NALCOM (Nonlinear Analysis of Laminated COMposites) developed for this study is described in Appendix B. A listing of the program is available from the author on request.

5.1 Isotropic Material

As a check of the elastic-plastic capabilities of the program, an isotropic material was analyzed. The material was a chromium-nickel steel for which the stress-strain curve is presented as Figure 11 of Reference 60. The Ramberg-Osgood coefficients are given in Table 5.1. The yield stresses were chosen as the points of significant deviation from linearity. A comparison of experimental and computed values is shown in Figure 5.1. The program predicts linear elastic unloading and subsequent yield when the stress state reattains the yield hypersurface through some loading cycle. Also note that the isotropic hardening model does not predict any Bauschinger effect. As stated in the initial derivation, this is a known shortcoming of

49

50

TABLE 5.1. ROOM TEMPERATURE MATERIAL PROPERTIES

Cr-Ni Steel

Parameter	Elastic (msi)	σ^e, τ^e (ksi)	n_1	β_1	σ^*(ksi)	n_2	β_2
E_1	25.77	60.	4.83	1.0999×10^{-28}	--	--	--
E_2	29.66	60.	4.81	6.5403×10^{-29}	--	--	--
G_{12}	9.9115	30.	4.83	1.0999×10^{-28}	--	--	--
ν_{12}	0.3	--	--	--	--	--	--
ν_{23}	0.3	--	--	--	--	--	--

NARMCO 5505 Boron/Epoxy

Parameter	Elastic (msi)	σ^e, τ^e (ksi)	n_1	β_1	σ^*(ksi)	n_2	β_2
E_1	30.1	180	1.0	0	--	--	--
E_2	2.87	3.34	3.0	8.2187×10^{-16}	--	--	--
G_{12}	.88	1.5	2.134	3.33×10^{-11}	6.3	4.0	2.6668×10^{-16}
ν_{12}	0.225	--	--	--	--	--	--
ν_{23}	0.35	--	--	--	--	--	--

T300/5208 Graphite/Epoxy

Parameter	Elastic (msi)	σ^e, τ^e (ksi)	n_1	β_1	σ^*(ksi)	n_2	β_2
E_1	19.2	90	2.0369	0.30754×10^{-13}	--	--	--
E_2	1.56	13.5	1.0681	0.13324×10^{-7}	--	--	--
G_{12}	0.82	3.5	1.1471	0.44882×10^{-7}	3.9757	3.3985	1.0953×10^{-16}
ν_{12}	0.238	--	--	--	--	--	--
ν_{23}	0.49	--	--	--	--	--	--

FIGURE 5.1 σ_x VS e_x FOR ISOTROPIC MATERIAL

the isotropic hardening model.

5.2 Off-axis Tensile Specimens

One common test for orthotropic materials which has received considerable attention is the off-axis tension test [68,69 70]. Shown schematically in Figure 5.2, the test involves applying tensile loading to a unidirectional material which is oriented in the test fixture such that the fibers are at some angle θ with respect to the load axis. Chamis [68] has proposed the use of a 10 degree off-axis tensile test for determination of the shear modulus G_{12}. Cole and Pipes [69,71] performed a series of off-axis tensile tests on NARMCO 5505 Boron/Epoxy. Sandhu [70] found their 15° off-axis data suspect and performed the test again, with significantly different results.

The computer program NALCOM was used to predict the linear elastic and elastic-plastic response of Boron/Epoxy off-axis tensile specimens. Material properties are shown in Table 5.1. The finite element grid used for all off-axis tensile modeling is shown in Figure 5.3. The model is symmetric about the x-y plane. The ends are assumed to remain straight and are free to move only in the x-direction for the linear elastic computations. For the nonlinear predictions, the load was a uniform stress applied to the end of maximum x, which was constrained to no rotation and no y or z direction motion. These end conditions were intended to simulate perfect gripping, no end tabs, and no rotation of the grips.

5.2.1 Linear Elastic Off-axis Tensile Specimen Modeling

Off-axis tensile specimens of NARMCO 5505 Boron/Epoxy and
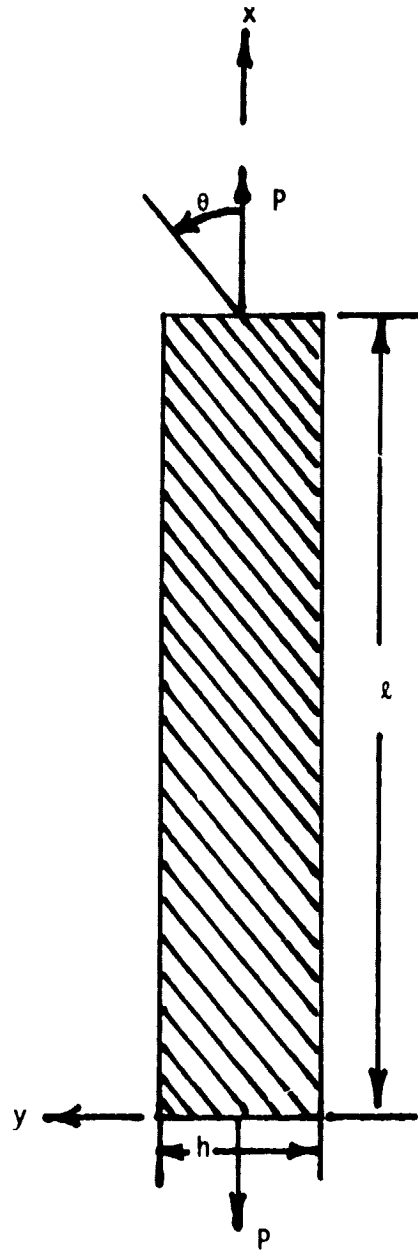
FIGURE 5.2   OFF-AXIS TENSILE SPECIMEN ($\ell/h > 14$)
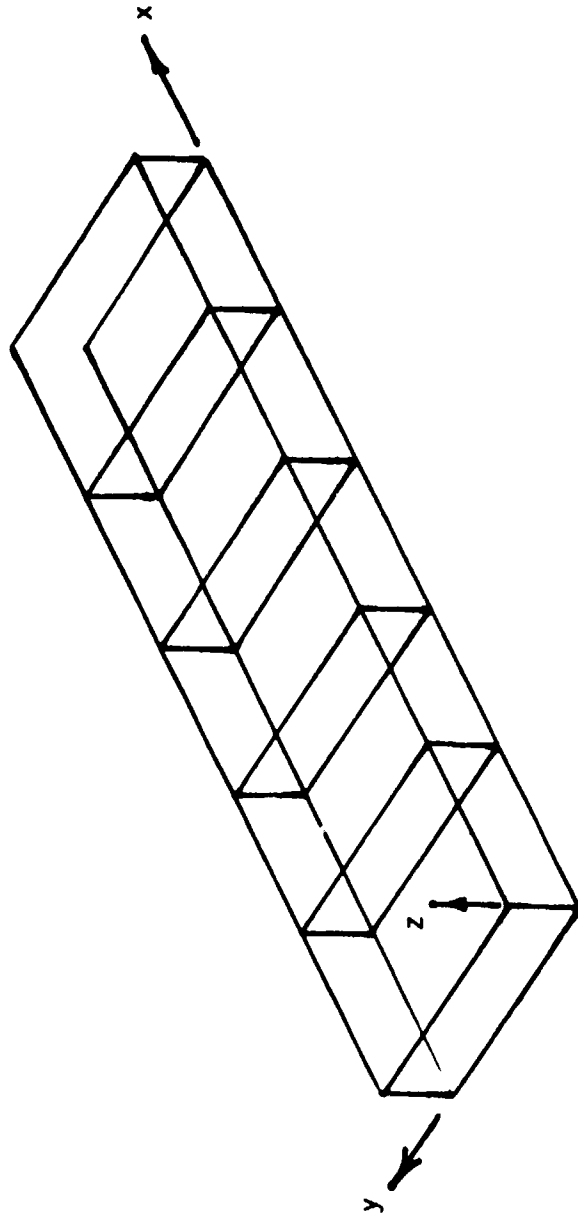
FIGURE 5.3 GRID FOR OFF-AXIS TENSILE STUDIES

T300/5208 Graphite/Epoxy were modeled using linear elastic material properties from Cole and Pipes [69,71] and unpublished data obtained from the Lockheed Company. Unless otherwise specified, all experimental data for T300/5208 were taken from the Lockheed data package. The finite element grid shown in Figure 5.3 was used for these analyses. The dimensions are given in Table 5.2. To simulate the effect of bonding end tabs to the composite as an aid to gripping, a length at each end equal to 20% of the total coupon length was constrained to no y-direction motion. This has the same effect as a perfectly bonded tab which allows extensional but no in-plane bending deflection along the tab length.

The linear elastic characteristics of Boron/Epoxy off-axis tensile coupons as determined by an x-direction strain loading are shown in Figures 5.4 and 5.5 and Table 5.2. The quantity S_{11}^{-1} as computed from the transformation equations is included for comparison. Note the close agreement between the model and Cole and Pipes' experimental data with the exception of the apparent modulus E_{xx} at 15°. As previously mentioned, Sandhu [70] found the 15° data suspect. Sandhu's 15° data is also shown on Figure 5.4, with significantly improved comparison. Note the small effect of the end tabs (Table 5.2). The effect of the end tabs is to decrease the coupon aspect ratio L/h. Since Cole and Pipes used aspect ratios ranging from 18.7 to 28, even the decrease due to the tabs is not sufficient in most cases to bring the ratios below the value of 14 to 16 which is generally regarded as an acceptable value for

TABLE 5.2. LINEAR ELASTIC RESULTS FOR OFF-AXIS EXTENSION OF NARMCO 5505

Angle (degrees)	Specimen		Computed - no tabs		Computed - tabs		$\frac{1}{S_{11}}$ (msi)	Experimental [69]	
	length (in)	width (in)	E_{xx} (msi)	ν_{xy}	E_{xx} (msi)	ν_{xy}		E_{xx} (msi)	ν_{xy}
0	9	0.5	30.1	.225	30.2	.225	30.1	30.1	.225
5	11.65	0.5	24.27	.325	--	--	24.28	--	--
10	11.65	0.5	15.65	.476	--	--	15.54	--	--
15	11.65	0.5	9.63	.558	9.37	.549	9.94	8.0	.53
20	11.65	0.5	6.53	.597	--	--	6.83	--	--
25	11.65	0.5	4.81	.610	--	--	5.05	--	--
30	14.	0.5	3.79	.606	3.78	.601	3.99	3.85	.58
45	14.	0.5	2.55	.536	2.54	.531	2.66	2.64	.56
60	14.	0.5	2.38	.378	2.38	.375	7.45	2.32	.38
75	9.35	0.5	2.64	.152	2.64	.150	2.68	2.52	.16
90	9	0.5	2.88	.0216	2.86	.0211	2.87	2.87	--

FIGURE 5.4   LOAD DIRECTION MODULUS VS. FIBER ANGLE
FOR OFF-AXIS TENSION OF BORON/EPOXY
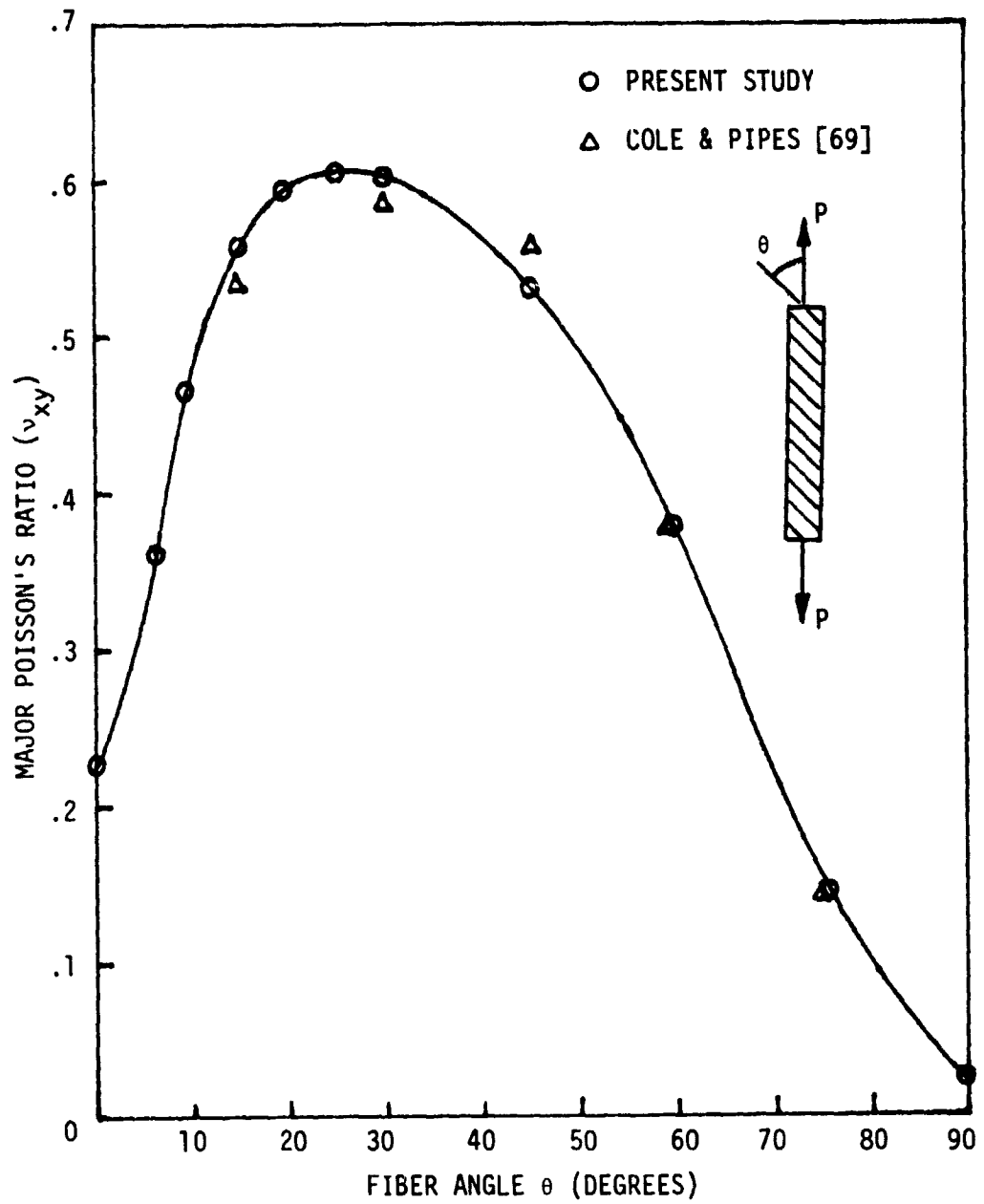
FIGURE 5.5   MAJOR POISSON'S RATIO VS. FIBER ANGLE
FOR OFF-AXIS TENSION OF BORON/EPOXY

elimination of end effects. Figure 5.6 is a plot of the deformed
finite element grid for Boron/Epoxy and θ = 15°. Note the in-plane
warping which is characteristic of off-axis tensile specimens. Such
warping gives rise to substantial variations in stress and strain
across the width of the specimen. Such variations raise the question
of accuracy of strain measurements on such specimens, since strain
gauges are of finite dimensions.

The computed linear elastic moduli and Poisson's ratios of
Graphite/Epoxy are shown in Figures 5.7 and 5.8. No experimental data
appear to exist for off-axis tensile testing of Graphite/Epoxy, so no
comparisons are possible. The basic shape of the curves is the
same as for Boron/Epoxy. Note that the major Poisson's ratio is
again a maximum at approximately 20°.

5.2.2 Nonlinear Response of Off-axis Tensile Specimens

As a check of the orthotropic plasticity model developed in
Chapter 3, the elastic-plastic response of Boron/Epoxy off-axis
tensile specimens was computed for comparison to the nonlinear data
of Cole and Pipes [69]. As with the linear case, the 15° data of
Sandhu [70] was also considered. Ramberg-Osgood coefficients were
determined from the 0°, 90°, and pure shear (from tube torsion) data
of Cole and Pipes. Comparisons for Boron/Epoxy were made to two
sets of experimental data and two other analytical models. The
elastic-plastic computations were also run for Gr/Ep and are
presented without comparison, since no off-axis tensile data
for Gr/Ep are known to exist. Comparisons of all the models to

FIGURE 5.6   DEFORMED GRID OF 15° OFF-AXIS TENSILE SPECIMEN
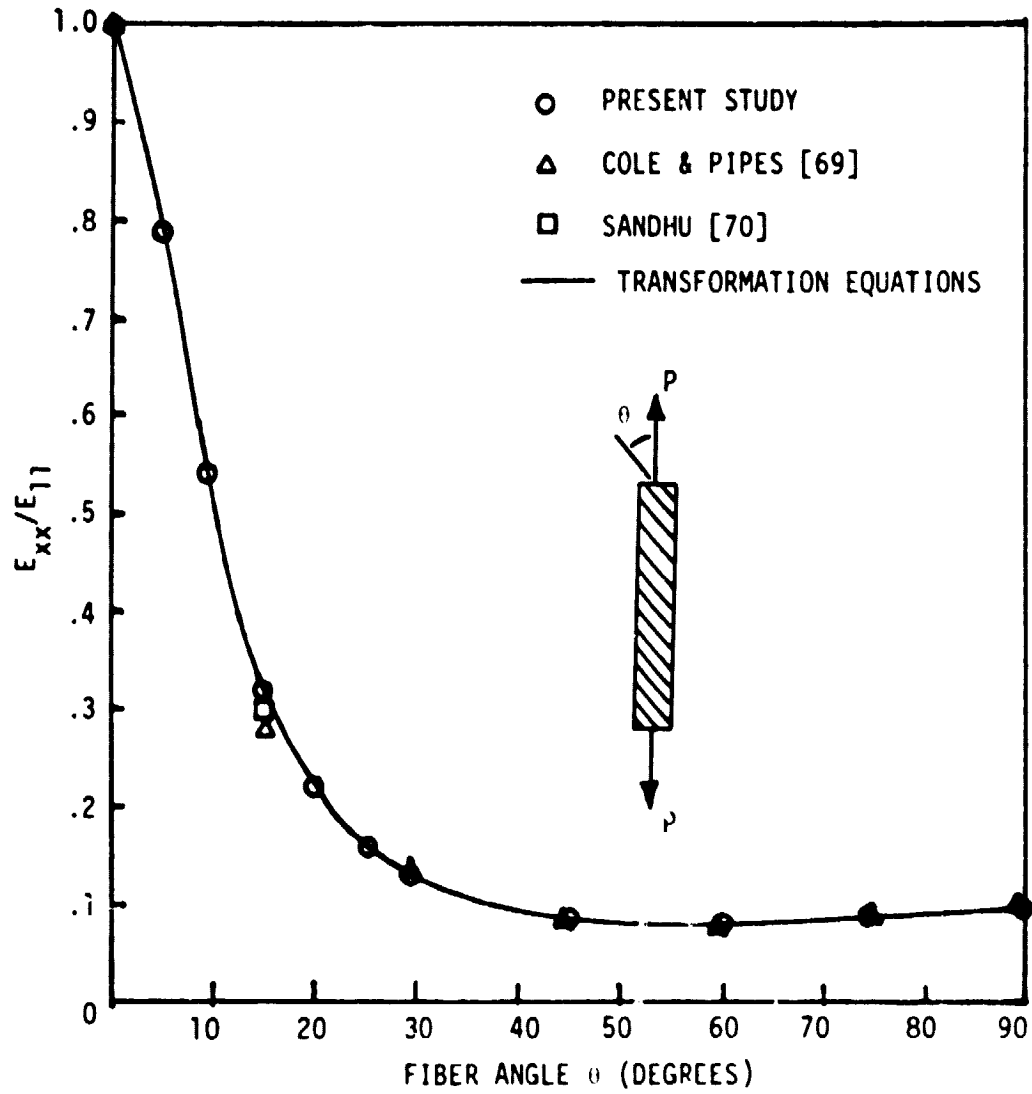(ℓ/h = 23.3, e_x = 0.1)
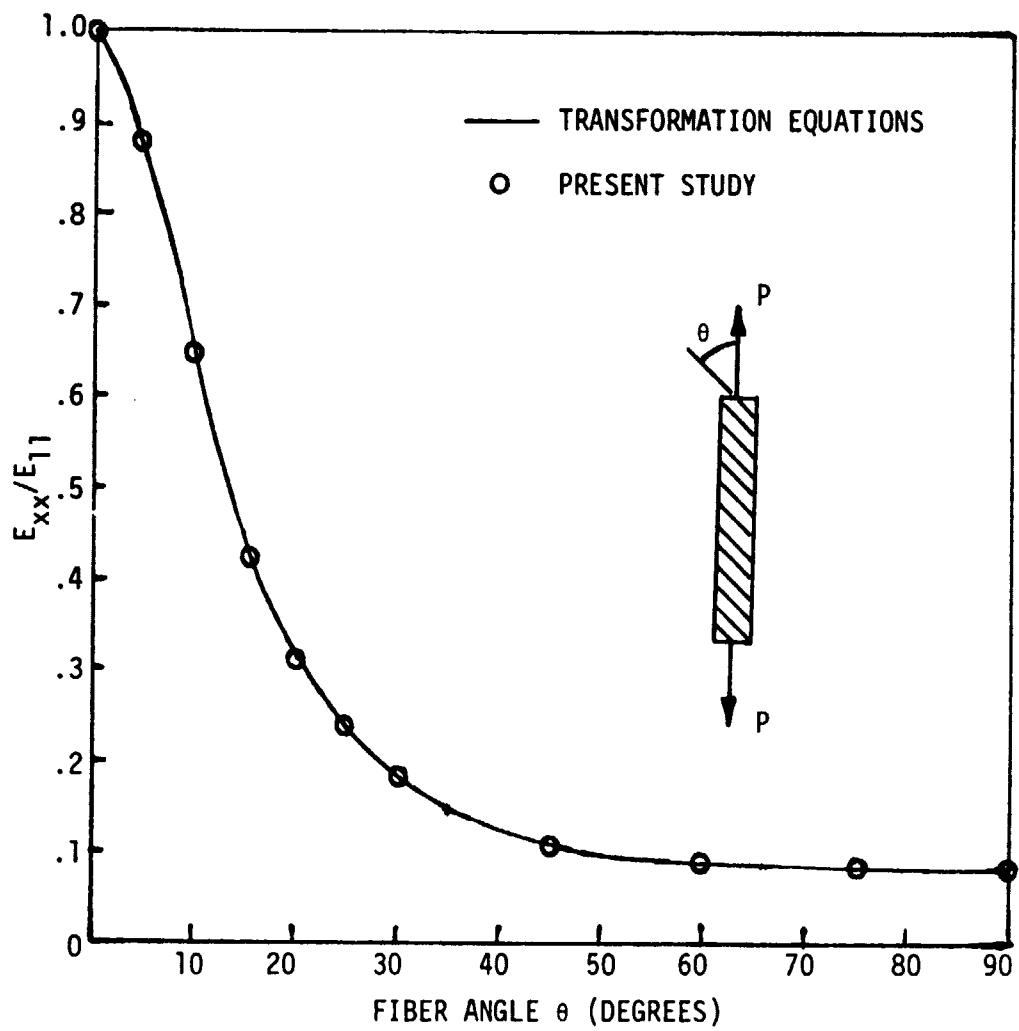
FIGURE 5.7 LOAD DIRECTION MODULUS VS. FIBER ANGLE
FOR OFF-AXIS TENSION OF GRAPHITE/EPOXY
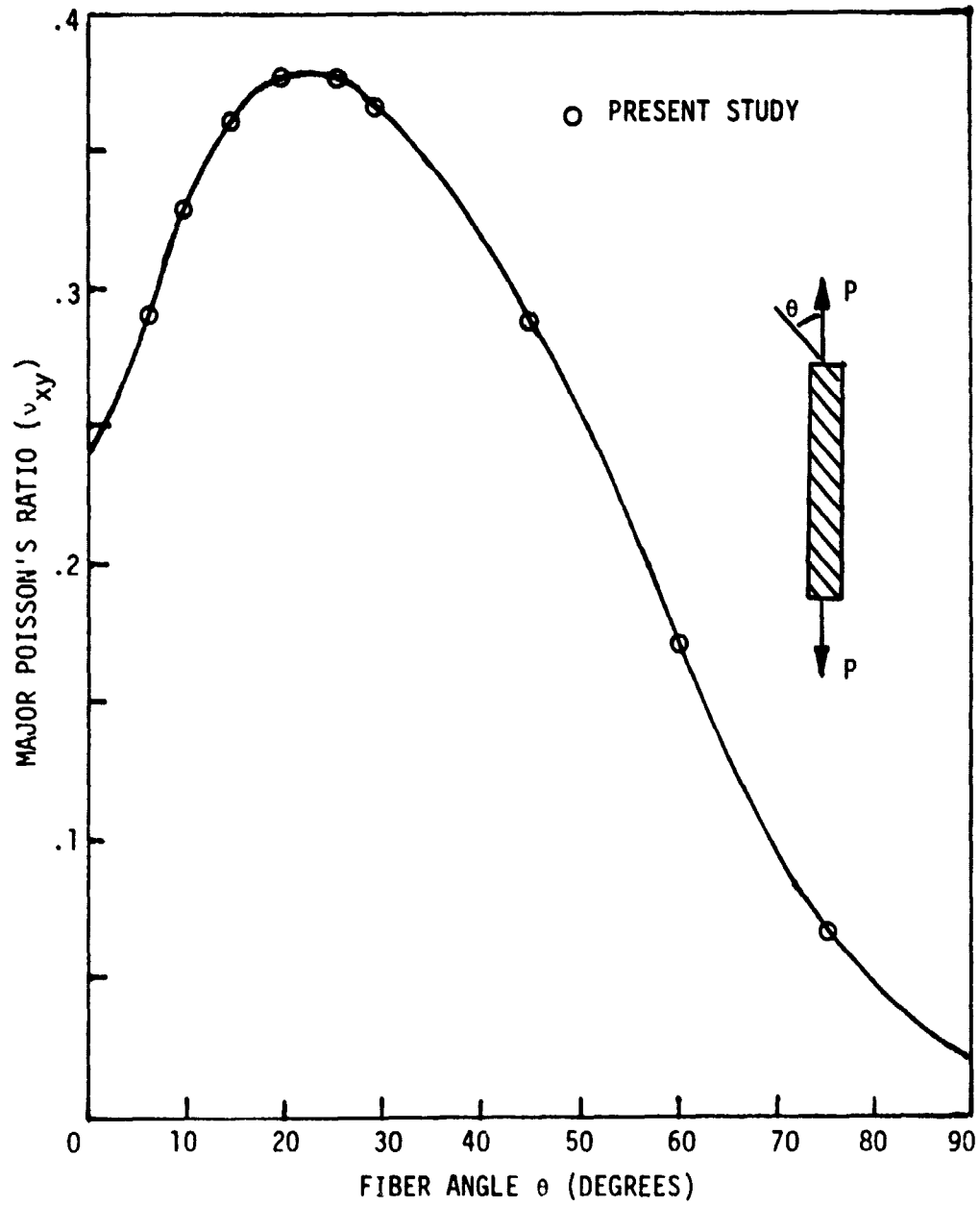
FIGURE 5.8   MAJOR POISSON'S RATIO VS. FIBER ANGLE
FOR OFF-AXIS TENSION OF GRAPHITE/EPOXY

the Boron/Epoxy data are good, with the results of the present study showing better agreement in some areas and worse in others. Note that the present study deviates from experiment primarily when plastic she:r strains are more significant. Plastic shear strains were determined to exist at all angles other than 0° and 90°. However, at 15°, 30°, and 45°, the plastic shear straining was noted to be the dominant plastic strain component. Since agreement between computed and experimental results is good for angles where plastic shearing strain is relatively low and significant differences occur when plastic shear strains are large, one must question either the manner in which plastic shear strains are included or the numerical values which were used as input. It appears that for all angles the plastic strain is initially underestimated, gradually becoming overestimated. The program NALCOM allows a two segement Ramberg-Osgood approximation to the stress-strain data. The method of determination of the coefficients is to plot stress versus plastic strain on a log-log scale and determine the best bilinear or linear fit. The tube torsion data from Tube 111B from Cole and Pipes [69] is plotted in this manner in Figure 5.9. It appears that the data are not well approximated by a bilinear fit. This assures that the model will have difficulty in duplicating the experimental data. Fortunately, a linear or bilinear Ramberg-Osgood fit is sufficient for most engineering materials.

The nonlinear response of Boron/Epoxy off-axis tensile specimens is shown in Figures 5.10-5.15. The results of the present study are
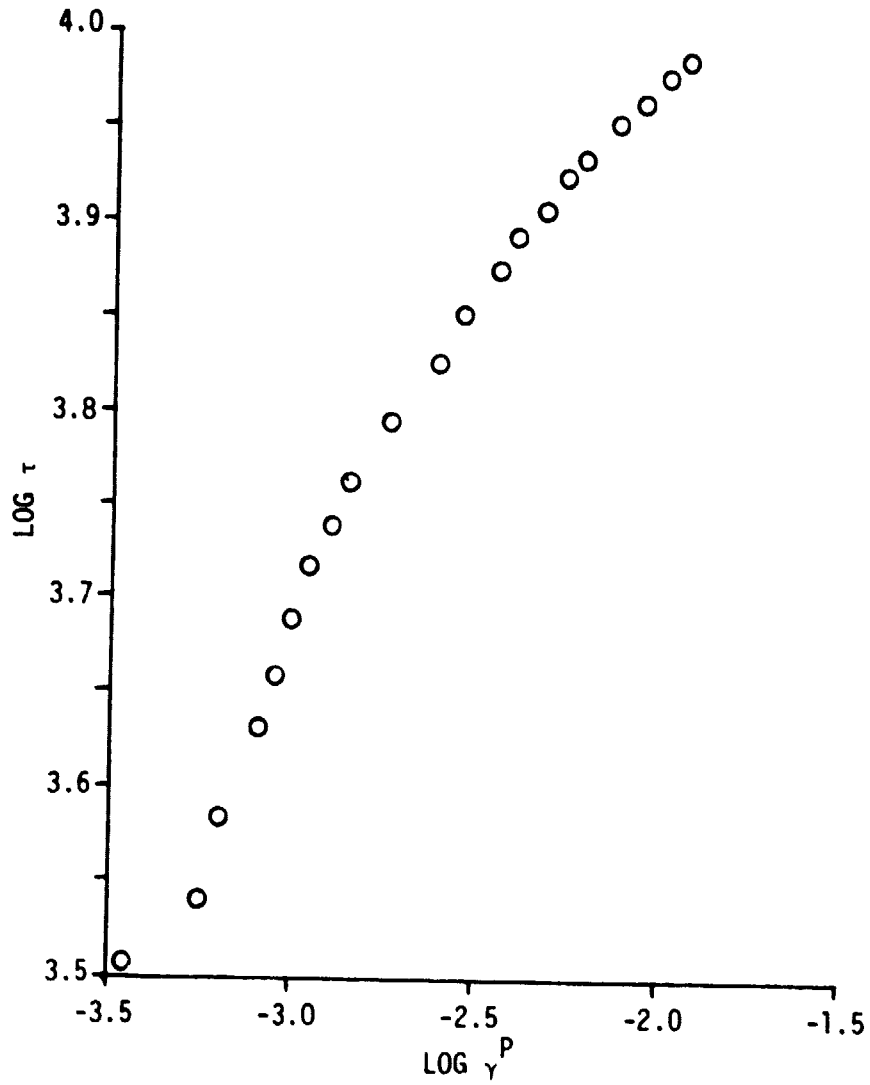
FIGURE 5.9   LOG τ VS. LOG γ^P, BORON/EPOXY

compared to the experimental results of Cole and Pipes [69] for all angles, the experimental results of Sandhu [70] for 15°, the computed results of the model of Hashin [12,13] as programmed by Pindera [72], and a modified form of Hashin's model due to Pindera [72].

The 15° off-axis response of Boron/Epoxy is shown in Figure 5.10. The shearing effects are strong at 15°, and it is believed that this fact in conjunction with the previously mentioned inability to accurately prescribe the shear behavior with a two segment Ramberg-Osgood approximation is at least part of the reason for the difference in computed and experimental results. Also, the Ramberg-Osgood parameters were taken from Cole and Pipes' data, which show considerable variations from one specimen to the next. Recall that the 15° data of Cole and Pipes is suspect, adding additional complication to meaningful comparisons.

The off-axis response of Boron/Epoxy at angles of 30°, 45°, 60°, 75°, and 90° is shown in Figures 5.11, 5.12, 5.13, 5.14 and 5.15, respectively. The comparison at 90° is very good, and the discrepancy at the other angles is again believed due to the poor shear data used as input to NALCOM.

The nonlinear off-axis response of Gr/Ep is shown in Figure 5.16. As with the linear elastic results, no experimental results are available except at 0°, which is linear. The angles 15°-75°, in which plastic shear straining is large (i.e. 15°-45°) show significant nonlinearity and become increasingly linear as the linear behavior of the 90° direction is approached. Note that the response
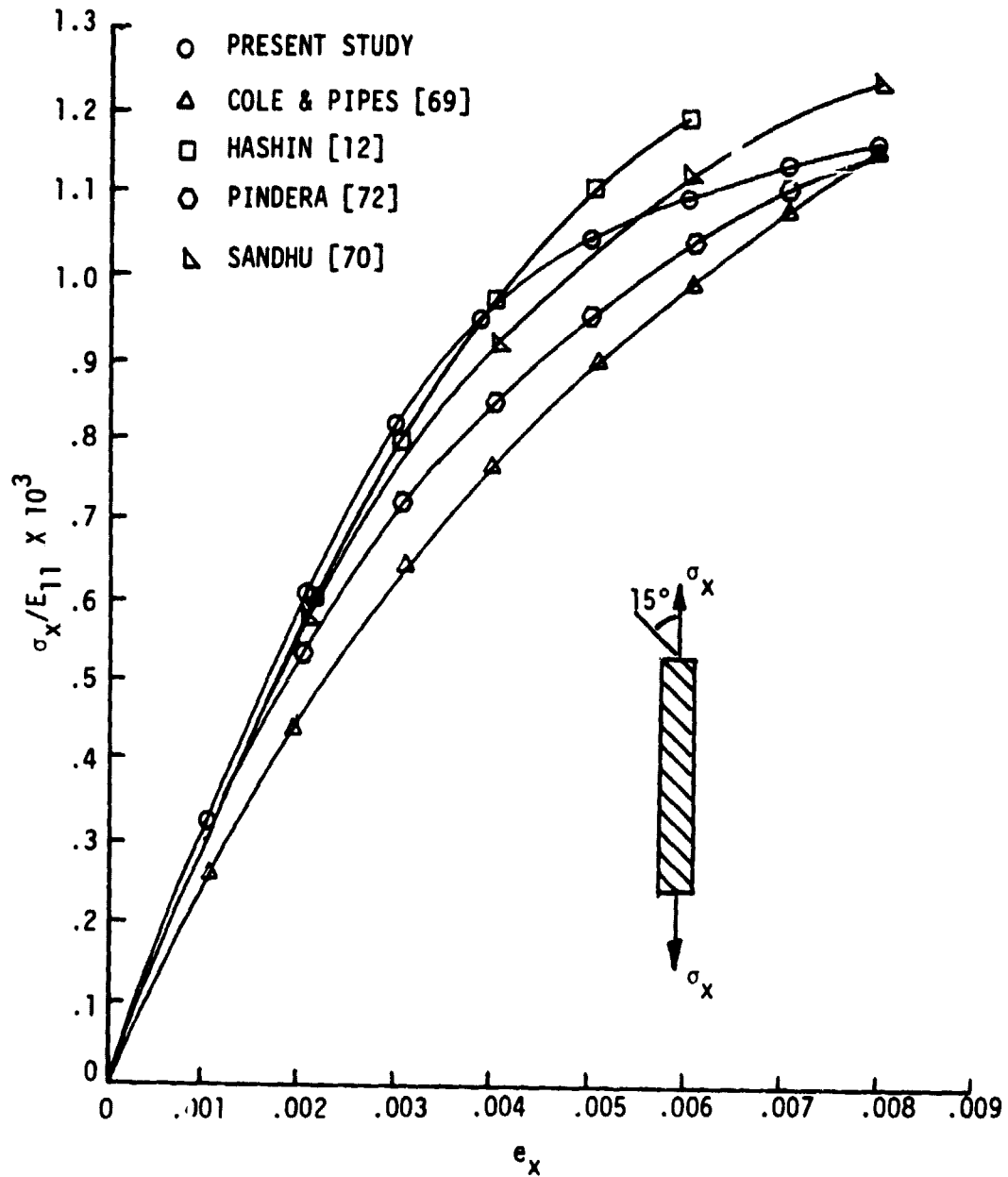
FIGURE 5.10   OFF-AXIS TENSION OF BORON/EPOXY, FIBER ANGLE = 15°
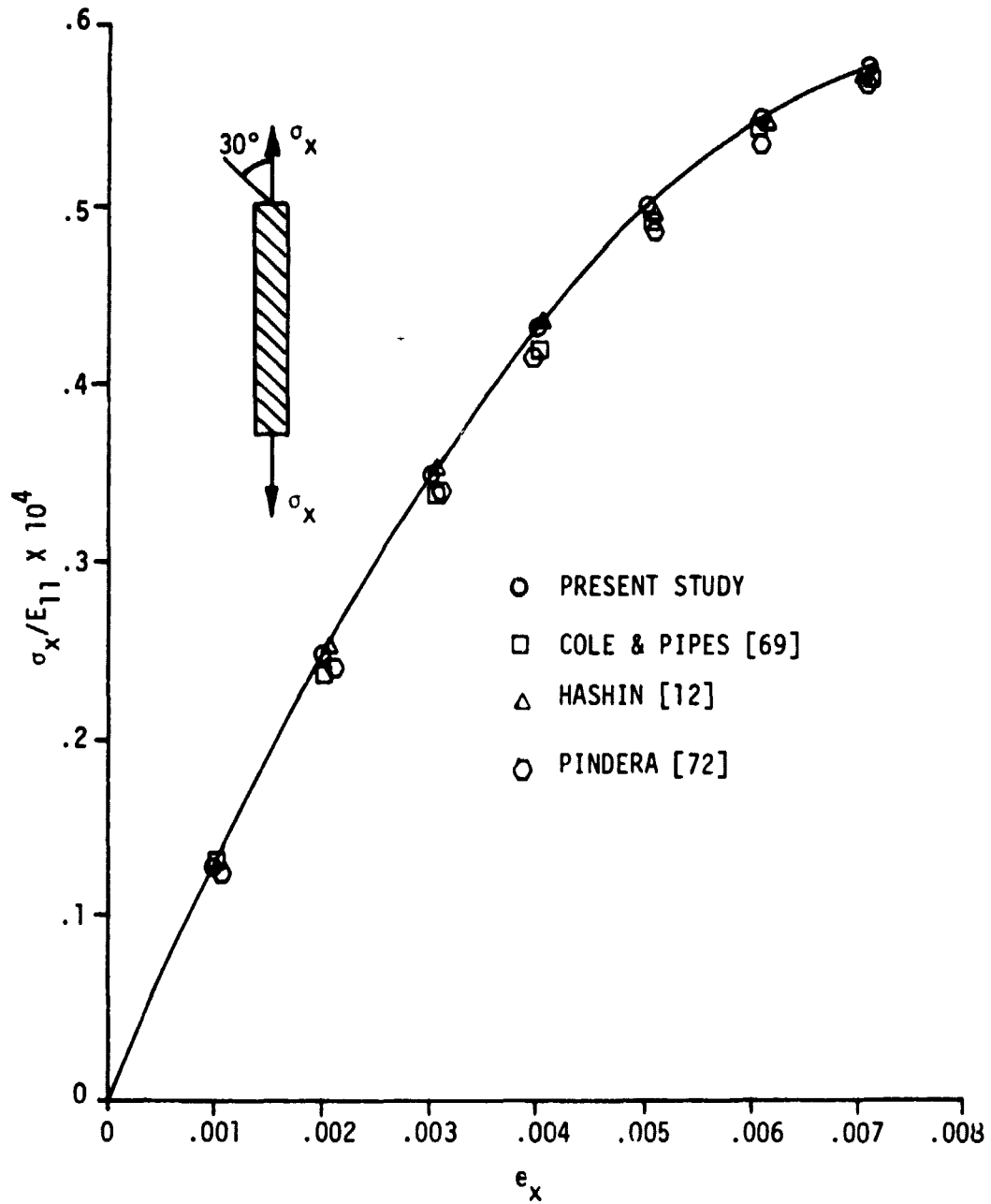
FIGURE 5.11   OFF-AXIS TENSION OF BORON/EPOXY, FIBER ANGLE = 30°
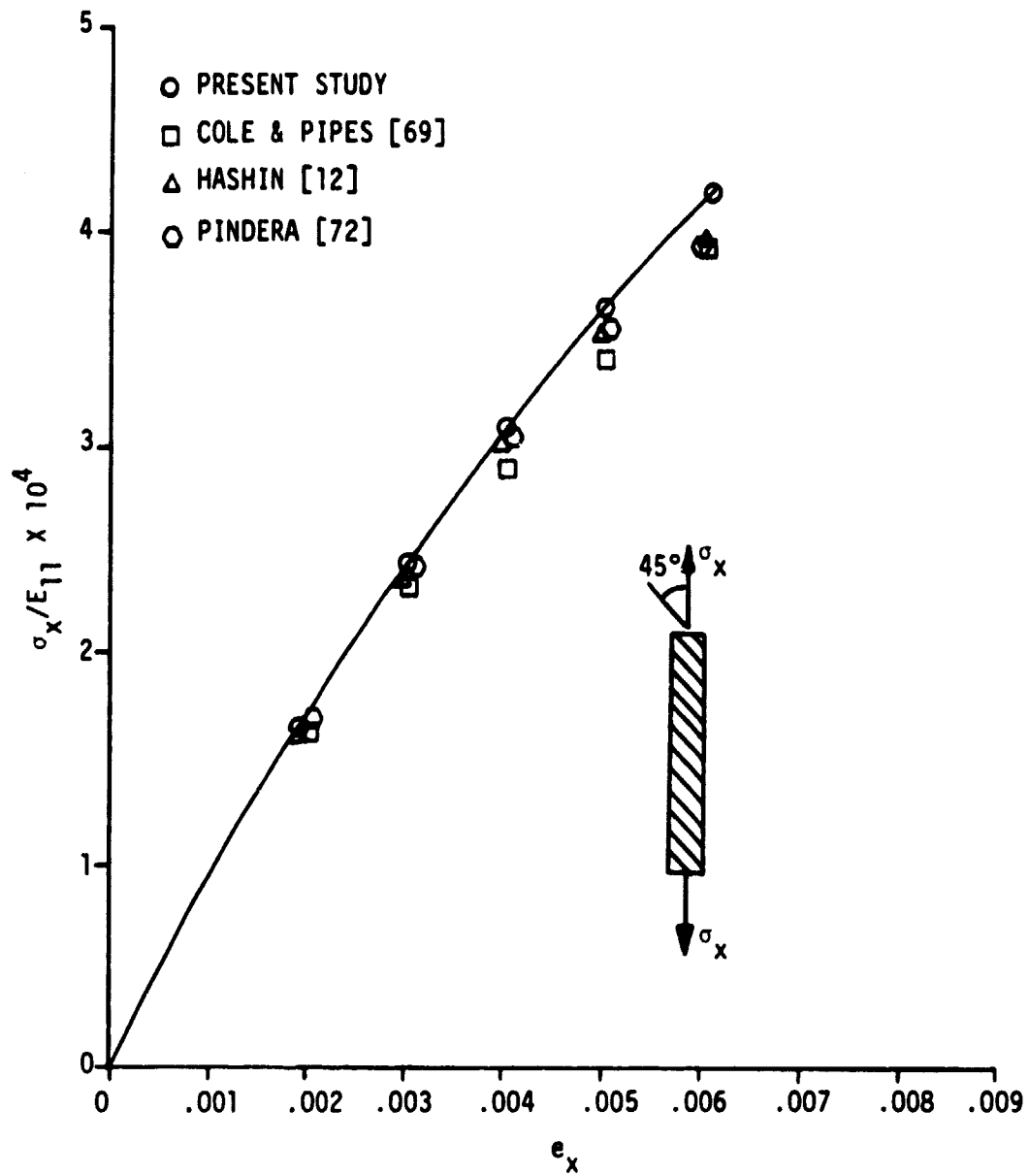
FIGURE 5.12   OFF-AXIS TENSION OF BORON/EPOXY, FIBER ANGLE = 45°
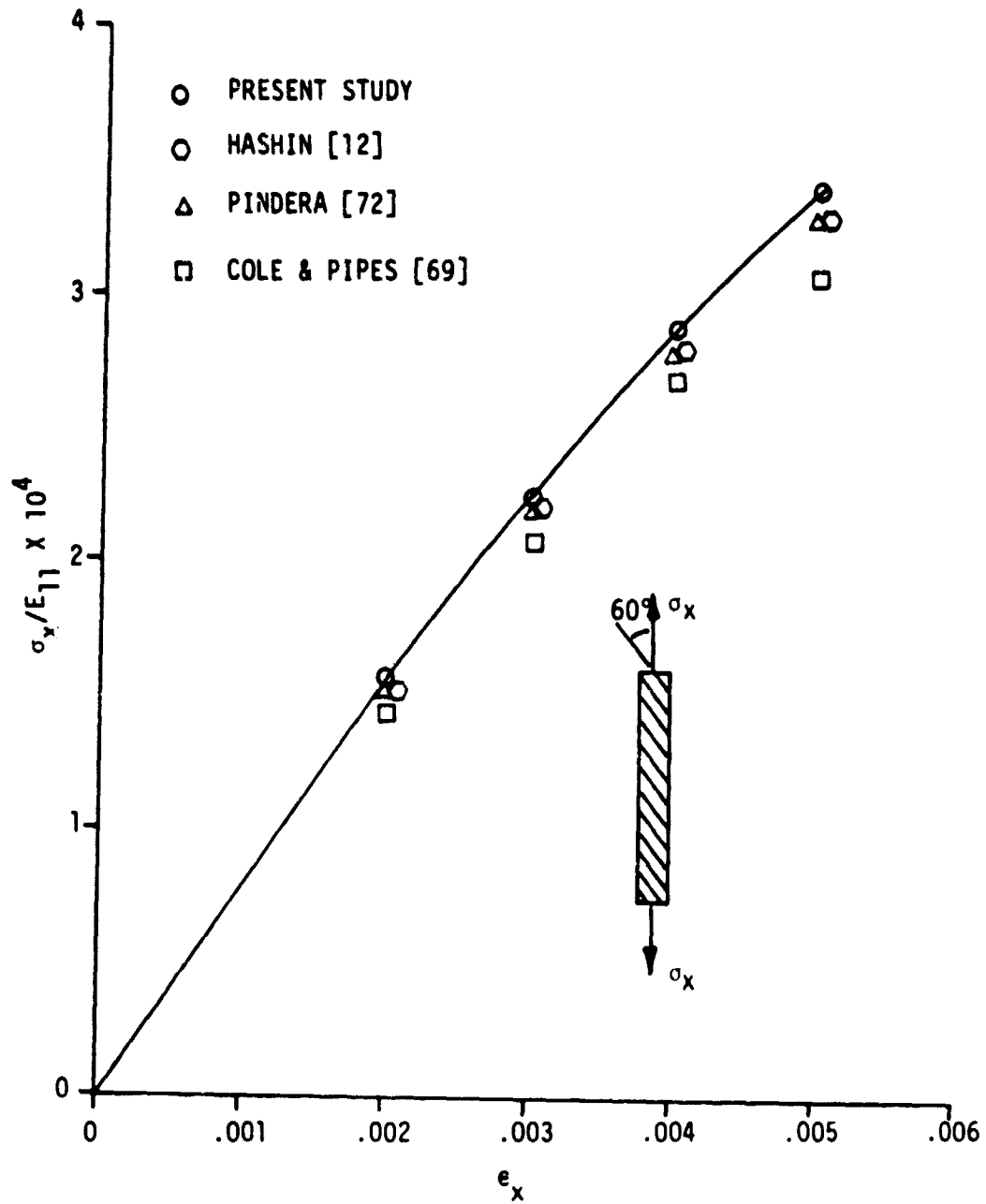
FIGURE 5.13 OFF-AXIS TENSION OF BORON/EPOXY, FIBER ANGLE = 60°
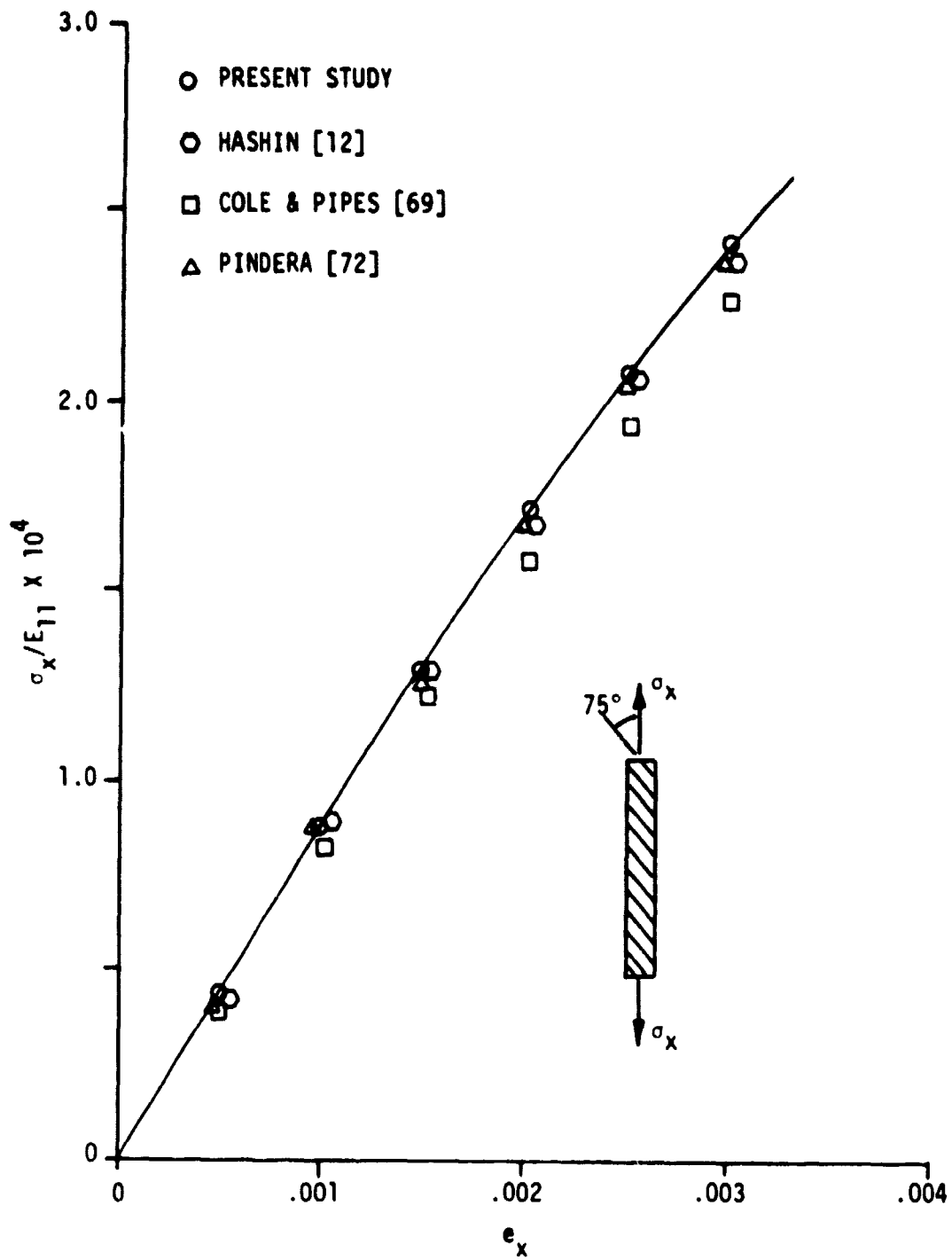
FIGURE 5.14   OFF-AXIS TENSION OF BORON/EPOXY, FIBER ANGLE = 75°
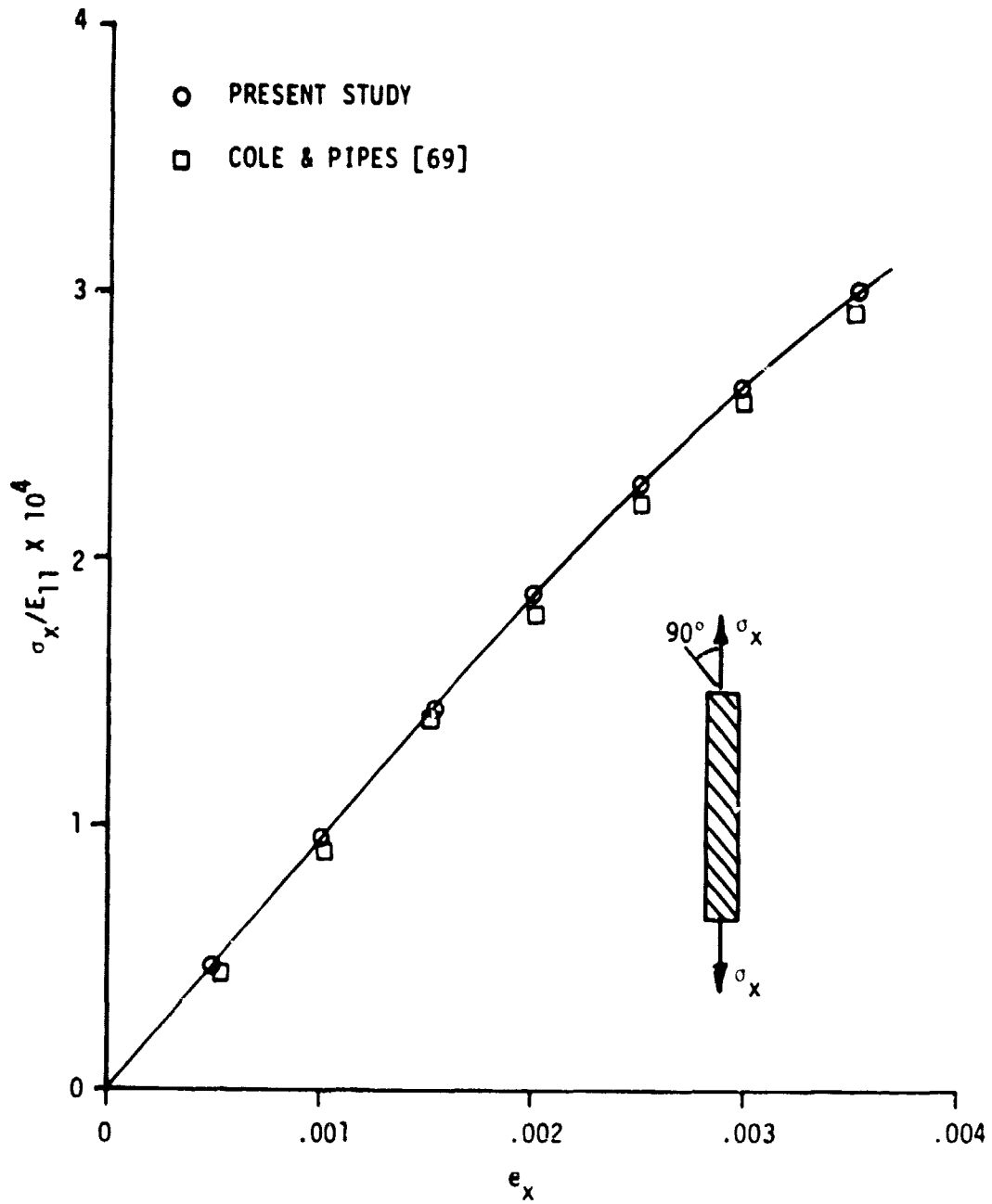
FIGURE 5.15   OFF-AXIS TENSION OF BORON/EPOXY, FIBER ANGLE = 90°

FIGURE 5.16 σ_x VS. e_x FOR OFF-AXIS TENSION OF GRAPHITE/EPOXY
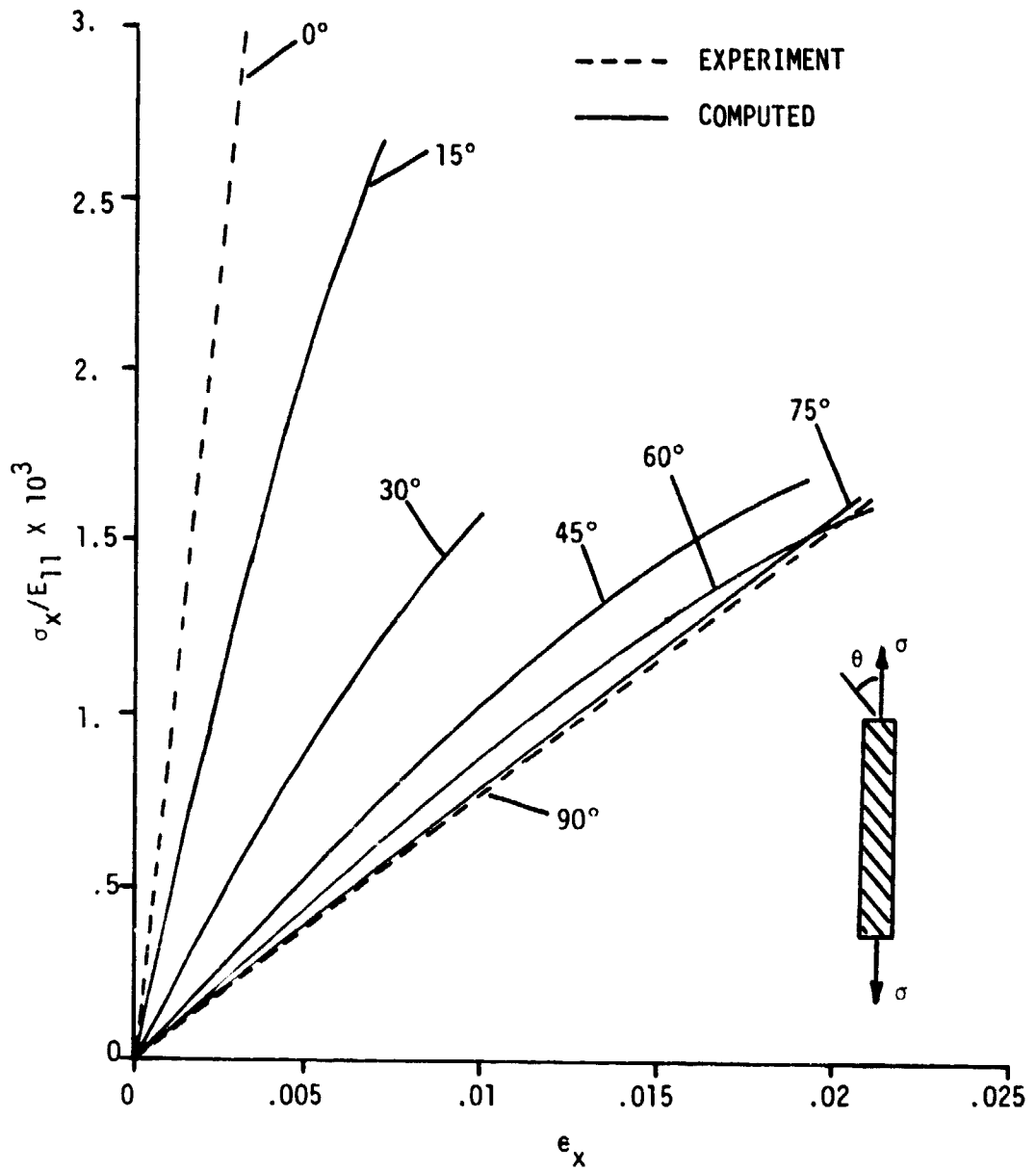
of $\theta = 90°$ is linear to failure.

5.3 Laminate Studies

The final test of the model developed for the present study is to compute the residual stress state resulting from the curing of symmetric composite laminates. Various geometries and material models were considered. Laminates were limited to symmetric layups consisting of two fiber orientations. This limitation was introduced in order to hold the expenditure of computer resources to a reasonable level while considering problems of significance. Comparisons to experimental data and the results of other models are made whenever possible. Such comparisons are often complicated for a variety of reasons. For example, Rybicki and Schmuesser [32], Pagano [6], and Wang and Crossman [16,73] used material models which set all three shear moduli (G_{12}, G_{13}, G_{23}) and all three Poisson's ratios (ν_{23}, ν_{13}, ν_{12}) equal. These assumptions are inconsistent with the theory of elasticity for transversely isotropic materials and also with the material model of NALCOM. In addition, the models of Wang and Crossman [73] and Renieri and Herakovich [40] are quasi-three dimensional, while NALCOM is fully three dimensional. The nonlinear material model used by Herakovich and his associates [40,74,75] is nonlinear elastic, while the material model implemented in NALCOM is based on a plasticity theory. The only other study known to have considered second order thermal effects is that of Hahn and Pagano [15], which was used in conjunction with a lamination theory model and

other simplifying assumptions. Dana [26] and Dana and Barker [27] did not consider thermal effects. In the light of these differences in the models, comparisons are often possible only in a qualitative sense.

The basic laminate geometries for the present study are shown in Figures 5.17 and 5.18. For simplicity, only one-eighth of the laminate is shown. For symmetric cross-ply (i.e. θ =0,90) laminates, there is symmetry about all three coordinate planes, and one eighth of the plate is sufficient for computations, provided that the loads are also symmetric. For symmetric angle ply laminates, there is symmetry only about the x-z plane, so one-half of the laminate must be modeled. As previously stated, three elements are required through the thickness of each fiber orientation. The object of the present study is to examine the stress fields near the edge and end of the solid laminates and near the hole in the laminates with central holes. Accordingly, the finite element grids used for the solid and central hole cross-ply laminates are shown in Figures 5.19 and 5.20, respectively. For accuracy in angle ply laminates, the upper half of the laminates must be modeled. This requirement will be discussed later in more detail.

The one eighth symmetric sections (Figures 5.19 and 5.20) contain six layers of four elements each. More elements in each layer would have yielded better results, but at considerable expense in computer time and storage. Each element contains 32 (4x4x2) Gauss points. The stress is computed at each Gauss point and averaged through the element thickness to obtain through the thickness stress distributions. Of primary concern is σ_z, the interlaminar normal stress.
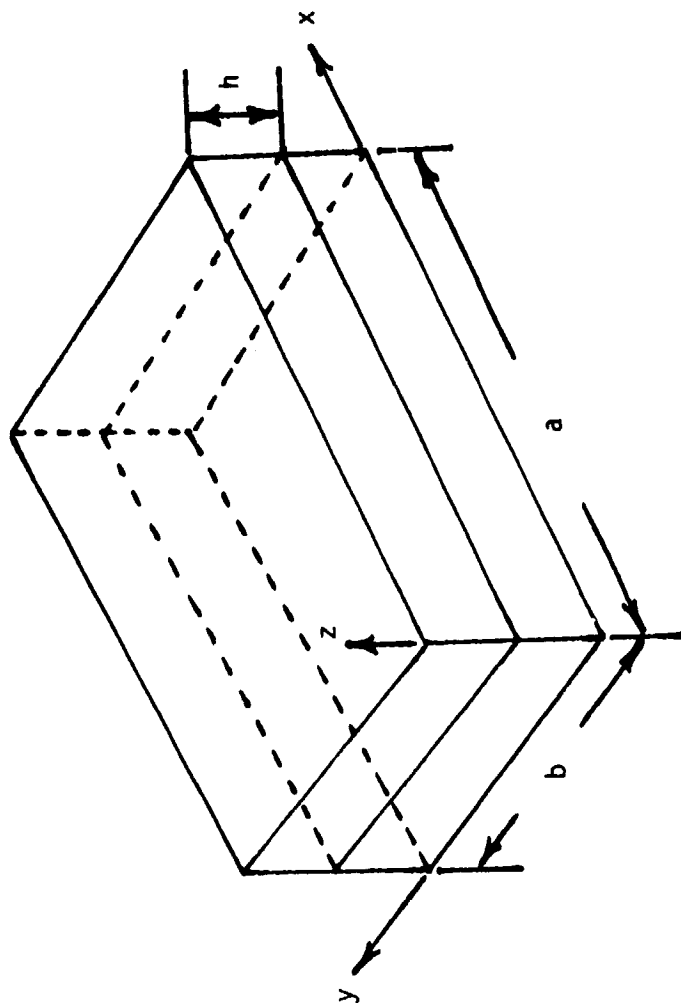
FIGURE 5.17 GEOMETRY OF ONE-EIGHTH OF A SOLID LAMINATE
(b/h = 16, b/a = 1.125)
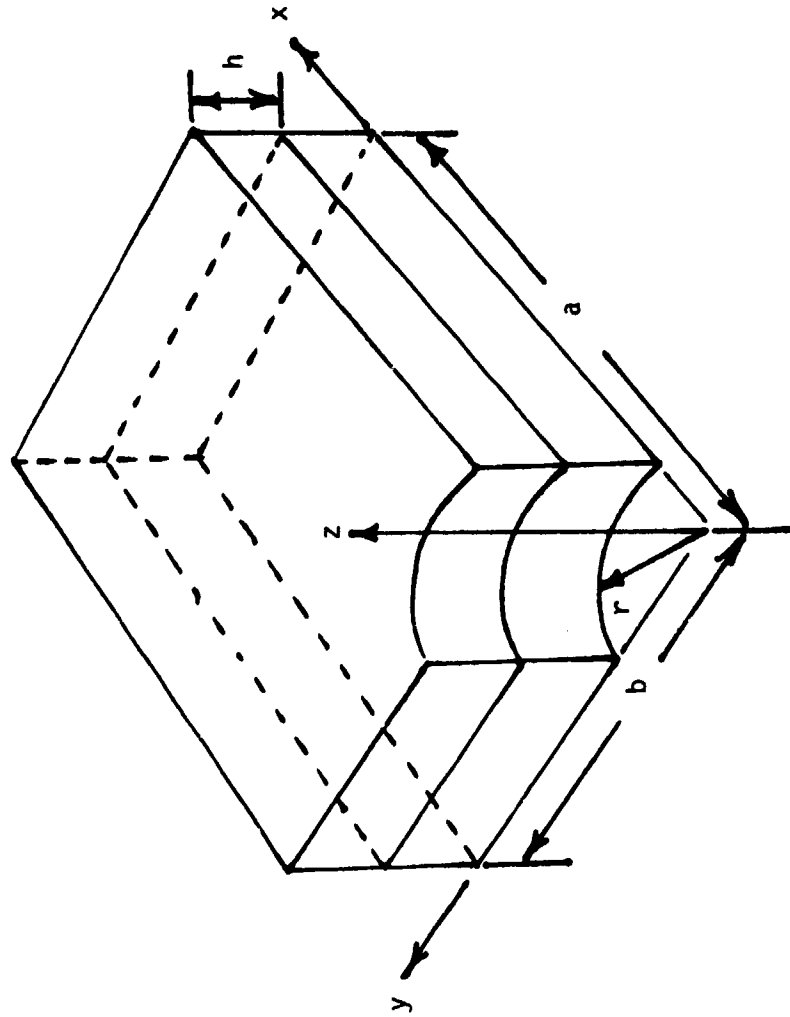
FIGURE 5.18   GEOMETRY OF ONE-EIGHTH OF A LAMINATE WITH CENTRAL HOLE
(b/h = 13.33, b/a = 0.8, r/a = 0.1)
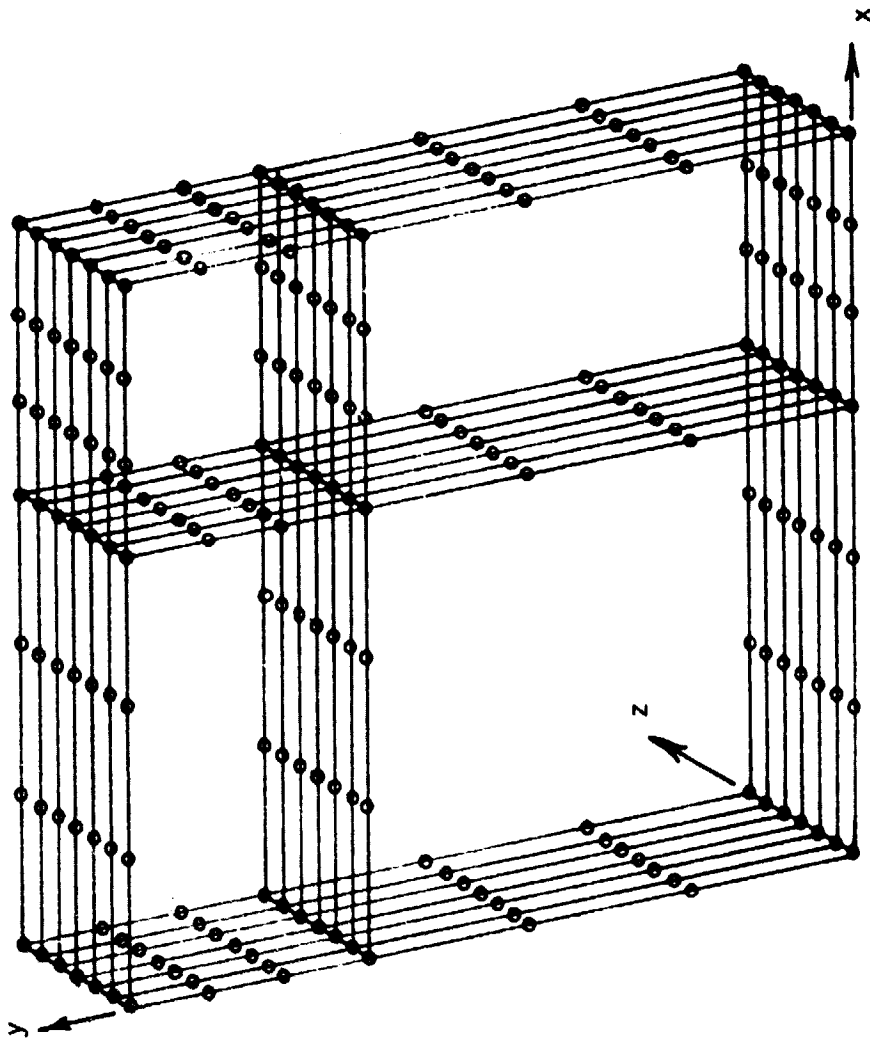
FIGURE 5.19 FINITE ELEMENT GRID FOR LAMINATE EDGE STUDIES
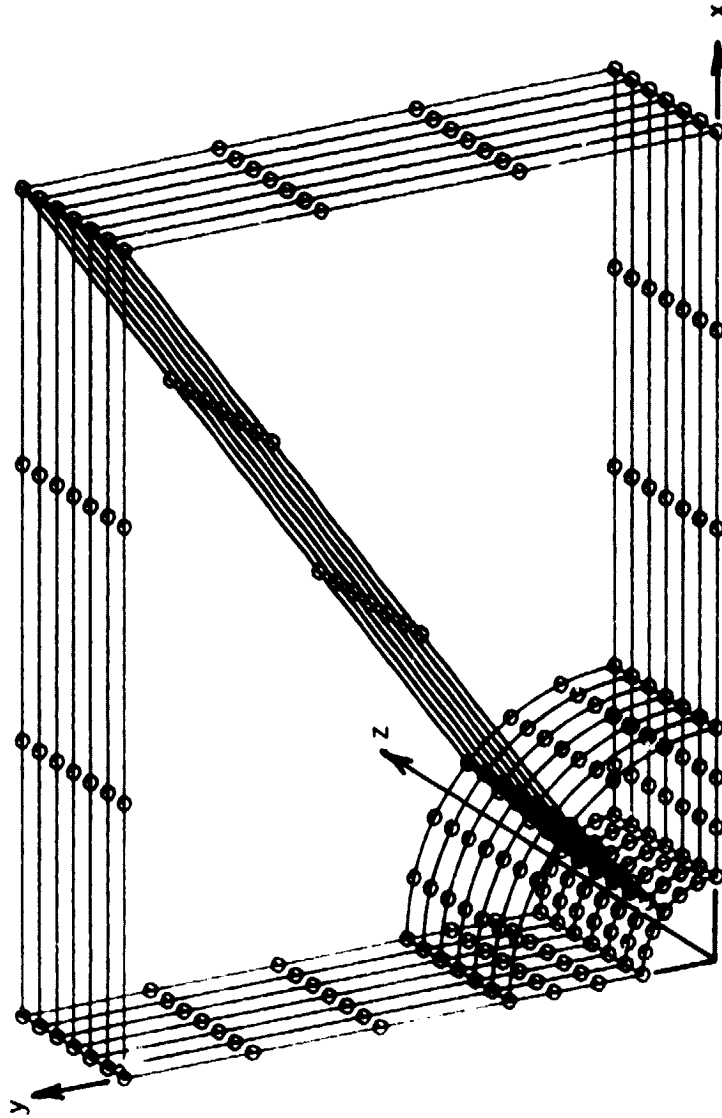
FIGURE 5.20 FINITE ELEMENT GRID FOR LAMINATE WITH CIRCULAR HOLE

Results are computed for both linear elastic and elastic-plastic

material models with constant, first order nonlinear, and second

order nonlinear thermal behavior. The following paragraphs detail

these analyses.

5.3.1 Uniform $[0/90]_s$ Laminate Studies

   5.3.1.1 Strain Loading

As a first comparison to other models, a $[0/90]_s$ boron/epoxy

laminate was subjected to a uniaxial strain loading. Figures 5.21

and 5.22 show the comparison of results of the present study with the

results of Pagano [6] and Wang and Crossman [73]. Note that the

comparison is excellent. The material model of NALCOM was modified

to conform to the simplified model of the other investigators for

this comparison.

   5.3.1.2 Thermal Loading

The next problems of concern were the linear elastic cooling from

the elevated curing temperature to room temperature followed by

imposition of mechanical load. For these analyses, the three thermal

effect options (i.e constant properties, first order nonlinear and

second order nonlinear) were considered. The finite element grid of

Figure 5.19 was subjected to temperature changes totaling -180°F,

in one step for the constant property case, using average properties

over the range, and in nine steps of -20°F each for the nonlinear

cases. The material for these analyses was T300/5208 graphite/epoxy.

The material properties used are given in Table 5.3. As previously

stated, the interlaminar stresses are of primary concern for this study.
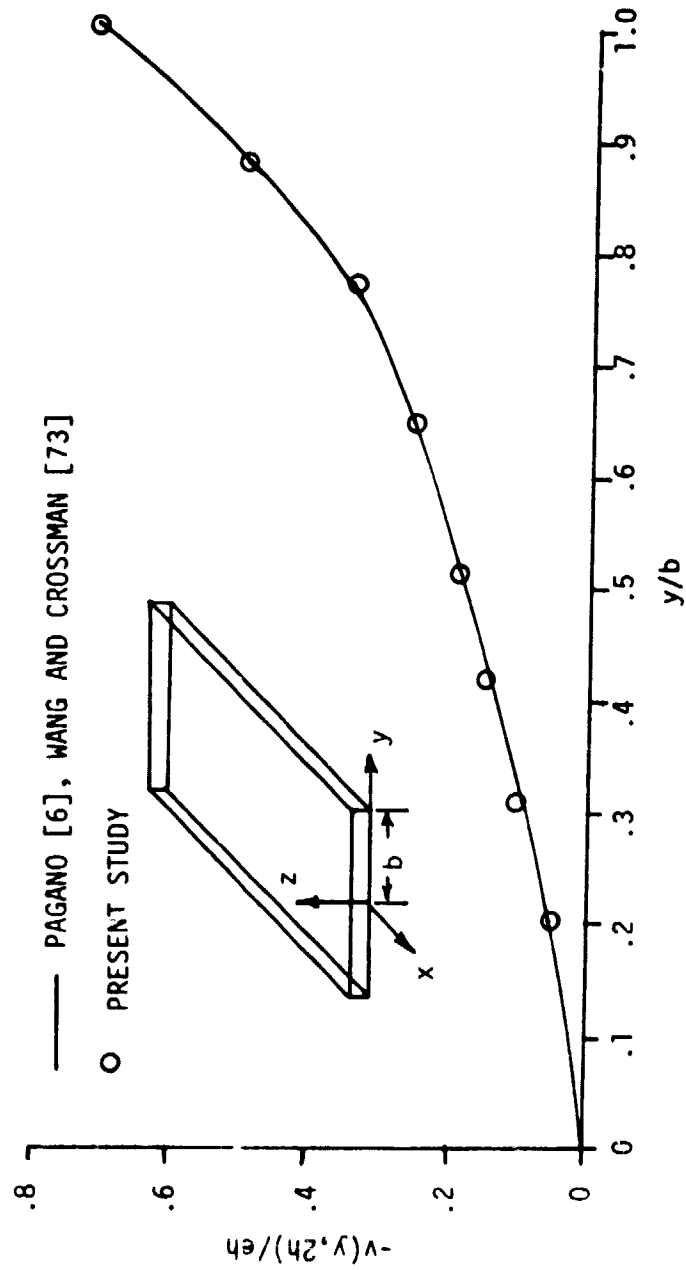
FIGURE 5.21 TRANSVERSE DISPLACEMENT ACROSS TOP SURFACE (z = 2h), $[0/90]_s$ B/Ep LAMINATE, $e_x = 10^{-6}$
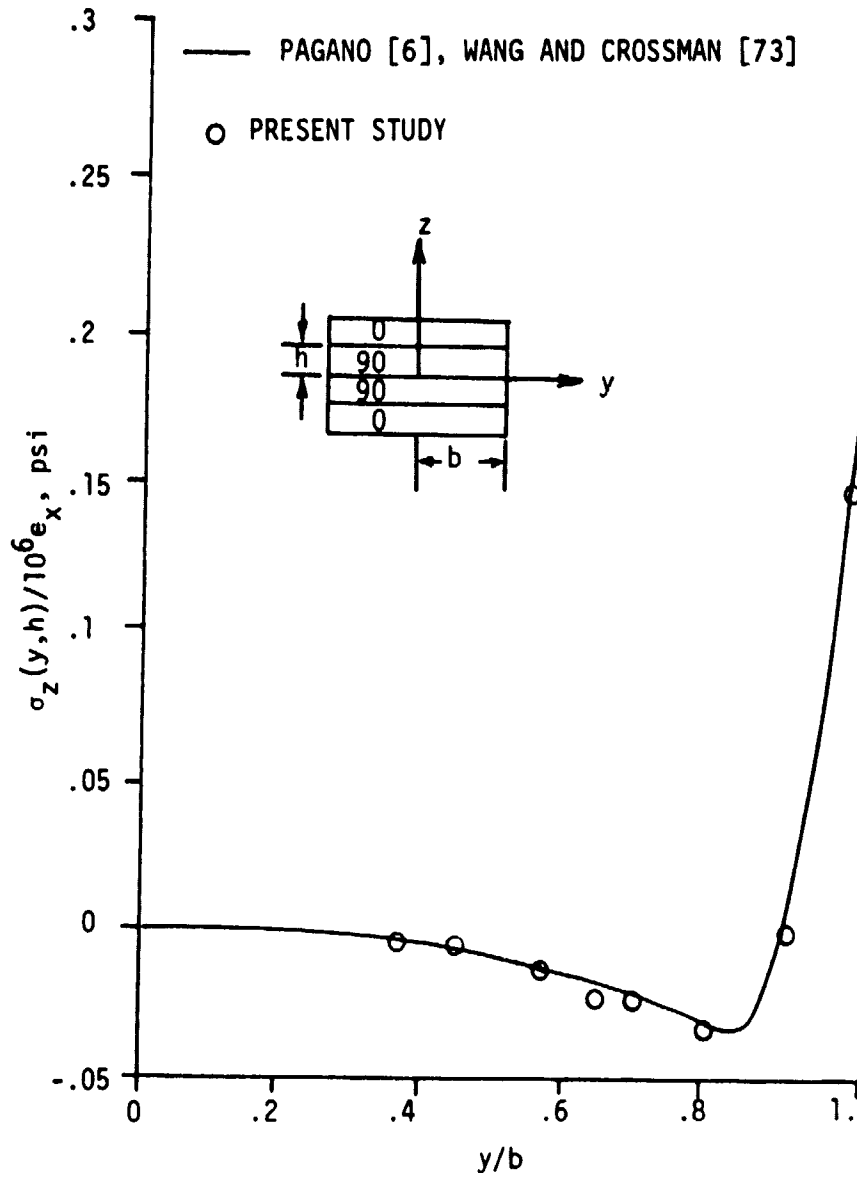
FIGURE 5.22 σ_z ACROSS 0/90 INTERFACE, $[0/90]_s$ B/Ep LAMINATE, $e_x^z = 10^{-6}$

TABLE 5.3.   ELEVATED TEMPERATURE PROPERTIES OF T300/5208 GRAPHITE/EPOXY

Ramberg-Osgood Coefficients

Direction	Temp (°F)	B_1	n_1	σ^e(ksi)	B_2	n_2	σ^*
1	70	$.30754 \times 10^{-15}$	2.0369	87000	--	--	--
2	70	$.13324 \times 10^{-7}$	1.0681	6300	--	--	--
12	70	$.44882 \times 10^{-7}$	1.1471	2100	$.10953 \times 10^{-15}$	3.3985	3975.7
1	260	$.30754 \times 10^{-13}$	2.0369	82000	--	--	--
2	260	$.13324 \times 10^{-7}$	1.0681	6000	--	--	--
12	260	$.44882 \times 10^{-7}$	1.1471	1800	$.10953 \times 10^{-15}$	3.3985	3975.7

Thermal Expansion Coefficients

Temp	α_1(μin/in/°F)	α_2(μin/in/°F)
70	.193	13.8
120	.193	13.8
121	.226	13.8
350	.226	13.8

Fraction Retention of Room Temperature Property

Temp	E_1/E_1 R.T.	E_2/E_2 R.T.	G_{12}/G_{12} R.T.	ν_{12}/ν_{12} R.T.	ν_{23}/ν_{23} R.T.
70	1.	1.	1.	1.	1.
260	1.	.934	.962	.8	.8
350	1.	.793	.854	.75	.75

Figure 5.23 shows residual interlaminar normal (σ_z) stress vs. y/b near the midplane (z/2h = 0.035) of a [0/90]$_s$ laminate of Graphite/Epoxy. Unless otherwise stated, all laminate analyses were performed for T300/5208 graphite/epoxy. Figure 5.23 shows the effect of the three thermal models. The effects are small, amounting to maximum differences of approximately 10%. Note that in the region away from the boundary layer (y/b < 0.6) the lamination theory solution $(\sigma_z = 0)$ is recovered exactly. An earlier version of NALCOM with no equilibrium iteration did not recover the lamination theory solution at y/b = 0. The curves of 5.23 were generated using the elastic-plastic analysis of NALCOM. The maximum value of Hill's yield function at z/2h = 0.035 was 0.419. This occurred in the region where the end boundary layer interacts with the edge boundary layer (x/a = 0.65, y/b = 0.89). At this point it should be emphasized that the three dimensional analysis shows the existence of the end (x/a = 1) boundary layer as well as the edge (y/b = 1) boundary layer normally discussed by investigators using two-dimensional or quasi three-dimensional models. The boundary layers interact at corners (x/a > 0.6, y/b > 0.6), often with surprising results, which are dependent on through the thickness location and the laminate layup. For linear elastic models, the interaction is basically a superposition, but the introduction of a yield condition and flow rule results in a considerably more complex situation.

Figure 5.24 shows residual σ_z vs y/b at x/a = 0.093 at the 0/90° interface for the [0/90]$_s$ Gr/Ep laminate. The difference between
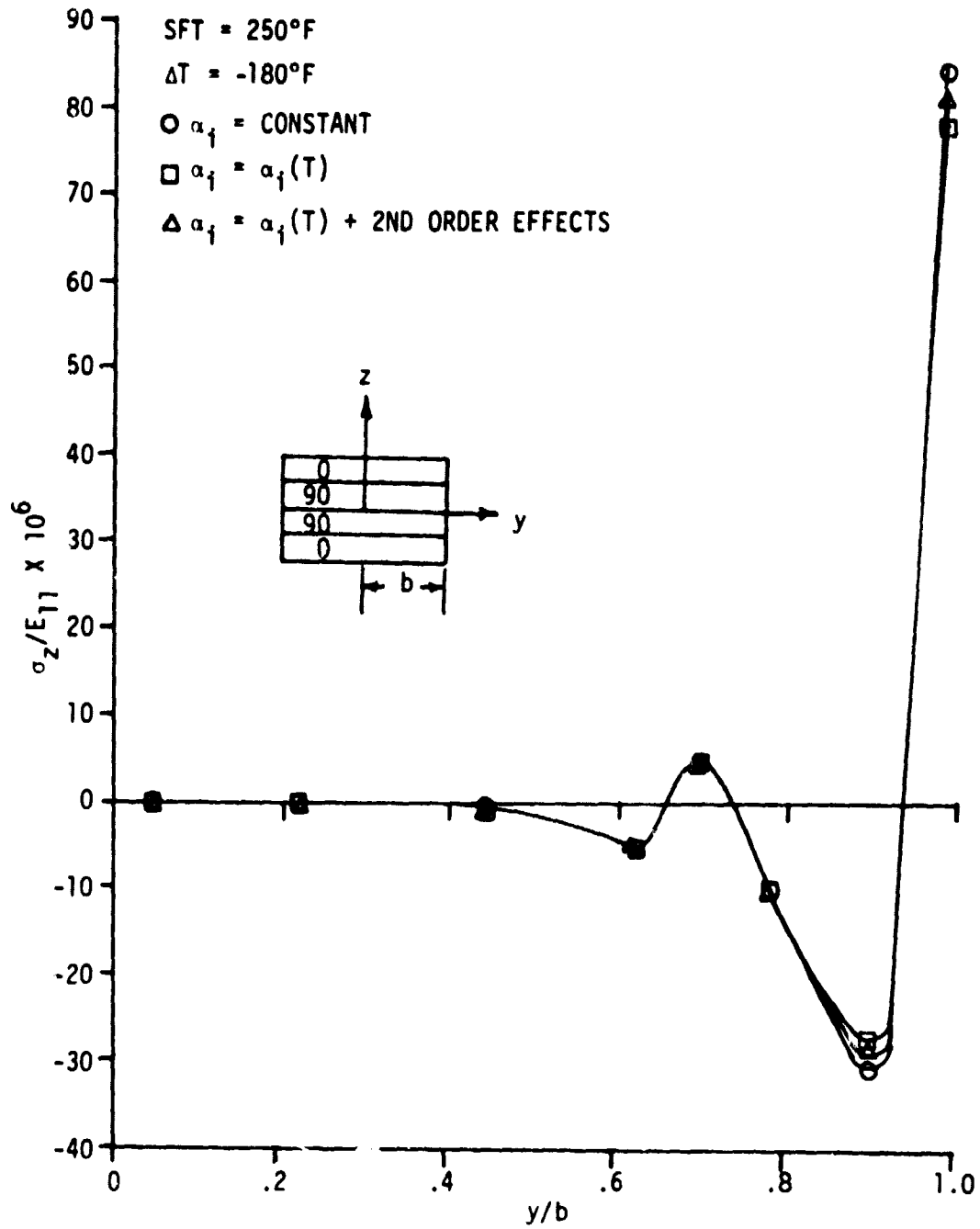
FIGURE 5.23 σ_z VS. y/b NEAR MIDPLANE OF $[0/90]_s$ Gr/Ep LAMINATE
(z/2h = .035, x/a = .043)
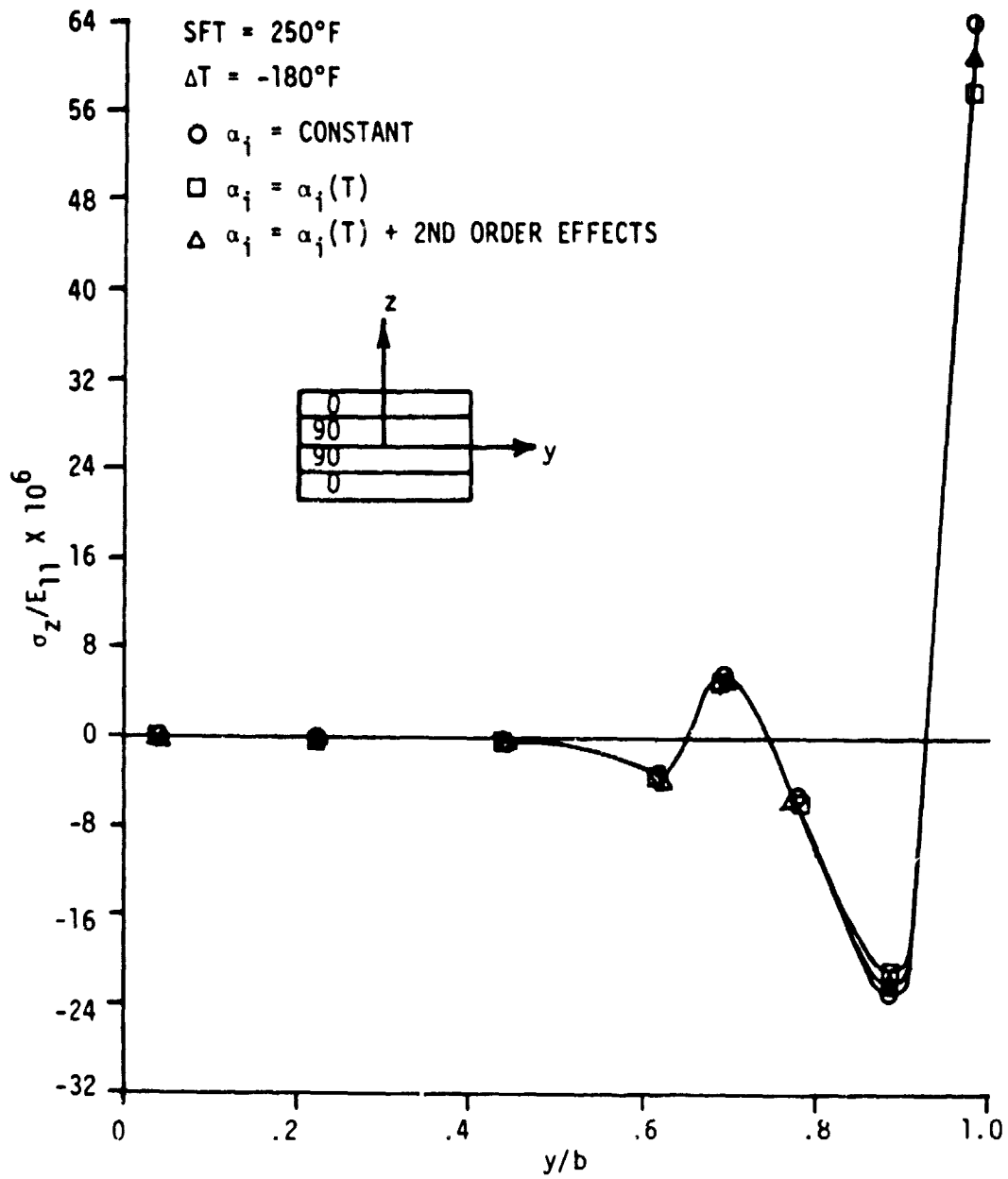
FIGURE 5.24 σ_z VS. y/b AT 0/90 INTERFACE, $[0/90]_s$ Gr/Ep LAMINATE

the different thermal models is again approximately ten percent. The lamination theory solution of σ_z = 0 is again satisfied for y/b < 0.6. As before, previous results with no equilibrium iteration did not satisfy this condition. Thermal loading was accomplished incrementally, and equilibrium was normally achieved in one to two iterations at each increment. Yielding of the material on both sides of the 0/90 interface was predicted. The amount of plastic deformation was small, and stress differentials between elastic and elastic-plastic models is thus small. Yielding occurred near the corner (x/a = 1, y/b = 1) of the laminate, with yielding being more pronounced in the top (0°) layer. The reason for yielding at the 0/90 interface when none occurred at the midplane is the thermal expansion mismatch of the 0° and 90° directions, resulting in large axial (σ_x) and transverse (σ_y) stresses near the corner. Since yielding depends on absolute value of stress, even though the algebraic sign of σ_x and σ_y are different, the combination results in yielding. Values of interlaminar shear stress (τ_{xz} and τ_{yz}) are also large near the corner. This is a good example of how a three-dimensional analysis reveals phenomena not treated by two dimensional models. No yielding was predicted for x/a ≈ 0 (corresponding to a 2-D analysis of [0/90]$_s$) or y/b ≈ 0 (corresponding to a 2-D analysis of [90/0]$_s$), but the interaction was sufficient to result in yielding. Yielding occurred in the -20°F thermal increment from 90°F to 70°F.

Figure 5.25 shows the variation of σ_z through the laminate thickness near the edge (y/b = 0.977) and away from the end

C-2
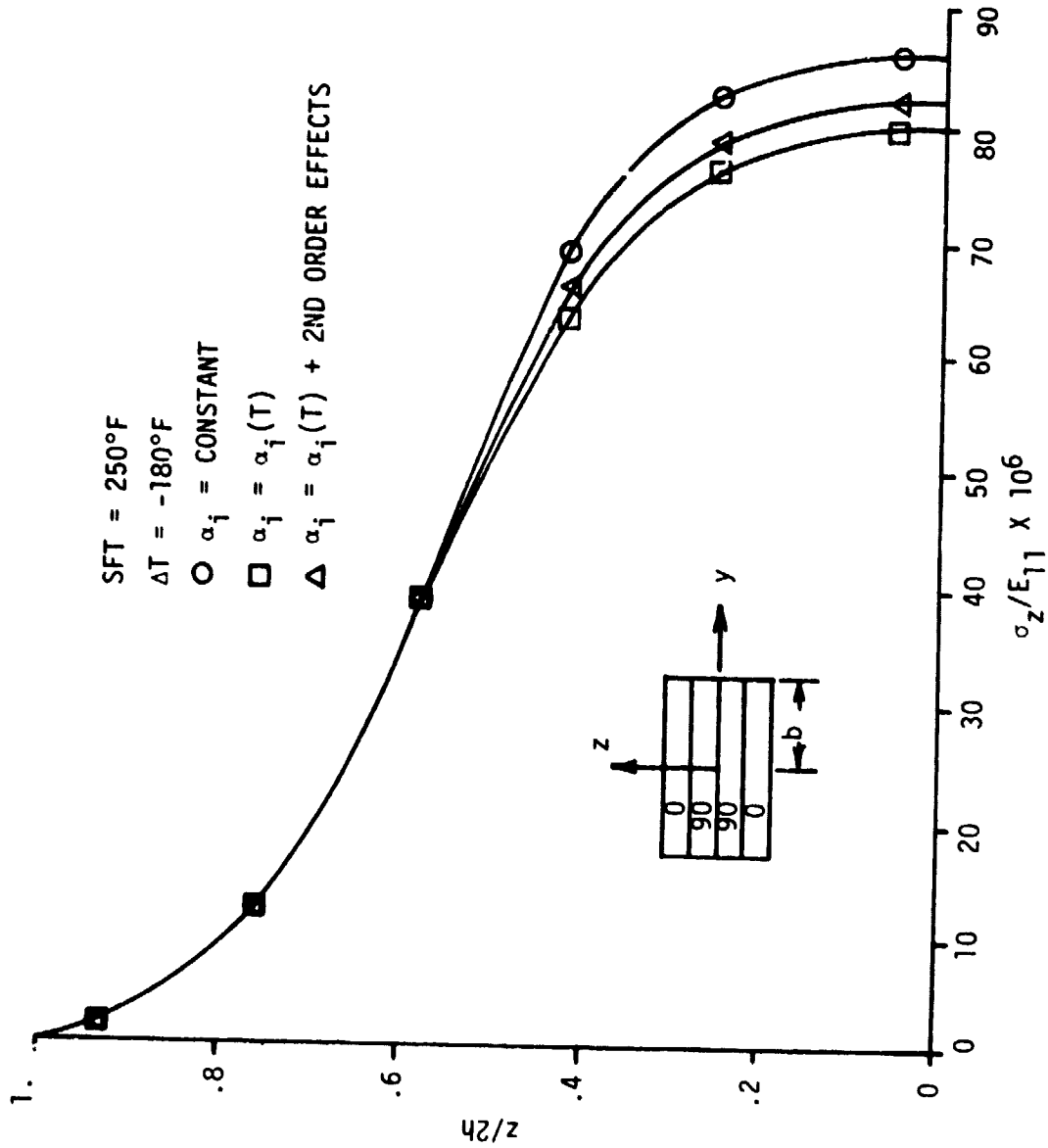
FIGURE 5.25 σ_z VS. z/2h, [0/90]$_s$ Gr/Ep LAMINATE (y/b = .977, x/a = .043)

(x/a = 0.043). The effect of the different thermal analyses is more pronounced near the midplane, with little difference in the upper (0°) layer. All models converge to the equilibrium solution (σ_z = 0) at the top surface (z/2h = 1.).

Several comments concerning the laminate analyses may be made. The addition of second order nonlinear thermal effects was found to have the effect of reducing the axial (σ_x) stress near the origin (x/a = y/b = 0), as predicted by Hahn and Pagano [15]. This effect cannot be ignored, especially in the investigation of elastic-plastic interlaminar effects. When yielding is imminent, even small changes in stress become significant.

5.3.1.3 Combined Mechanical and Thermal Loading

All thermal cooling (ΔT = -180°F) was followed by the application of a uniform x-direction traction (σ_x) of 1000 psi. Although the magnitude of the load was small, the effects are significant. All the Gauss points near the free corner which were exhibiting plastic behavior started to unload in the plastic sense. This is easily explained if we consider that certain of the stress terms exhibit reversal in algebraic sign when going from thermal cooling to x-direction extension. Had the x-direction traction been continued, yielding would undoubtedly have been resumed, although not necessarily in the same location. Again, the three-dimensional effect of the free corner must be considered. The two dimensional and quasi three dimensional analyses of previous investigators is valid away from three dimensional effects of ends and holes, but one must realize the

limitations. Also, one must be aware that intuition gained from examin-
ation of two dimensional analyses may not extend to three dimensional
problems, and may actually be misleading if used in attempts to predict
three dimensional effects.

5.3.2 Uniform $[\pm\theta]_s$ Laminates

Also of concern is the response of symmetric angle ply laminates.
Previous investigators [26,32,40] have analyzed $[\pm\theta]_s$ configurations
($\theta \neq 0,90$) assuming varying degrees of symmetry. With the exception of
Dana, et al [26,27], no consideration seems to have been given to the
question of symmetry. In order for symmetry to exist about a plane,
all nodal points originally on the plane must undergo displacements only
in that plane. A symmetry plane may be thought of as a mirror, where
all quantities (material properties, displacements, loads, stresses)
must be mirrored by the plane. If we consider a $[\pm\theta]_s$ laminate,
$\theta \neq 0°,90°$, the only symmetry which exists is across the midplane (Z=0).

The symmetry conditions for a long laminate advanced by Hsu and
Herakovich [8] are

$$u(x,y,z) = u(x,y,-z) \tag{5.1a}$$

$$v(x,y,z) = v(x,y,-z) \tag{5.1b}$$

$$w(x,y,z) = -w(x,y,-z) \tag{5.1c}$$

$$v(x,y,z) = -v(x,-y,z) \tag{5.1d}$$

$$w(x,y,z) = w(x,-y,z) \tag{5.1e}$$

plus an experimentally verified condition [8] that

$$u(0,y,h) = -u(0,-y,h) \tag{5.2}$$

where Z=h is the top surface. The condition (5.2) is generalized to

$$u(0,y,z) = -u(0,-y,z). \qquad (5.3)$$

NALCOM was used to model the top half of a $[\pm 45]_s$ laminate, with one element being used for each quadrant of the laminate, and six elements through the thickness as before. The load was a uniform x-direction extension of $\varepsilon_x = 0.001$. For uniform x-direction extension, if symmetry exists about the x-z plane as proposed by other investigators, the y-direction displacements along the initial lines of y=0 should all be zero. Figures 5.26 and 5.27 show the seven lines of initial y=0 after load application for thick (a/h=15) and thin (a/h=150) laminates, respectively. Note that the only locations where all are zero is at the ends (x/a=±1) where the ends were rigidly clamped, and at the axial center, x/a=0. Everywhere else the displacements are small, but nonzero. The symmetry condition is thus seen to be nonexistent. The assumption of symmetry about y=0 is seen to be increasingly poor as the laminate becomes thicker. The coarse grid used for these analyses did not permit what were considered accurate stress determinations. It is possible that while the violation of the y=0 symmetry may be small with regard to displacements, the symmetry of stresses which results may contain severe inaccuracies. The symmetry conditions which are not satisfied are 5.1d and 5.1e. For infinitely long laminates, the conclusion is that the usual symmetry assumptions are valid. However, three dimensional studies (e.g. [30]) which have assumed symmetry must be questioned, especially in regions
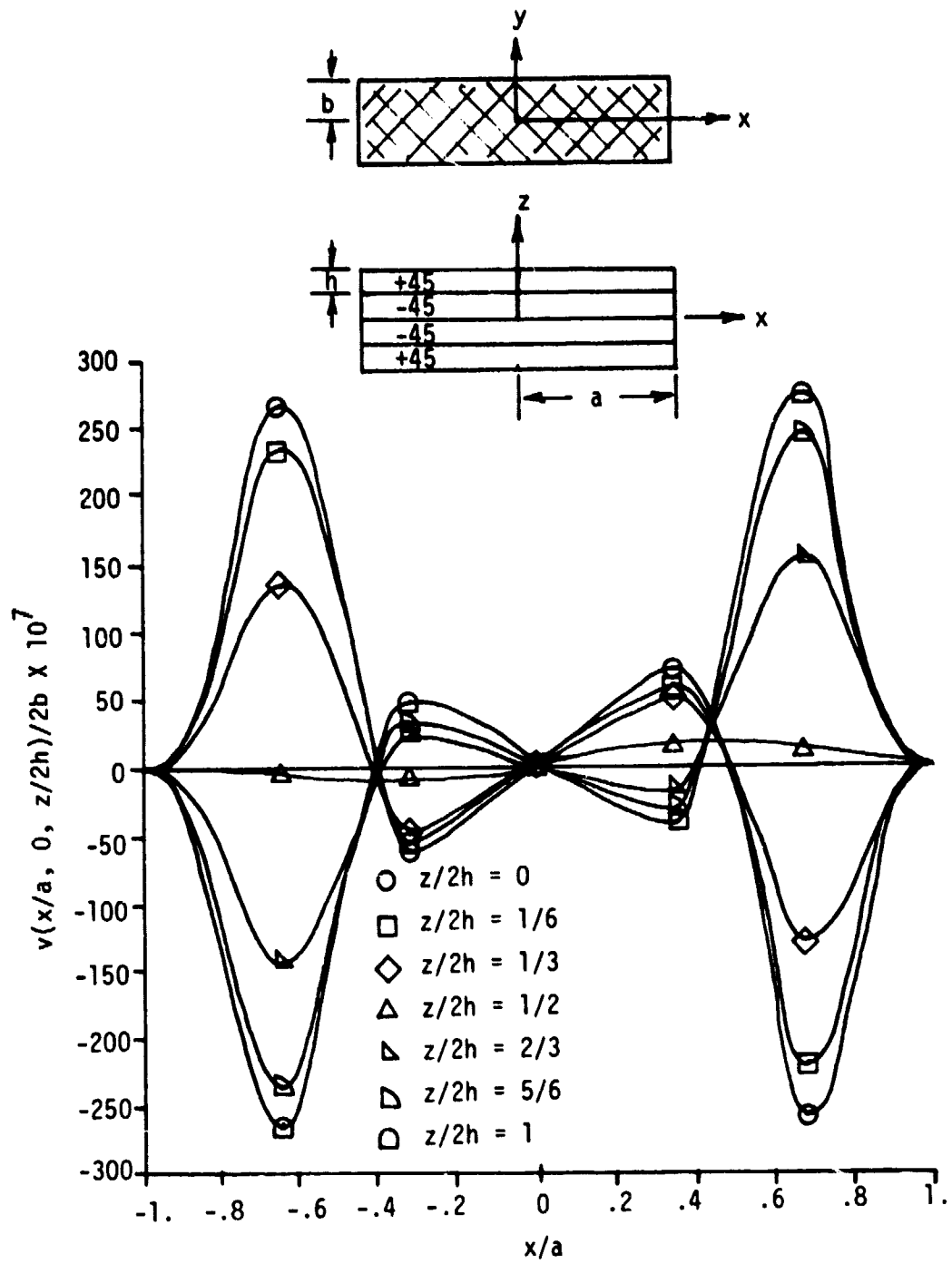
FIGURE 5.26   TRANSVERSE DISPLACEMENT OF LAMINATE CENTERLINE,
$[\pm 45]_s$, a/h = 15
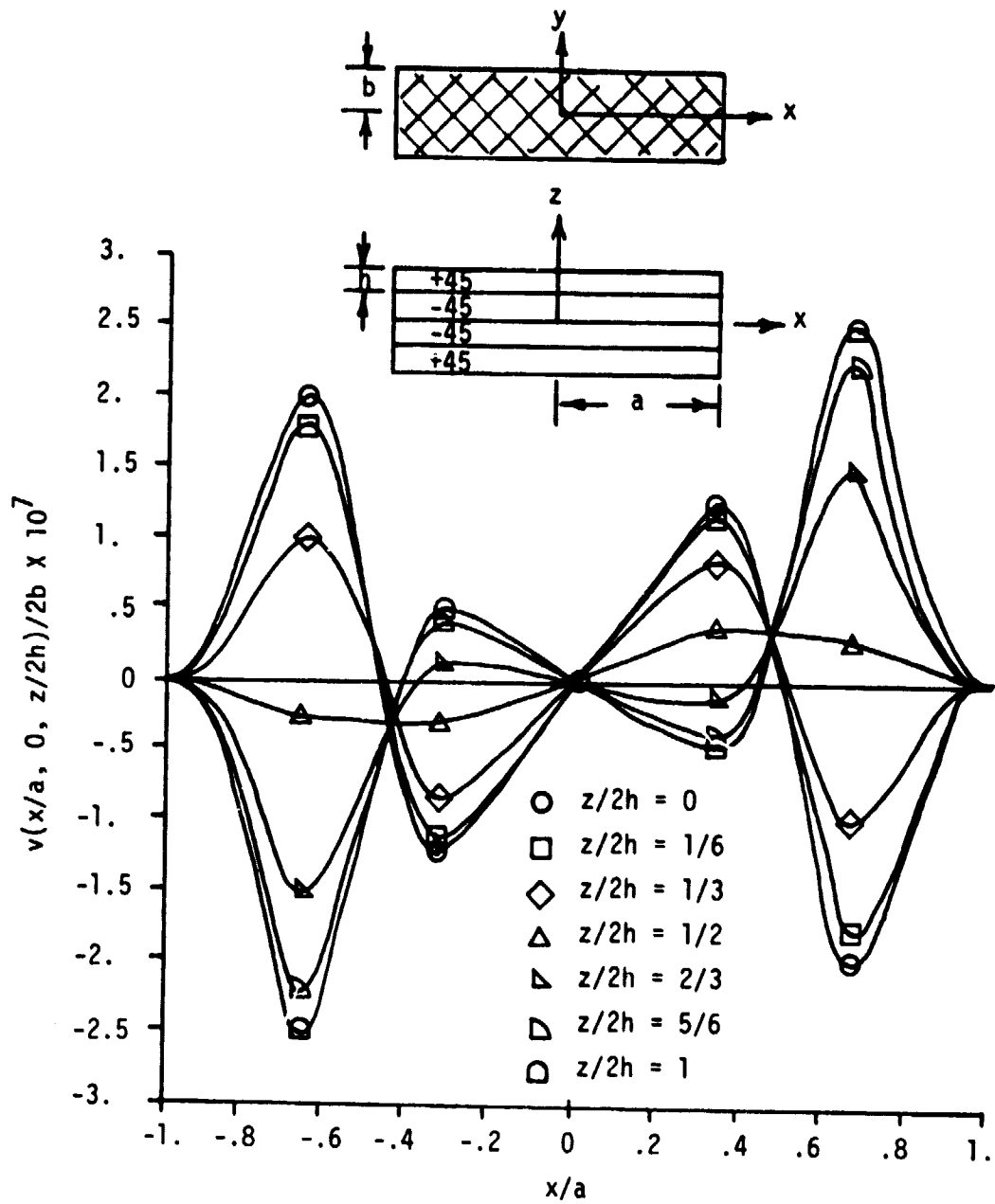
FIGURE 5.27 TRANSVERSE DISPLACEMENT OF LAMINATE CENTERLINE,
$[\pm 45]_s$, $a/h = 150$

near planes where symmetry has been improperly assumed. By invoking St. Venant's Principle, one might be able to use results from other regions of the laminate. Additional investigation into this problem is indicated.

5.3.3 Laminates with Central Circular Holes

Due to core limitations, only $[0/90]_s$ laminates with central circular holes were modeled. The geometry is shown schematically in Figure 5.18, and the finite element grid is shown in Figure 5.20. The material system considered was T300/5208 graphite/epoxy. As for the uniform laminates, the interlaminar normal stress (σ_z) was of prime concern.

Figure 5.28 shows σ_z vs. position around the hole near the mid-plane. The difference in the three thermal models is more pronounced at the extreme values of ϕ. The difference is approximately ten percent. No yielding of the material was predicted at the midplane. Figure 5.29 shows σ_z around the hole at the 0°/90° interface. Yielding was initiated in the upper (0°) layer near $\theta=45°$. The degree of plasticity was small, resulting in little stress relief. Yielding occurred during the -20°F increment from 90°F to 70°F. As with the uniform laminates, the thermal cooling was followed by a uniform x-direction traction of 1000 psi. The yielded area unloaded elastically, the value of Hill's yield function undergoing a slight decrease. Interlaminar shear stresses τ_{yz} and τ_{xz} were significant (~1400 psi) near the interface and $\theta=45°$.

Figures 5.30 and 5.31 show the through the thickness variation
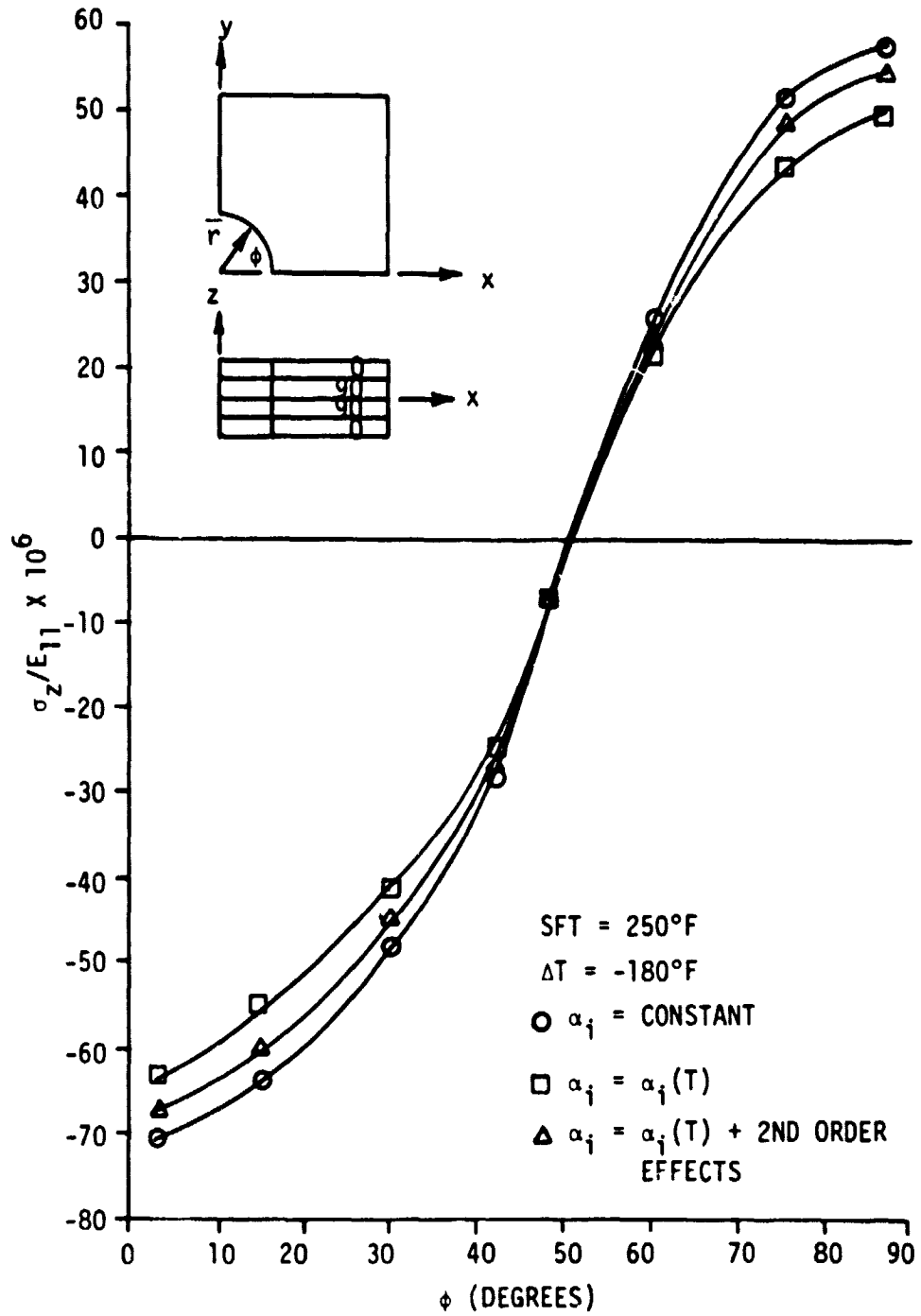
FIGURE 5.28 σ_z VS. ϕ NEAR MIDPLANE AT HOLE, $[0/90]_s$ Gr/Ep LAMINATE ($r/\bar{r} = 1.12$)
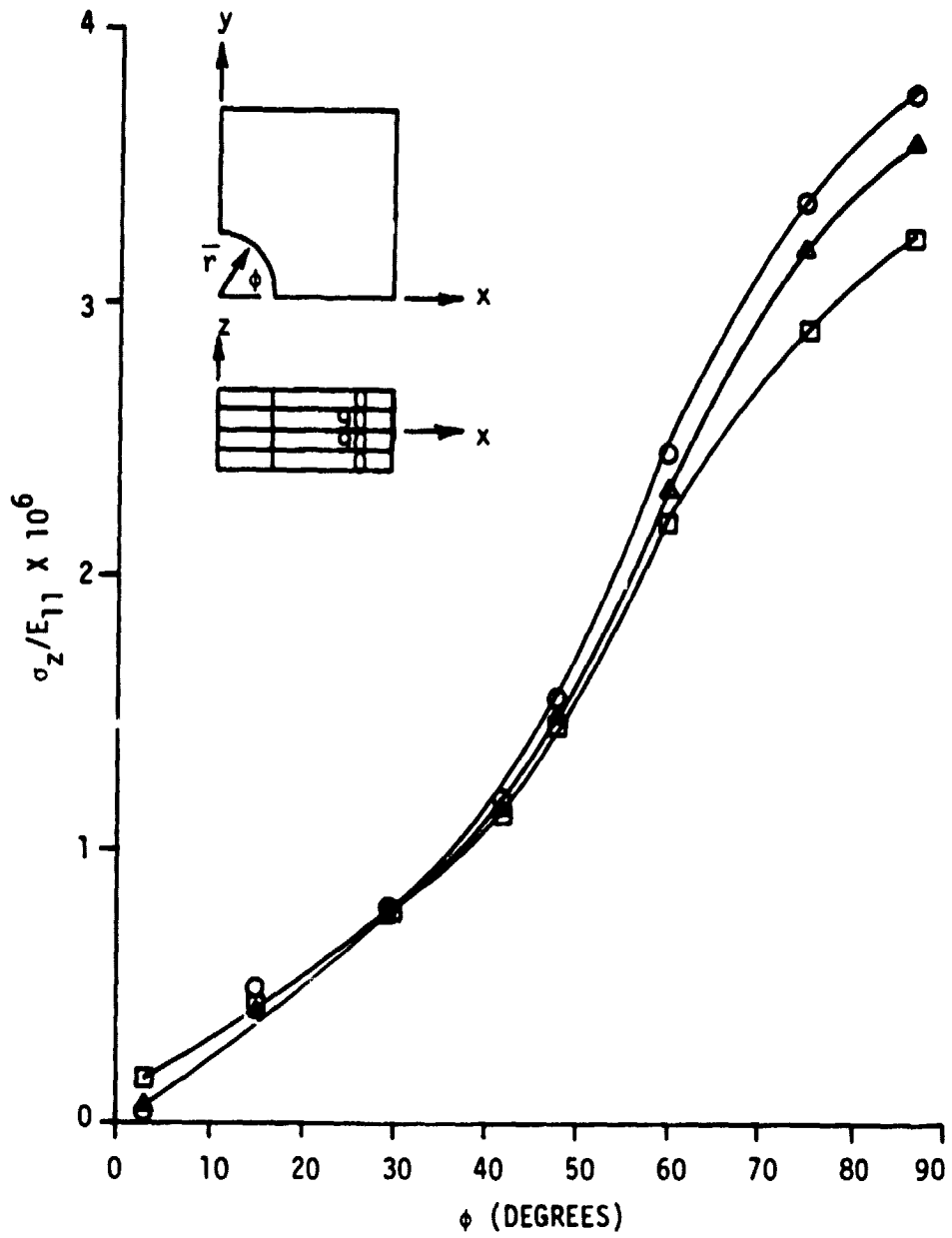
FIGURE 5.29 σ_z VS. ϕ AT 0/90 INTERFACE NEAR HOLE, $[0/90]_s$
Gr/Ep LAMINATE ($r/\bar{r} = 1.12$)
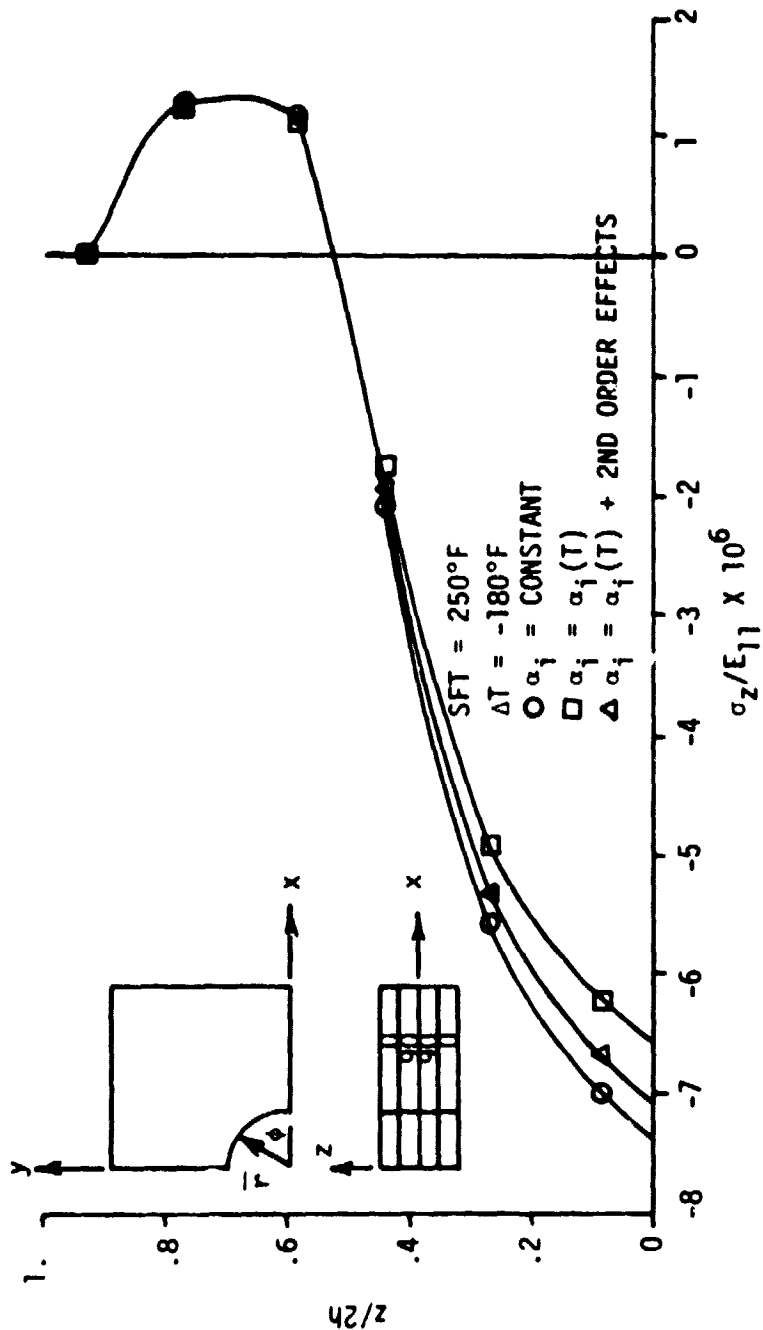
FIGURE 5.30 σ_z VS. z/2h, [0/90]$_s$ Gr/Ep LAMINATE WITH HOLE, ϕ = 3.13° (r/$\bar{r}$ = 1.12)
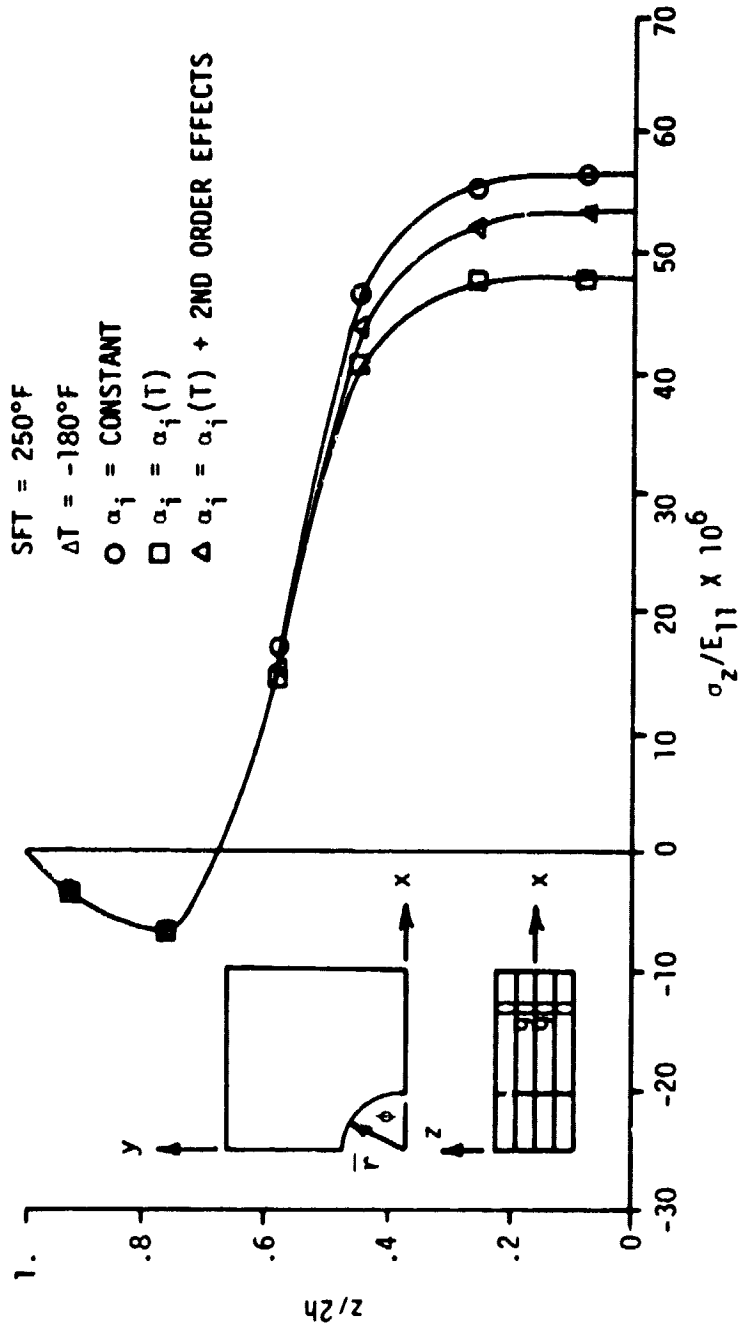
FIGURE 5.31 σ_z VS. z/2h, [0/90]$_s$ Gr/Ep LAMINATE WITH HOLE, ϕ = 86.87° ($r/\bar{r}$ = 1.12)

of σ_z near the hole for $\phi = 3.13$ and $86.87°$, respectively. The effect of the different thermal models is again approximately ten percent, with the differences more pronounced near the midplane. The equilibrium condition $\sigma_z = 0$ is recovered for $z/2h = 1$.

Chapter 6

SUMMARY AND CONCLUSIONS

The present study was concerned with a number of facets of the analysis of laminated composite materials. A plasticity theory, based on Hill's orthotropic yield criterion and the incremental flow theory of plasticity was formulated and made compatible with the finite element method of stress analysis. Techniques of including nonlinear hardening of orthotropic materials via unidirectional Ramberg-Osgood coefficients as well as temperature dependent plasticity, and linear, first and second order nonlinear thermal expansions was included. A computer implementation was formulated, coded, and utilized to study a number of problems relevant to composite materials.

Based on the work done in this study, the following conclusions, comments, and recommendations for future research are presented.

1. Three dimensional effects are definitely present in laminate composites, especially near free edges, holes, and corners. Treatment of these effects requires a fully three dimensional analysis capability.

2. For problems (e.g. cross-ply laminates, long laminates) which are closely approximated by generalized plane strain models, quasi-three dimensional analyses agree well with fully three dimensional results. They have the advantage of substantially lower cost, plus easier input generation and output assimilation.

3. Nonlinear behavior is a factor in composite materials, and

99

can significantly alter stress distributions. However, plasticity theories for orthotropic materials are not well developed, and the analyst must take care that spurious results do not lead to wrong decisions and faulty structural designs.

4. In material systems which are temperature dependent, as are composites, nonlinear thermal effects may be important, and should not be ignored. Where stress and/or temperature gradients are high, second order nonlinear thermal effects may also be important.

5. Symmetry conditions which have been advanced and widely used for angle ply laminates appear to be identically correct for an extremely limited number of positions in the laminate. Both the analyst and experimentor should take care not to assume symmetry where none exists. In addition, experimenters should be continually aware of the large gradients of strain which may exist when composites are extended off-axis. Variations may exist over the length of a strain gauge.

6. The initial strain technique of finite element analysis is a viable technique for modeling thermal and plasticity effects. It has the severe drawback of not being able to treat properties which differ in tension and compression. It is possible that a tangent stiffness method could be made competitive with respect to execution time and have the advantage of different properties in tension and compression.

7. An element with as many degree of freedom as the one used in the present study rapidly lead to stiffness matrices with large

bandwidth, often resulting in catastrophic storage problems. Out of core solvers are very slow in assembly and suffer somewhat in solution. A minimization technique which does not require assembly of the global stiffness matrix is indicated as a viable solution algorithm.

8. Thick cross-ply graphite/epoxy laminates are not highly susceptible to plasticity during the cooling cycle, even when free edge influence is considered. Were the transverse modulus raised, plasticity might be a problem.

9. When modeling nonlinear effects, an equilibrium iteration is essential. Omission of equilibrium iteration or failure to converge can result in instabilities which render useless any values computed after deviation from equilibrium.

10. When using any nonlinear model and describing stress-strain relationships, the tangent modulus is of the utmost importance. Even if σ is correctly computed given ϵ, a faulty tangent modulus yields poor results when used to extrapolate to the next step. Exponential models such as Ramberg-Osgood suffer severely from this problem since small deviations raised to a power greater than unity are magnified. Such errors propagate and grow very rapidly.

REFERENCES

1. Smith, C. B., "Some New Types of Orthotropic Plates Laminated of Orthotropic Materials," J. App. Mech., Vol. 20, June 1953, pp. 286-288.

2. Reissner, E., Stavsky, Y., "Bending and Stretching of Certain Types of Heterogeneous Aeolotropic Elastic Plates," J. App. Mech., Vol. 28, Sept. 1961, pp. 402-408.

3. Ashton, J. E., Whitney, J. M., Theory of Laminated Plates, Technomic Publishing Company Inc., Stamford, Conn., 1970.

4. Jones, R. M., Mechanics of Composite Materials, McGraw-Hill:New York, 1975.

5. Herakovich, C. T., Ed. Inelastic Behavior of Laminated Composite Materials, ASTM Publication AMD-Vol. 13, 1975.

6. Pagano, N. J., "Stress Fields in Composite Laminates," Int. J. Sol. Struc., Vol. 14, 1978, pp. 385-400.

7. Pagano, N. J., "Free Edge Stress Fields in Composite Laminates," Int. J. Sol. Struc., Vol. 14, 1978, pp. 401-406.

8. Hsu, P. W., Herakovich, C. T., "Interlaminar Stresses in Composite Laminates -- A Perturbation Analysis," VPI-E-76-1, January, 1976.

9. Pipes, R. B., "Interlaminar Stresses in Composite Laminates," AFML-TR-72-18, 1972.

10. Tsai, S. W., Wu, E. M., "A General Theory of Strength for Anisotropic Materials," J. Comp. Mat., Vol. 5, January, 1971, pp. 58-80.

11. Petit, P. H., Waddoups, M. E., "A Method of Predicting the Non-linear Behavior of Laminated Composites," J. Comp. Mat., Vol. 3, January, 1969, pp. 2-19.

12. Hashin, Z., Rosen, B. W., Pipes, R. B., "Non-linear Behavior of Fiber Composite Laminates," Mat. Sci. Corp. Rept., TFR/7309, NASA, September, 1973.

13. Hashin, Z., Rosen, B. W., Pipes, R. B., "Non-linear Effect on Composite Laminate Thermal Expansion," NASA Contractor Report 3088, Contract NAS1-14964, February, 1979.

14. Sandhu, R. S., Computer Program (NOLAST) for Nonlinear Analysis of Composite Laminates, AFFDL-TR-76-1, February, 1976.

15. Hahn, H. T., Pagano, N. J., "Curing Stresses in Composite Laminates," J. Comp. Mat., Vol. 9, January, 1975, pp. 91-106.

16. Wang, A. S. D., Crossman, F. W., "Edge Effects on Thermally Induced Stresses in Composite Laminates," J. Comp. Mat., Vol. 11, July, 1977, pp. 300-312.

17. Mauri, R. E., Crossman, F. W., Warren, W. J., "Assessment of Moisture Altered Dimensional Stability of Structural Composites," SAMPE, Vol. 23, 1978, pp. 1202-1217.

18. Pipes, R. B., Pagano, N. J., "Interlaminar Stresses in Composite Laminates Under Uniform Axial Extension," J. Comp. Mat., Vol. 4, October 1970, pp. 538-548.

19. Pipes, R. B., Pagano, N. J., "Interlaminar Stresses in Composite Laminates - An Approximate Elasticity Solution," J. App. Mech., Vol. 41, September 1974, pp. 668-672.

20. Isakson, G., Levy, A., "Finite Element Analysis of Interlaminar Shear in Fibrous Composites," J. Comp. Mat., April, 1971, pp. 273-276.

21. Puppo, A. H., Evensen, H. A., "Strength of Anisotropic Materials Under Combined Stresses," AIAA/ASME 12th SDM Conf. Anaheim, April 19-21, 1971, AIAA Paper No. 71-368.

22. Levy, A., Armen, H., Whiteside, J., "Elastic and Plastic Interlaminar Shear Deformation in Laminated Composites under Generalized Plane Stress," 3rd Conf. Wright Patterson, October 19-21, 1971, Grumman Research Dept., Memorandum RM-535J, February, 1972.

23. Herakovich, C. T., Brooks, E. W., Jr., "Tensile Strength Behavior of Composite Reinforced Metals," VPI-E-73-5, January, 1973.

24. Herakovich, C. T., "On Thermal Edge Effects in Composite Laminates," Int. J. Mech. Sci., Vol. 18, 1976, pp. 129-134.

25. Lin, F. T., "The Finite Element Analysis of Laminated Composites," Ph.D. Dissertation, VPI&SU, 1972.

26. Dana, J. R., "Three Dimensional Finite Element Analysis of Thick Laminated Composites - Including Interlaminar and Boundary Effects near Circular Holes," Ph.D. Dissertation, VPI&SU, 1974.

27. Dana, J. R., Barker, R. M., "Three-Dimensional Finite-Element Computer Program - User's Guide," VPI-E-74-19, August, 1974.

28. Rybicki, E. F., Schmit, Jr., L. A., "An Incremental Complementary Energy Method of Nonlinear Stress Analysis," <u>AIAA J.</u>, Vol. 8, October 1970, pp. 1805-1812.

29. Rybicki, E. F., "Approximate Three-Dimensional Solutions for Symmetric Laminates Under Inplane Loading," <u>J. Composite Materials</u>, Vol. 5, July 1971, pp. 354-360.

30. Rybicki, E. F., Kanninen, M. F., "A Finite Element Calculation of Stress Intensity Factors by a Modified Crack Closure Integral," <u>Engr. Fract. Mech.</u>, Vol. 9, 1977, pp. 931-938.

31. Rybicki, E. F., Schmueser, D. W., Fox, J., "An Energy Release Rate Approach for Stable Crack Growth in the Free-Edge Delamination Problem," <u>J. Composite Materials</u>, Vol. 11, October 1977, pp. 470-487.

32. Rybicki, E. F., Schmueser, D. W., "Three-Dimensional Finite Element Stress Analysis of Laminated Plates Containing a Circular Hole," AFML-TR-76-92, August 1976.

33. Stanton, E. L., Crain, L. M., Neu, T. F., "A Parametric Cubic Modelling System for General Solids of Composite Material," <u>Int. J. Num. Meth. Engr.</u>, Vol. 11, 1977, pp. 653-670.

34. Stanton, E. L., "A General Three-Dimensional Computational Model for Nonlinear Composite Structures and Materials," PDA TR 1045-00, June 1977.

35. Foye, R. L., "Inelastic Micromechanics of Curing Stresses in Composites," <u>Inelastic Behavior of Composite Materials</u>, ASME, AMD Vol. 13, 1975, C. T. Herakovich, Ed.

36. Hill, R., <u>The Mathematical Theory of Plasticity</u>, Oxford University Press, London, 1971.

37. Pifko, A., Levine, H. S., Armen, H. Jr., "PLANS - A Finite Element Program for Nonlinear Analysis of Structures, Volume I - Theoretical Manual," NASA CR-2568, November 1975.

38. Mendelson, A.. <u>Plasticity: Theory and Application</u>, The MacMillan Company, New York, 1970.

39. Isakson, G., Armen, H. Jr. and Pifko, A., "Discrete Element Methods for the Plastic Analysis of Structures," NASA Contractor Report NASA CR-803, October 1967.

40. Renieri, G. D., Herakovich, C. T., "Nonlinear Analysis of Laminated Fibrous Composites," VPI-E-76-10, June, 1976.

41. Lee, S. W., "An Assumed Stress Hybrid Finite Element for Three Dimensional Elastic Structural Analysis," M. S. Thesis, M.I.T., May, 1974.

42. Wang, S. S., Mandell, J. F., McGarry, F. J., "Three-Dimensional Solution for a Through-Thickness Crack in a Cross-Plied Laminate," Fracture Mechanics of Composites, ASTM STP 593, 1975, pp. 36-60.

43. Wang, S. S., Mandell, J. F., McGarry, F. J., "Three-Dimensional Solution for a Through-Thickness Crack with Crack Tip Damage in a Cross-Plied Laminate," Fracture Mechanics of Composites, ASTM STP 593, 1975, pp. 61-85.

44. Pian, T. H. H., Tong, P., "Finite Element Methods in Continuum Mechanics," Advances in Applied Mechanics, Vol. 12, Academic Press, N.Y., 1972.

45. Kathiresan, K., "Three-Dimensional Linear Elastic Fracture Mechanics by a Displacement Hybrid Finite-Element Model," Ph.D. Dissertation, Ga. Inst. Tech., September 1976.

46. Atluri, S. N., Kathiresan, K., "Stress Analysis of Typical Flaws in Aerospace Structural Components Using 3-D Displacement Finite Element Method," AIAA/ASME 19th SDM Conf., Bethesda, Md., April 3-5, 1978.

47. Ueda, Y., Yamakawa, T., "Thermal Nonlinear Behavior of Structures," Advances in Computational Methods in Structural Mechanics and Design, The University of Alabama in Huntsville, Huntsville, Alabama, 1972.

48. Time-Dependent Environmental Behavior of Gr/Ep Composites, Quarterly Prog. Rept. 5, Contract F33615-77-C-5109, Prepared for AFML by General Dynamics, Fort Worth, Texas, 10 December 1978.

49. Zienkiewicz, O. C., Cormeau, I. C., "Visco-Plasticity - Plasticity and Creep in Elastic Solids - A Unified Numerical Approach," Int. J. Num. Meth. Eng., Vol. 8, 1974, pp. 821-845.

50. Desai, C. S., Abel, J. F., Introduction to the Finite Element Method: A Numerical Method for Engineering Analysis, Van Nostrand Reinhold Company, New York, 1972.

51. Yamada, Y., "Incremental Formulation for Problems with Geometric and Material Nonlinearities," Advances in Computational Methods in Structural Mechanics and Design, The University of Alabama in Huntsville, Huntsville, Alabama, 1972.

52. Lin, T. H., Salinas, D., Ito, Y. M., "Effects of Hydro-Static Stress on the Yielding of Cold Rolled Metals and Fiber - Reinforced Composites," J. Comp. Mat., Vol. 6, 1972, p. 409.

53. Drucker, D. C., "Plasticity," Structural Mechanics, Proceedings of the First Symposium on Naval Structural Mechanics, August 11-14, 1958, Pergamon Press, New York, 1960.

54. Krieg, R. D., "A Practical Two Surface Plasticity Theory," J. App. Mech., Vol. 42, September 1975, pp. 641-646.

55. Bazant, Z. P., "Endochronic Inelasticity and Incremental Plasticity," Int. J. Solids Structures, Vol. 14, 1978, pp. 691-714.

56. Mroz, Z., "On the Description of Anisotropic Workhardening," J. Mech. Phys. Solids, Vol. 15, 1967, pp. 163-175.

57. Axelsson, K., Samuelsson, A., "Finite Element Analysis of Elastic-Plastic Materials Displaying Mixed Hardening," Int. J. Num. Meth. Engr., Vol. 14, 1979, pp. 211-225.

58. Marcal, P. V., "Finite Element Analysis with Material Nonlinearities - Theory, and Practice," Recent Advances in Matrix Methods of Structural Analysis and Design, The University of Alabama Press, Huntsville, Alabama, 1971, pp. 257-282.

59. Biffle, J. H., "Finite Element Analysis for Wave Propagation in Elastic-Plastic Solids," Ph.D. Dissertation, The University of Texas at Austin, 1973.

60. Ramberg, W., Osgood, W. R., "Description of Stress-Strain Curves by Three Parameters," National Advisory Committee for Aeronautics, NACA TN 902, July 1943.

61. Conte, S. D. and de Boor, C., Elementary Numerical Analysis, McGraw-Hill, New York, 1972.

62. Brinson, H. F., Yeow, Y. T., "A Comparison of Simple Shear Characterization Methods for Composite Laminates," VPI-E-77-7, February, 1977.

63. Bathe, K. J., Wilson, E. L., Numerical Methods in Finite Element Analysis, Prentice-Hall, Inc., New Jersey, 1976.

64. Everstine, G. C., "The BANDIT Computer Program for the Reduction of Matrix Bandwidth for NASTRAN," Naval Ship Research and Development Center Report 3827, March 1972.

65. Gibbs, N. E., Poole, W. G., Jr. and Stockmeyer, P. K., "An Algorithm for Reducing the Bandwidth and Profile of a Sparse Matrix," Institute for Computer Applications in Science and Engineering (ICASE) Report, Hampton, Virginia, July 1974.

66. Cuthill, E., McKee, J., "Reducing the Bandwidth of Sparse Symmetric Matrices," Proc. 24th National Conf. ACM, 1969, pp. 157-172.

67. Rosen, R., "Matrix Bandwidth Minimization," Proceedings - 1968 ACM Conference, pp. 585-595.

68. Chamis, C. C., Sinclair, J. H., "Ten-deg Off-axis Test for Shear Properties in Fiber Composites," Experimental Mechanics, Sept. 1977, pp. 339-346.

69. Cole, B. W. and Pipes, R. B., "Filamentary Composite Laminates Subjected to Biaxial Stress Fields," AFFDL-TR-73-115, June 1974.

70. Sandhu, R. S., "Nonlinear Behavior of Unidirectional and Angle Ply Laminates," J. Aircraft, Vol. 13, No. 2, Feb. 1976, pp. 104-111.

71. Pipes, R. B., Cole, B. W., "On the Off-Axis Strength Test for Anisotropic Materials," J. Composite Materials, Vol. 7, April 1973, pp. 246-256.

72. Pindera, M. J., "Nonlinear Behavior and Failure of Off-axis Unidirectional Composites," unpublished project report, March, 1979.

73. Wang, A. S. D., Crossman, F. W., "Some New Results on Edge Effect in Symmetric Composite Laminates," J. Composite Materials, Vol. 11, January 1977, pp 92-106.

74. O'Brien, D., Herakovich, C. T., "Finite Element Stress Analysis of Idealized Composite Damage Zones," VPI-E-78-6, February 1978.

75. Humphreys, E. A. and Herakovich, C. T., "Nonlinear Analysis of Bonded Joints with Thermal Effects," VPI-E-77-19, June, 1977.

76. Zienkiewicz, O. C., The Finite Element Method in Engineering Science, Second Edition, McGraw-Hill:London, 1971.

77. Scarborough, J. B., Numerical Mathematical Analysis, Sixth Edition, Johns Hopkins Press: Baltimore, 1966, pp. 152-159.

APPENDIX A

LINEAR ELASTIC FINITE ELEMENT RELATIONSHIPS

APPENDIX A

LINEAR ELASTIC FINITE ELEMENT RELATIONSHIPS

The finite element used is shown in Figure A.1. The sides with
four nodes are described by the cubic "serendipity" interpolation
functions as described by Zienkiewicz [76]. The details of the isopara-
metric finite element concept are also given in Reference 76. The
technique basically involves mapping a distorted shape in the
Cartesian (x,y,z) coordinate system into a cube in a local (ξ,η,ζ)
coordinate system where ξ, η, and ζ range from -1 to $+1$. The
relationship between the global Cartesian and the local curvilinear
coordinates is

$$x = N_1 x_1 + N_2 x_2 + \ldots + N_{24} x_{24} = N_i x_i \qquad i = 1,24$$

$$y = N_1 y_1 + N_2 y_2 + \ldots + N_{24} y_{24} = N_i y_i \qquad i = 1,24 \qquad (A.1)$$

$$z = N_1 z_1 + N_2 y_2 + \ldots + N_{24} z_{24} = N_i z_i \qquad i = 1,24$$

where the N_i are the interpolation functions for the 24 nodal points
and the x_i, y_i, z_i are the Cartesian coordinates of the nodes. If
we introduce the notation

$$\xi_0 = \xi\xi_i \qquad \eta_0 = \eta\eta_i \qquad \zeta_0 = \zeta\zeta_i, \qquad (A.2)$$

then for the corner nodes $\zeta = \pm1 \qquad \eta_i = \pm1 \qquad \xi_i = \pm1$

$$N_i = \frac{1}{64}(1+\xi_0)(1+\eta_0)(1+\zeta_0)[9(\xi^2+\eta^2)-10] \qquad i = 1,4,5,8,17,20,21,24.$$

$$(A.3)$$

FIGURE A.1 LOCAL ELEMENT COORDINATE SYSTEM
AND NODE INPUT SEQUENCE

For the triside nodes $\xi_i = \pm 1 \quad \eta_i = \pm \frac{1}{3} \quad \zeta_i = \pm 1$

$$N_i = \frac{9}{64}(1+\xi_0)(1+9\eta_0)(1+\zeta_0)(1-\eta^2) \qquad i = 9,10,11,12,13,14,15,16.$$

(A.4)

For the triside nodes $\eta_i = \pm 1 \quad \xi_i = \pm \frac{1}{3} \quad \zeta_i = \pm 1$

$$N_i = \frac{9}{64}(1+9\xi_0)(1+\eta_0)(1+\zeta_0)(1-\xi^2) \qquad i = 2,3,6,7,18,19,22,23.$$

(A.5)

For an isoparametric element, the same interpolation functions are used for the assumed displacements as for the geometry. Hence,

$$u = N_i u_i$$

$$v = N_i v_i \qquad (A.6)$$

$$w = N_i w_i$$

where u, v, and w are the x, y, and z displacements, respectively, and the u_i, v_i, and w_i are the values at the ith node.

The strain-displacement relationships are derived based on small strain-small displacement theory. For the three dimensional case, these relationships may be written as

$$
\begin{Bmatrix} \epsilon_x \\ \epsilon_y \\ \epsilon_z \\ \gamma_{yz} \\ \gamma_{xz} \\ \gamma_{xy} \end{Bmatrix}
=
\begin{bmatrix}
\frac{\partial}{\partial x} & 0 & 0 \\
0 & \frac{\partial}{\partial y} & 0 \\
0 & 0 & \frac{\partial}{\partial z} \\
0 & \frac{\partial}{\partial z} & \frac{\partial}{\partial y} \\
\frac{\partial}{\partial z} & 0 & \frac{\partial}{\partial x} \\
\frac{\partial}{\partial y} & \frac{\partial}{\partial x} & 0
\end{bmatrix}
\begin{Bmatrix} u \\ v \\ w \end{Bmatrix}
\qquad (A.7)
$$

Substituting (A.6) into (A.7),

$$
\begin{Bmatrix} \epsilon_x \\ \epsilon_y \\ \epsilon_z \\ \gamma_{yz} \\ \gamma_{xz} \\ \gamma_{xy} \end{Bmatrix} = \begin{bmatrix} \frac{\partial}{\partial x} & 0 & 0 \\ 0 & \frac{\partial}{\partial y} & 0 \\ 0 & 0 & \frac{\partial}{\partial z} \\ 0 & \frac{\partial}{\partial z} & \frac{\partial}{\partial y} \\ \frac{\partial}{\partial z} & 0 & \frac{\partial}{\partial x} \\ \frac{\partial}{\partial y} & \frac{\partial}{\partial x} & 0 \end{bmatrix} [IN_i \mid IN_2 \mid \ldots \mid IN_{24}]\{q\} \qquad (A.8)
$$

where

I is the 3x3 identity matrix

$\{q\}$ is the 72x1 vector of nodal displacements given by

$$
\{q\} = \begin{Bmatrix} u_1 \\ v_1 \\ w_1 \\ u_2 \\ v_2 \\ w_2 \\ \cdot \\ \cdot \\ \cdot \\ u_{24} \\ v_{24} \\ w_{24} \end{Bmatrix} \qquad (A.9)
$$

We define the [B] matrix (strain-displacement relationships) by

$$
\{\epsilon\} = [B]\{q\}. \qquad (A.10)
$$

By comparison of (A.10) and (A.8),

$$[B] = \begin{bmatrix} \frac{\partial}{\partial x} & 0 & 0 \\ 0 & \frac{\partial}{\partial y} & 0 \\ 0 & 0 & \frac{\partial}{\partial z} \\ 0 & \frac{\partial}{\partial z} & \frac{\partial}{\partial y} \\ \frac{\partial}{\partial z} & 0 & \frac{\partial}{\partial x} \\ \frac{\partial}{\partial y} & \frac{\partial}{\partial x} & 0 \end{bmatrix} [IN_1 | IN_2 | \ldots | IN_{24}]. \qquad (A.11)$$

From (A.3), (A.4), and (A.5), we recall that the N_i are functions of the local coordinates ξ, η, ζ. In order to determine the elements of $[B]$ we require a relationship between the derivatives in the global (x,y,z) and local (ξ,η,ζ) coordinate systems. This relationship is given by the Jacobian matrix $[J]$ of the transformation where

$$[J] = \begin{bmatrix} \frac{\partial x}{\partial \xi} & \frac{\partial y}{\partial \xi} & \frac{\partial z}{\partial \xi} \\ \frac{\partial x}{\partial \eta} & \frac{\partial y}{\partial \eta} & \frac{\partial z}{\partial \eta} \\ \frac{\partial x}{\partial \zeta} & \frac{\partial y}{\partial \zeta} & \frac{\partial z}{\partial \zeta} \end{bmatrix}. \qquad (A.12)$$

and

$$\begin{Bmatrix} \frac{\partial N_i}{\partial \xi} \\ \frac{\partial N_i}{\partial \eta} \\ \frac{\partial N_i}{\partial \zeta} \end{Bmatrix} = [J] \begin{Bmatrix} \frac{\partial N_i}{\partial x} \\ \frac{\partial N_i}{\partial y} \\ \frac{\partial N_i}{\partial z} \end{Bmatrix} \qquad (A.12a)$$

Inverting (A.12a),

$$\begin{Bmatrix} \dfrac{\partial N_i}{\partial x} \\[6pt] \dfrac{\partial N_i}{\partial y} \\[6pt] \dfrac{\partial N_i}{\partial z} \end{Bmatrix} = [J]^{-1} \begin{Bmatrix} \dfrac{\partial N_i}{\partial \xi} \\[6pt] \dfrac{\partial N_i}{\partial \eta} \\[6pt] \dfrac{\partial N_i}{\partial \zeta} \end{Bmatrix} \qquad (A.13)$$

where $[J]^{-1}$ is the inverse of $[J]$. Note that if $[J]$ is singular, the inverse does not exist. Physically, this indicates that the $x,y,z \rightarrow \xi,\eta,\zeta$ mapping is improper. Furthermore, if $|J|$ (determinant of $[J]$) is negative an improper mapping is indicated. Improper mappings indicate faulty geometry input or elements which are so distorted that a unique mapping is impossible. Substituting (A.1) into (A.12),

$$[J] = \begin{bmatrix} \dfrac{\partial N_1}{\partial \xi} & \cdots & \dfrac{\partial N_{24}}{\partial \xi} \\[8pt] \dfrac{\partial N_1}{\partial \eta} & \cdots & \dfrac{\partial N_{24}}{\partial \eta} \\[8pt] \dfrac{\partial N_1}{\partial \zeta} & \cdots & \dfrac{\partial N_{24}}{\partial \zeta} \end{bmatrix} \begin{bmatrix} x_1 & y_1 & z_1 \\ \cdot & \cdot & \cdot \\ \cdot & \cdot & \cdot \\ x_{24} & y_{24} & z_{24} \end{bmatrix} \qquad (A.14)$$

For the application of finite elements to laminates, several assumptions are made. The material properties are assumed to be transversely isotropic, with the stiffer of the two directions always being in the plane of the element. The fiber direction so defined is oriented at an arbitrary angle. The material is assumed to be homogeneous. This approach has been termed the macroscopic approach, as opposed to the micromechanics approach of considering the fiber and matrix materials individually. In reality, one cannot ignore the

fiber-matrix interactions which exist on the microscopic level. In practice, microscopic analyses cannot be handled for problems of significant size. The purpose of this investigation is to determine the stress distributions between laminae, an effect which is manifested near the microscopic level. However, the physical dimensions of the solids to be treated preclude a microscopic analysis. Macroscopic analysis techniques will therefore be used with the tacit understanding that microscopic effects of possibly significant magnitude have been omitted.

The elasticity matrix $[D]$ for a homogeneous orthotropic material is

$$[D] = \begin{bmatrix} D_{11} & D_{12} & D_{13} & 0 & 0 & 0 \\ & D_{22} & D_{23} & 0 & 0 & 0 \\ & & D_{33} & 0 & 0 & 0 \\ & & & D_{44} & 0 & 0 \\ & \text{symmetric} & & & D_{55} & 0 \\ & & & & & D_{66} \end{bmatrix} \quad (A.15)$$

where

$$D_{11} = \frac{1-\nu_{23}\nu_{32}}{F} E_{11} \qquad D_{12} = \frac{\nu_{12}+\nu_{13}\nu_{32}}{F} E_{22} \qquad D_{13} = \frac{\nu_{13}+\nu_{12}\nu_{23}}{F} E_{33}$$

$$D_{22} = \frac{1-\nu_{13}\nu_{31}}{F} E_{22} \qquad D_{23} = \frac{\nu_{23}+\nu_{21}\nu_{13}}{F} E_{33} \qquad D_{33} = \frac{1-\nu_{12}\nu_{21}}{F} E_{33}$$

$$D_{44} = G_{23} \qquad\qquad D_{55} = G_{13} \qquad\qquad D_{66} = G_{12}$$

$$F = 1-\nu_{12}\nu_{21}-\nu_{13}\nu_{31}-\nu_{23}\nu_{32}-\nu_{12}\nu_{23}\nu_{31}-\nu_{21}\nu_{13}\nu_{32}.$$

The stress-strain relations for the material in the principal material axis system (1,2,3) is

$$\begin{Bmatrix} \sigma_1 \\ \sigma_2 \\ \sigma_3 \\ \tau_{23} \\ \tau_{13} \\ \tau_{12} \end{Bmatrix} = [D] \begin{Bmatrix} \varepsilon_1 \\ \varepsilon_2 \\ \varepsilon_3 \\ \gamma_{23} \\ \gamma_{13} \\ \gamma_{12} \end{Bmatrix} \qquad (A.16)$$

where the 1-direction is assumed to be coincident with the fibers. The material is isotropic in the 2-3 plane, leading to the reduction of the nine material constants of (A.15) to the five required for a transversely isotropic material. The additional relationships due to the 2-3 isotropy are

$$E_2 = E_3 \qquad G_{31} = G_{12} \qquad \nu_{21} = \nu_{31}$$

$$G_{23} = \frac{E_2}{2(1+\nu_{23})} . \qquad (A.17)$$

If the in-plane principal material axes (1,2) are not coincident with the in-plane global axes (x,y), the equations (A.16) must be modified to result in a stress-strain relationship in the global system. Since σ_{ij} and ε_{ij} are actually second order Cartesian tensors and follow the transformation law of second order tensors,

$$\sigma_{ij} = a_{ik}a_{jl}\sigma_{kl}^{(1)}$$

$$\varepsilon_{ij} = a_{ik}a_{jl}\varepsilon_{kl}^{(1)} , \qquad (A.18)$$

where σ_{ij} and ε_{ij} are referred to the global axes, $\sigma_{kl}^{(1)}$ and $\varepsilon_{kl}^{(1)}$ are referred to the material axes, and a_{ik} are the direction cosines of the

global axes with respect to the material axes. For an angle θ measured from the x axis to the 1 axis,

$$a_{ij} = \begin{bmatrix} \cos\theta & -\sin\theta & 0 \\ \sin\theta & \cos\theta & 0 \\ 0 & 0 & 1 \end{bmatrix} , \qquad (A.19)$$

which corresponds to an angular rotation θ about the 3 (coincident with z) axis. Performing the operations (A.18) with (A.19), and replacing tensor strain ε_{ij} ($i{\neq}j$) with engineering strain γ_{ij} ($i{\neq}j$),

$$\begin{Bmatrix} \varepsilon_1 \\ \varepsilon_2 \\ \varepsilon_3 \\ \gamma_{23} \\ \gamma_{13} \\ \gamma_{12} \end{Bmatrix} = [T_2] \begin{Bmatrix} \varepsilon_x \\ \varepsilon_y \\ \varepsilon_z \\ \gamma_{yz} \\ \gamma_{xz} \\ \gamma_{xy} \end{Bmatrix} \qquad (A.20)$$

where

$$[T_2] \begin{bmatrix} m^2 & n^2 & 0 & 0 & 0 & mn \\ n^2 & m^2 & 0 & 0 & 0 & -mn \\ 0 & 0 & 1 & 0 & 0 & 0 \\ 0 & 0 & 0 & m & -n & 0 \\ 0 & 0 & 0 & n & m & 0 \\ -2mn & 2mn & 0 & 0 & 0 & m^2-n^2 \end{bmatrix} \qquad (A.21)$$

and $m = \cos\theta \qquad n = \sin\theta$.

Furthermore, the stresses in the global and material axis systems are related by

$$\begin{Bmatrix} \sigma_1 \\ \sigma_2 \\ \sigma_3 \\ \tau_{23} \\ \tau_{13} \\ \tau_{12} \end{Bmatrix} = [T_1] \begin{Bmatrix} \sigma_x \\ \sigma_y \\ \sigma_z \\ \tau_{yz} \\ \tau_{xz} \\ \tau_{xy} \end{Bmatrix} \tag{A.22}$$

where

$$[T_1] = \begin{bmatrix} m^2 & n^2 & 0 & 0 & 0 & 2mn \\ n^2 & m^2 & 0 & 0 & 0 & -2mn \\ 0 & 0 & 1 & 0 & 0 & 0 \\ 0 & 0 & 0 & m & -n & 0 \\ 0 & 0 & 0 & n & m & 0 \\ -mn & mn & 0 & 0 & 0 & m^2-n^2 \end{bmatrix} \tag{A.23}$$

and $m = \cos\theta$, $n = \sin\theta$. The matrices $[T_1]$ and $[T_2]$ are referred to as the stress and strain transformation matrices, respectively. Note that the presence of the factor two in $[T_1]$ and $[T_2]$ in the shear terms accounts for the difference in tensor shear strain and engineering shear strain.

Substituting (A.21) and (A.22) into (A.16) and premultiplying both sides by $[T_1]^{-1}$,

$$\begin{Bmatrix} \sigma_x \\ \sigma_y \\ \sigma_z \\ \tau_{yz} \\ \tau_{xz} \\ \tau_{xy} \end{Bmatrix} = [T_1]^{-1}[D][T_2] \begin{Bmatrix} \epsilon_x \\ \epsilon_y \\ \epsilon_z \\ \gamma_{yz} \\ \gamma_{xz} \\ \gamma_{xy} \end{Bmatrix} . \qquad (A.24)$$

Equations (A.24) are the stress strain relationships in the global coordinate system. The rotated elasticity matrix $[\bar{D}]$ is defined by

$$[\bar{D}] = [T_1]^{-1}[D][T_2]. \qquad (A.25)$$

The finite element used is formulated based on linear elasticity and the theory of minimum potential energy. Material nonlinearities may be introduced as pseudo-loads acting on the elastic body. This technique is discussed in Chapter 3.

The total potential energy, Π, of a given finite element is the sum of the strain energy, U, and the work of the external loads, V. In the following developments the matrix notation will be dropped and index notation used. The strain energy U of the element is

$$U = \frac{1}{2} \int_\Omega \sigma_{ij}\epsilon_{ij}^e d\Omega \qquad (A.26)$$

where

σ_{ij} is the stress tensor in global (x,y,z) axes

ϵ_{ij}^e is the elastic strain tensor in global (x,y,z) axes

Ω is the volume of the element.

If we introduce the initial strain tensor ϵ_{ij}^o, (A.26) becomes

$$U = \frac{1}{2} \int_{\Omega} \sigma_{ij}(\epsilon_{ij} - \epsilon_{ij}^{o}) d\Omega \qquad (A.27)$$

where ϵ_{ij} is the total strain tensor. The initial strains ϵ_{ij}^{o} may be due to thermal expansion,

$$\epsilon_{ij}^{o\,t} = \alpha_{ij}\theta \qquad (A.28)$$

where

α_{ij} is the matrix of thermal expansion coefficients

θ is the temperature change from some reference state.

Initial strains may also be due to moisture expansion

$$\epsilon_{ij}^{o\,m} = \beta_{ij}\mu \qquad (A.29)$$

where

β_{ij} is the matrix of moisture expansion coefficients

μ is the moisture concentration.

Initial strains may also be used to include material nonlinearities (either static or time dependent). The initial strain method for nonlinear analysis is discussed in the text by Desai and Abel [50]. With the inclusion of initial stresses, σ_{ij}^{o}, the linear elastic constitutive equations become

$$\sigma_{ij} = \bar{D}_{ij}\epsilon_{ij}^{e} + \sigma_{ij}^{o} \qquad (A.30)$$

where $\bar{D}_{ij}$ is as defined by (A.25) and the initial stresses may be a residual stress field due to some previous loading. Inserting (A.30) into (A.27),

$$U = \frac{1}{2} \int_{\Omega} [(\epsilon_{kj} - \epsilon_{kj}^{o})\bar{D}_{ik}(\epsilon_{ij} - \epsilon_{ij}^{o}) + 2\sigma_{ij}^{o}(\epsilon_{ij} - \epsilon_{ij}^{o})] d\Omega \qquad (A.31)$$

and

$$U = \frac{1}{2} \int_\Omega [\epsilon_{kj}\bar{D}_{ik}\epsilon_{ij} + \epsilon^\circ_{kj}\bar{D}_{ik}\epsilon^\circ_{ij} - 2\epsilon_{kj}\bar{D}_{ik}\epsilon^\circ_{ij} + 2\sigma^\circ_{ij}\epsilon_{ij} - 2\sigma^\circ_{ij}\epsilon^\circ_{ij}]d\Omega \quad (A.32)$$

The potential of the external loads, V, is

$$V = -q_i Q_i \quad (A.33)$$

where

q_i is the vector of nodal displacements

Q_i is the applied mechanical load vector.

The total potential energy, π, of the element is

$$\pi = U + V \quad (A.34)$$

where U and V are given by (A.32) and (A.33), respectively. Converting (A.32) and (A.33) to vector-matrix notation and inserting into (A.34),

$$\pi = \frac{1}{2} \int_\Omega [\lfloor\epsilon\rfloor[\bar{D}]\{\epsilon\} + \lfloor\epsilon^\circ\rfloor[\bar{D}]\{\epsilon^\circ\} - 2\lfloor\epsilon\rfloor[\bar{D}]\{\epsilon^\circ\} + 2\lfloor\epsilon\rfloor\{\sigma^\circ\} - 2\lfloor\sigma^\circ\rfloor\{\epsilon^\circ\}]d\Omega - \lfloor q\rfloor\{Q\}.$$
$$(A.35)$$

Using (A.10) in (A.35),

$$\pi = \frac{1}{2} \int_\Omega [\lfloor q\rfloor[B]^T[\bar{D}][B]\{q\} + \lfloor\epsilon^\circ\rfloor[\bar{D}]\{\epsilon^\circ\} - 2\lfloor q\rfloor[B]^T[\bar{D}]\{\epsilon^\circ\}$$

$$+ 2\lfloor q\rfloor[B]^T\{\sigma^\circ\} - 2\lfloor\sigma^\circ\rfloor\{\epsilon^\circ\}]d\Omega - \lfloor q\rfloor\{Q\}. \quad (A.36)$$

Taking the variation of π with respect to the unknown nodal displacements $\{q\}$ and setting to zero,

$$\delta\pi = 0 = \frac{1}{2} \int_\Omega (2\lfloor\delta q\rfloor[B]^T[\bar{D}][B]\{q\} - 2\lfloor\delta q\rfloor[B]^T[\bar{D}]\{\epsilon^\circ\}$$

$$+ 2\lfloor\delta q\rfloor[B]^T\{\sigma^\circ\})d\Omega - \delta\lfloor q\rfloor\{Q\}. \quad (A.37)$$

Rearranging (A.37),

$$[\delta q][\int_\Omega ([B]^T[\bar{D}][B]\{q\} - [B]^T[\bar{D}]\{\epsilon^\circ\} + [B]^T\{\sigma^\circ\})d\Omega - \{Q\}] = 0. \quad (A.38)$$

Since the [δq] are arbitrary variations, the quantity inside the
square brackets must vanish. Hence

$$\int_\Omega ([B]^T[\bar{D}][B]\{q\})d\Omega = \{Q\} + \int_\Omega [B]^T[\bar{D}]\{\epsilon^\circ\}d\Omega$$

$$- \int_\Omega [B]^T\{\sigma^\circ\}d\Omega. \qquad (A.39)$$

Defining the element stiffness matrix [k] by

$$[k] = \int_\Omega [B]^T[\bar{D}][B]d\Omega, \qquad (A.40)$$

(A.39) becomes

$$[k]\{q\} = \{Q\} + \int_\Omega [B]^T[\bar{D}]\{\epsilon^\circ\}d\Omega - \int_\Omega [B]^T\{\sigma^\circ\}d\Omega. \qquad (A.41)$$

The last two terms in (A.41) represent the pseudo-loads necessary to
account for the effects of initial strains and initial stresses. The
equations (A.41) are the linear load-displacement relations for a single
element. For an assemblage of elements, the equations (A.41) are
"assembled" by superposition. This technique is detailed in the text
by Bathe and Wilson [63].

The integrations required in the evaluation of (A.41) are computed
by Gaussian quadratures using a 4x4x2 rule. The integrations to
compute the element stiffness matrix will be discussed as an example.
Gaussian quadrature is discussed in detail in the text by
Scarborough [77]. Considering again equation (A.40),

$$[k] = \int_\Omega [B]^T[\bar{D}][B]d\Omega. \qquad (A.40)$$

When mapped into the local ξ,n,ζ coordinate system,

$$d\Omega = |J| d\xi d\eta d\zeta \qquad (A.42)$$

where $|J|$ is the determinant of the Jacobian $[J]$. The limits of the integration are -1 to +1 in all directions. Equation (A.40) becomes

$$[k] = \int_{-1}^{1} \int_{-1}^{1} \int_{-1}^{1} [B]^T [\bar{D}][B]|J| d\xi d\eta d\zeta \qquad (A.43)$$

$$= \int_{-1}^{1} \int_{-1}^{1} \int_{-1}^{1} G(\xi,\eta,\zeta) d\xi d\eta d\zeta.$$

The coordinates (a_i, b_j, c_k) of the 32 Gauss points are

$$a_i = \pm.86113, \pm.33998$$
$$b_j = \pm.86113, \pm.33998 \qquad (A.44)$$
$$c_k = \pm.57735$$

The corresponding weighting functions (H_i, H_j, H_k) are

$$H_i = .34785 \text{ (for } \pm.86113\text{)}, .65214 \text{ (for } \pm.33998\text{)}$$

$$H_j = .34785 \text{ (for } \pm.86113\text{)}, .65214 \text{ (for } \pm.33998\text{)} \qquad (A.45)$$

$$H_k = 1.0 \text{ (for } \pm.57735\text{)}.$$

Appling the rules of Gaussian quadratures,

$$[k] = \sum_{i=1}^{4} \sum_{j=1}^{4} \sum_{k=1}^{2} H_i H_j H_k G(a_i, b_j, c_k) \qquad (A.46)$$

where $G(\xi,\eta,\zeta) = [B]^T [\bar{D}][B]|J|$.

We note at this point that $[k]$ is a 72x72 matrix which is symmetric.

The other volume integrals required in (A.41) are similarly evaluated.

The result of the assembly process is a system of n linear

algebraic equations, where n is the total number of degrees of freedom of the finite element assemblage. Before imposition of boundary conditions sufficient to prevent rigid body motion, the system is indeterminate. After imposition of boundary conditions, the global stiffness matrix [K] is symmetric, banded, and positive definite. Once all the terms in (A.41) are evaluated, the nodal displacement vector {q} for the linear elastic problem is computed by inversion of the global stiffness matrix. Thus, for linear elasto-static problems,

$$\{q\} = [k]^{-1}(\{Q\} + \int_\Omega [B]^T[D]\{\epsilon^\circ\}d\Omega - \int_\Omega [B]^T\{\sigma^\circ\}d\Omega). \quad (A.47)$$

In practice, the global stiffness matrix is not actually inverted. The system of equations is generally solved by some triangularization and backsubstitution process. Bathe and Wilson [63] present a review of several commonly used equation solution techniques.

For a nonlinear analysis using an incremental intial strain technique, Equ. (A.41), in the absence of initial stresses, becomes for the kth increment

$$[K]\{\Delta q\}^k = \{\Delta Q\}^k \quad (A.48)$$

where

$$\{\Delta Q\}^k = \{\Delta Q\}^k + \{\Delta Q^\theta\}^k + \{\Delta Q_0^m\}^k + \{\Delta Q_0^p\}^{k-1} + \{R_0\}^{k-1} \quad (A.49)$$

and

$$[K] \quad = \text{stiffness matrix}$$

$\{\Delta Q\}^k$ = applied force increment

$\{\Delta Q_0^T\}^k$ = incremental temperature pseudoload

$\{\Delta Q_0^m\}^k$ = incremental moisture pseudoload

$\{\Delta Q_0^p\}^{k-1}$ = incremental plasticity pseudoload from prior step

$\{R_0\}^{k-1}$ = total equilibrium residual at end of prior step.

The incremental plasticity pseudoload is designated (k-1) since it is computed (see Chapter 3) using the plastic strain increment computed during the $(k-1)^{th}$ increment. The residual is computed from a total equilibrium check at the end of the $(k-1)^{th}$ increment, and is given by

$$\{R\}^{k-1} = [K]\left(\sum_{i=1}^{k-1} \{\Delta q\}^i\right) - \sum_{i=1}^{k-1} \{\Delta Q\}^i \qquad (A.50)$$

and represents a correction which compensates for any errors in total equilibrium which may have existed at the end of step (k-1). The mechanics of computing the various pseudoloads are discussed in detail in Chapter 3.

APPENDIX B

COMPUTER IMPLEMENTATION

APPENDIX B

COMPUTER IMPLEMENTATION

A computer program was written to test the theoretical developments previously presented. The program is called Nonlinear Analysis of Laminated Composites (NALCOM). This chapter presents a description of the cap⋅ʰ⋅lit⋅es of NALCOM as well as serves as a user's manual. Considerable effort was expended in choosing mnemonics consistent with the theoretical developments. The program is as modular as was deemed practical. Program development was done on the CDC 6700 computer at the United States Naval Surface Weapons Center, Dahlgren, Virginia. The program was later converted and run on the IBM S370/3303 at Virginia Polytechnic Institute and State University, Blacksburg, Virginia. Due to core limitations of the CDC system, considerable equivalencing is used, many parameters are passed in subroutine calls, and scratch files are used for storage of matrices, material properties, etc.

B.1 Summary of Capabilities

The only finite element currently implemented in NALCOM is the 24 node isoparametric element (Figure A.1) with transversely isotropic material properties. All capabilities are available for transversely isotropic materials. The nonlinear load-deflection equations are solved incrementally. Any combination of the three load types (with the exception of specified displacements with plasticity) may be applied to the finite element model, but only one type of load may be applied per load step. As with any nonlinear analysis program,

the choice of load step is left to the analyst.   Prospective users are encouraged to read and understand the theoretical basis of NALCOM. Violation of assumptions by an improper choice of load step will result in erroneous results.   NALCOM was developed as a research tool, and while some error checking is done, other operations are not monitored for quality.   To paraphrase, "If you don't know how it works, don't fool with it!"

B.2   Program Description

NALCOM is written in ANSI standard FORTRAN and consists of approximately 4000 source statements, may of which are comments.   A listing of the program is available from the author.   Core requirement for in-core solution on a CDC 6000 series computer is approximately 100000 octal words plus the number of stiffness matrix elements stored. The number of elements (or d.o.f.) which may be used in the finite element model is based on the available storage, number of element groups (see input description), and the bandwidth of the global elastic stiffness matrix.   The author has used a modified version of the NASTRAN preprocessor BANDIT [64] to minimize bandwith prior to any runs on the problems reported.   Due to the use of the skyline column storage algorithm of Bathe and Wilson [63], minimization of mean bandwith is important, since smaller mean bandwidths require less core storage and fewer arithmetic operations for triangularization and back-substitution.

NALCOM is specifically designed for nonlinear analysis. Consequently, linear analyses may be somewhat inefficient.   For

example, cooling of a linear elastic material with constant properties followed by load application would ordinarily be handled by superposition in one calculation. NALCOM, however, would require two load steps, first a cooling step, followed by a loading step. Such inefficiency would not be acceptable in a production code, but is believed acceptable in a research tool. Other inefficiencies include the carrying of all 36 terms of elasticity and compliance matrices. Other quantities, such as the B matrices (strain-displacement transformation), determinant of the Jacobian for the isoparametric mapping, stress and strain transformation matrices are stored in core or on scratch files to avoid recomputation.

The starting point for the development of NALCOM was the sample program STAP given in the text by Bathe and Wilson [65]. The concept of element groups, with properties stored on disk when not in use; the skyline column storage scheme utilizing the efficient equation solver COLSOL; and the semi-dynamic storage allocation technique all made STAP a perfect starting point. For details on the skyline column storage scheme and the routine, the reader is directed to the text by Bathe and Wilson [63]. The program STAP was modified to use the 24 node isoparametric element. Additional modifications were made, in a step-by-step manner, to introduce all capabilities. Checkout has included a wide variety of problems, some of which are discussed in Chapter 5. Complete checkout of all options for all possible loading combinations, material models, and geometries is beyond the scope of the present study. It is possible that future NALCOM users will encounter some

difficulties. This possibility places additional emphasis on the need for understanding of the theoretical basis of the program.

The high speed storage allocation for NALCOM is shown in Figures B.1. Note the similarity to Figure 6.6 of Reference 63. The significance of the arrays which are input is noted in the input guide presented later in this Appendix. For detailed discussions of the element connectivity array LM, the skyline diagonal pointer array MAXA, and the column height vector MHT, the reader is directed to the text by Bathe and Wilson [63]. The variable ITWO is an aid to machine-to-machine conversion. It has a value of one for single precision and two for double precision. A flow chart for NALCOM is shown in Figure B.2. Table B.2 is a list, along with a brief description, of the scratch files used.

Several comments are necessary regarding the implementation of the temperature dependent material properties and plasticity. All temperature dependency relationships are input as piecewise linear with a maximum of ten points (nine linear segments). The maximum of ten is easily changed by changing dimensions and loop ranges in the appropriate reading and interpolating subroutines. A minimum of two points is required, and if temperature dependent elastic constants are declared (ITLOAD.GE.2), all properties are automatically temperature dependent. Properties at points between the extremes are linearly interpolated on the appropriate segment. A temperature lower than the lowest input temperature will result in properties evaluated at the lowest input. Similarly, a temperature higher than the highest input

Address in Blank Common	Storage Required	Array
N1=1	3*NUMNP	ID array
N2	NUMNP*ITWO	X-coordinate array
N3	NUMNP*ITWO	Y-coordinate array
N4	NUMNP*ITWO	Z-coordinate array
N5		

FIGURE B-1a. INPUT PHASE STORAGE ALLOCATION

Address in Blank Common	Storage Required	Array
N1=1	3*NUMNP	ID array
N2	NEQ+1	MAXA array
N3	NWK*ITWO	Global stiffness matrix K
N4	NEQ*ITWO	R-load vector or DU- displacement vector
N5	MAXEST	Element group information
N6		

FIGURE B-1b. K ASSEMBLY, SOLUTION, STRESS COMPUTATION STORAGE ALLOCATION

Address in Blank Common	Storage Required	Array
N1=1	3*NUMNP	ID array
N2	NEQ+1	MAXA array
N3	NWK*ITWO	Global stiffness matrix K
N4	NEQ*ITWO	R-load vector
N5	MAXEST	Element group information
N6	NLOAD	NOD- loaded nodes
N7	NLOAD	IDIRN- load directions
N8	NLOAD*ITWO	FLOAD- load magnitudes
N9		

FIGURE B-1c. LOAD VECTOR GENERATION PHASE STORAGE ALLOCATION

Address in Blank Common	Storage Required	Array
N1=1	3*NUMNP	ID array
N2	NEQ+1	MAXA array
N3	NWK*ITWO	Global stiffness matrix K
N4	NEQ*ITWO	R-load vector
N5	MAXEST	Element group information
N6	NBC	NOD- nodes with specified displacements
N7	NBC	IDIRN-direction of specified displacements
N8	NBC*ITWO	BC- boundary condition vector
N9		

FIGURE B-1d. SPECIFIED DISPLACEMENT DEFINITION PHASE STORAGE ALLOCATION

Address in Blank Common	Storage Required	Array
N1=1	3*NUMNP	ID array
N2	NEQ+1	MAXA array
N3	NWK*ITWO	Global stiffness matrix K
N4	NEQ*ITWO	R-load vector
N5	NEQ*ITWO	BC- boundary condition vector
N6		

FIGURE B-1e. SPECIFIED DISPLACEMENT IMPOSITION PHASE STORAGE ALLOCATION

Address in Blank Common	Storage Required	Array
N101	5*ITWO	E- room temperature elastic constants
N102	6*ITWO	ALP- room temp thermal expansion coefficients
N103	6*ITWO	not currently used
N104	ITWO	ANG- ply orientation, degrees
N105	36*ITWO	D- room temp elasticity, global coordinates
N106	36*ITWO	D12- room temp elasticity matrix, material coordinates
N107	36*ITWO	COM- room temp compliance matrix, global coordinates
N108	36*ITWO	COM12- room temp compliance matrix, material coordinates
N109	36*ITWO	T1- stress transformation matrix
N110	36*ITWO	T1I- inverse of T1
N111	36*ITWO	T2- strain transformation matrix
N112	36*ITWO	T2I- inverse of T2
N113	72*NUME*ITWO	EGXYZ- element group coordinate array
N114	72*NUME	LM- element connectivity array
N115	NEQ*ITWO	V- scratch area
N116		

FIGURE B-1f. ELEMENT GROUP INFORMATION STORAGE ALLOCATION
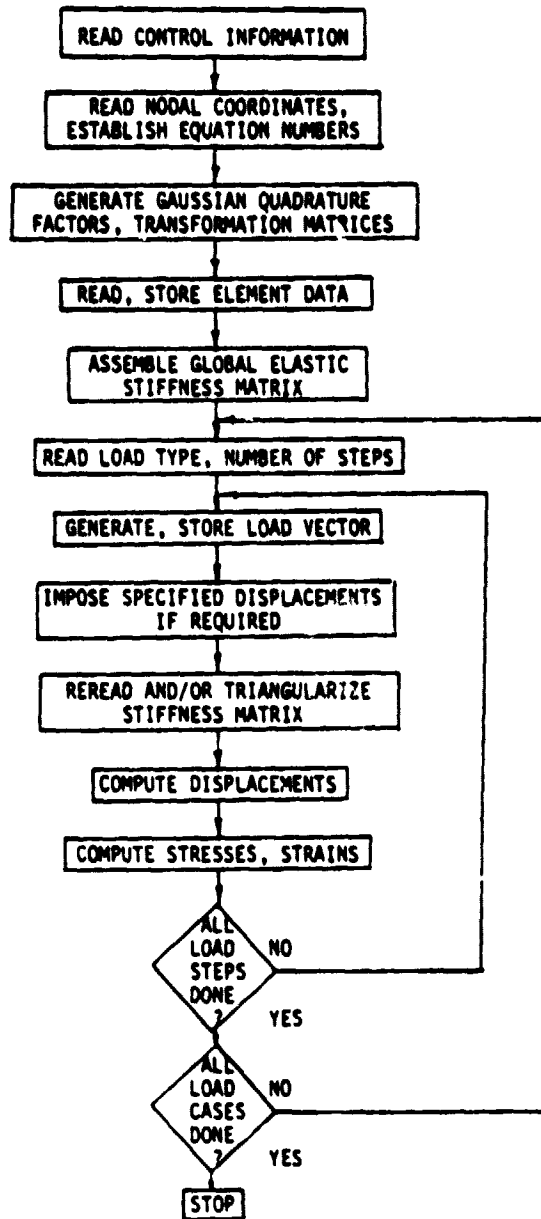
FIGURE B.2. FLOW CHART FOR NALCOM

TABLE B-1. NALCOM SCRATCH FILE ASSIGNMENTS

File Name	Unit Number	Use
IELMNT	1	element group information
ILOAD	2	incremental load vector
IBCTAP	3	specified displacement vector
ICTAPE	4	coordinate transformation matrices
IIN	5	input device
IOUT	6	output device
ISTRS	8 or 18	stress information
ISTRN	9 or 19	strain information
ISTF	14	global elastic stiffness matrix
IALPH	15	thermal expansion coefficients
IPCR	16	percent retention data
IRAMOS	17	Ramberg-Osgood coefficients
ISTRSO	8 or 18	stress information
ISTRNO	9 or 19	strain information
IDISP	20	total displacement vector
IPLAS	21 or 22	plasticity data
IPLASO	21 or 22	plasticity data
IBTAPE	23	B (strain-displacement transformation) and DETJ (Jacobian determinant) data
ISTFT	24	total mechanical force vector
IPLTAP	25	plasticity pseudoload vector

will result in properties <u>at</u> the highest input.

Linear interpolation is also used to compute the fraction of the step which was elastic for an element undergoing the transition from elastic to plastic behavior. The interpolation is done on the numerical value of Hill's yield condition evaluated at the beginning and end of the load step. Since Hill's criterion is quadratic in stress, this interpolation is accurate only for relatively small increments. Also, too many Gauss points should not be allowed to transition during a single load step due to mutual influence of the Gauss points on their neighbors.

B.3 Program Input

This section details the inputs to NALCOM. It should be noted that no preprocessing is currently implemented. This is due largely to core limitations of the CDC 6700 on which the program was developed. Also, due to the previously mentioned importance of bandwidth, it is recommended that grids should be generated by some other means and the bandwidth minimized before use of NALCOM.

B.3.1 Units

There is no dependence on the system of units used in NALCOM. Any set of consistent units may be used, but care must be taken that consistency is present. The one exception to this rule is that the ply orientation angle, ANG, must be input in degrees.

B.3.2 Inputs, Formats, Mnemonics, and Description

I. TITLE CARD (20A4)

Note	Columns	Variable	Description
(1)	1-80	HED(20)	80 columns of alphanumeric title info

NOTES -

(1) Two blank cards must be input at the end of the data deck for normal termination

II. MASTER CONTROL CARD (7I5)

Note	Columns	Variable	Description
(1)	1-5	NUMNP	Total number of nodal points, .EQ.0 for program stop
(2)	6-10	NUMEG	Number of element groups, .GT.0
(3)	11-15	NLCASE	Number of load cases, .GT.0
	16-20	MODEX	Solution mode. .EQ.1 execution, no plasticity .EQ.2 execution, with plasticity
	21-25	IPRINT(1)	Equation number print flag, .EQ.0 print equation numbers corresponding to nodal d.o.f. .EQ.1 no print equation numbers
	26-30	IPRINT(2)	Gauss point print flag .EQ.0 Compute and print Cartesian coordinates of Gauss points .EQ.1 No compute
(4)	31-35	NITER	Maximum number of equilibrium iterations per increment. Set .EQ.0 for no iteration.

NOTES -

(1) Controls number of cards of Type IV to be read

(2) An element group is a convenient collection of elements, all of which must have the same fiber orientation for orthotropic materials

(3) Number of unique load types or magnitudes to be applied

(4) Convergence occurs when the <u>change</u> in the Euclidean norm of the residual from the last iteration is less than 0.001 times the Euclidean norm of the incremental load vector

III. STRESS FREE TEMPERATURE (F10.0)

Note	Columns	Variable	Description
	1-10	SFT	Laminate stress free temperature or reference temperature for thermal expansion

IV. INPUT SCALE FACTORS (3F10.0)

Note	Columns	Variable	Description
	1-10	XFAC	Input x coordinates will be multiplied by this quantity
	11-20	YFAC	Input y coordinates will be multiplied by this quantity
	21-30	ZFAC	Input z coordinates will be multiplied by this quantity

V. NODAL POINT CARDS (4I5,3F10.0)

Note	Columns	Variable	Description
(1)	1-5	N	Nodal point number, .GE.0 and .LE.NUMNP
(2)	6-10	ID(1,N)	X translation code
	11-15	ID(2,N)	Y translation code
	16-20	ID(3,N)	Z translation code
	21-30	X(N)	X coordinate
	31-40	Y(N)	Y coordinate
	41-50	Z(N)	Z coordinate

NOTES -

(1) Data must be defined for all nodal points. Nodes may be input in any order.

(2) Translation codes define whether a node is free to move. ID(M,N)=0 means node N may translate in the M direction ID(M,N)=1 means node N is fixed in the M direction. Equation numbers are not assigned to degrees of freedom with ID=1. DOF with ID=1 are used to define rigid boundaries, symmetry lines, etc. Note that sufficient fixities must be present to prevent rigid body motion of the structure.

(3) The XYZ coordinate system is hereafter referred to as the global, or laminate coordinate system.

VI. ELEMENT GROUP DATA

The following sequence of cards is present for each of the NUMEG element groups. The only element currently implemented is the 24 node isoparametric element. Note that each element group may be a different material, different thermal, plasticity behavior, etc.

VI.1 Element Group Control Card (5I5)

Note	Columns	Variable	Description
	1-5	NPAR(1)	Enter the number 1
(1)	6-10	NPAR(2) or NUME	Number of elements in this group .GE.1
	11-15	NPAR(3) or ITLOAD	Thermal expansion type .EQ.0 No thermal effects .EQ.1 Constant coefficients of thermal expansion .EQ.2 First order nonlinear thermal effects .EQ.3 Second order nonlinear plus first order nonlinear thermal effects
	16-20		Not currently in use
	21-25	NPAR(5) or IDEN	Element group identity flag, .EQ.0 elements may be geometrically different .EQ.1 elements are geometrically identical

NOTES -

(1) Element numbers begin with 1 and end with NUME within each element group. Tnere is no limit, other than available core, on the value of NUME.

VI.2 ELASTIC PROPERTIES AND PLY ORIENTATION (6F10.0)

Note	Columns	Variable	Description
(1)	1-10	E(1)	Longitudinal Young's modulus, E_{11}
	11-20	E(2)	Transverse Young's modulus, E_{22}
	21-30	E(3)	Shear modulus, G_{12}
	31-40	E(4)	Major Poisson's ratio, ν_{12}
	41-50	E(5)	Minor Poisson's ratio, ν_{23}
	51-60	ANG	Ply orientation (angle) measured from X- (global) to 1- (longitudinal material) axis, DEGREES (see Figure B.3)

NOTES -

(1) Properties are input as room temperature (RT) values
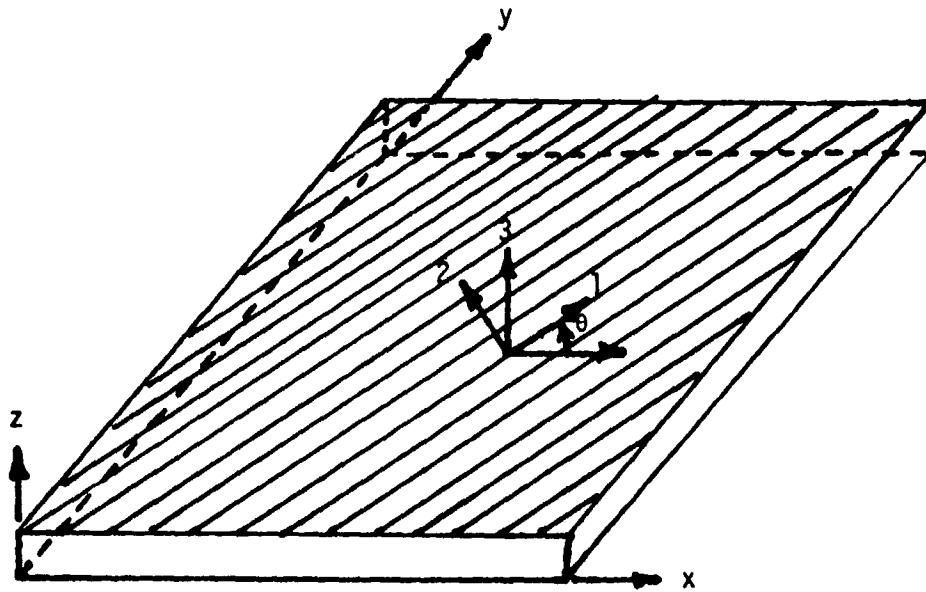
FIGURE B.3   RELATIONSHIP OF GLOBAL AND MATERIAL COORDINATE SYSTEMS

VI.3 RAMBERG-OSGOOD COEFFICIENTS

Two forms of Ramberg-Osgood coefficient inputs are available, the first constant with respect to temperature (ITLOAD.LE.1) and the other variable with respect to temperature (ITLOAD.GE.2). Recall the Ramberg-Osgood form is $\epsilon = \frac{\sigma}{E} + \beta\sigma^n$.

Ramberg-Osgood coefficients are read only if MODEX.EQ.2.

VI.3.1 Constant Ramberg-Osgood Coefficients (6E13.5)

These cards are read if ITLOAD.EQ.1. Three cards are required, the first for the material longitudinal direction, the second for the transverse direction, and the third for shear. Transition from n_1 and β_1 to n_2 and β_2 occurs at σ^*.

Note	Column	Variable	Description
(1)	1-13	ROB(I)	Ramberg-Osgood coefficient β_1
	14-26	RON(I)	Ramberg-Osgood coefficient n_1
	27-39	YIE(I)	Yield stress in I direction
	40-52	ROB(I+4)	Ramberg-Osgood coefficient β_2
	53-65	RON(I+4)	Ramberg-Osgood coefficient n_2
	66-78	YIE(I+4)	Transition stress, σ^*

NOTES -

(1) Directions are given by

I=1 longitudinal direction
I=2 transverse direction
I=3 shear direction

VI.3.2 Temperature Dependent Ramberg-Osgood Coefficients

These cards are read if ITLOAD.GE.1. Temperature dependent Ramberg-Osgood coefficients and yield strengths are input at up to ten temperatures, as specified on the following card.

VI.3.2.1 Number of Temperatures for Ramberg-Osgood Input (I5)

Note	Column	Variable	Description
	1-5	NTEMS	Number of temperatures for R-O and yield strength input, .GE.2 and .LE.10

NTEMS sets of the four R-O and yield data cards are required, in order of ascending temperature.

VI.3.2.2 Temperature for R-O and Yield Strength Input (F10.0)

Note	Column	Variable	Description
(1)	1-10	TEMP	Temperature

VI.3.2.3 R-O and Yield Data (6E13.5)

Note	Column	Variable	Description
(1)	1-13	ROB(I)	β_1 at TEMP
	14-26	RON(I)	n_1 at TEMP
	27-39	YIE(I)	Yield strength at TEMP
	40-52	ROB(I+4)	β_2 at TEMP
	53-65	RON(I+4)	n_2 at TEMP
	66-78	YIE(I+4)	σ^* at TEMP

NOTES -

(1) Three of these cards are required at each value of TEMP, one for longitudinal, transverse, and shear behavior, in that order. If a bilinear R-O fit is not desired, leave Columns 40-78 blank.

VI.4 THERMAL EXPANSION COEFFICIENTS

Thermal expansion coefficients are read only if ITLOAD.GT.0. If ITLOAD.EQ.1, properties are constant. If ITLOAD.GE.2, properties vary with temperature, and piecewise linear (up to ten po'nts) curves are input.

VI.4.1 Constant Thermal Expansion Coefficients (2F10.0)

Read if ITLOAD.EQ.1.

Note	Column	Variable	Description
	1-10	ALP(1)	Longitudinal thermal expansion coefficient
	11-20	ALP(2) =ALP(3)	Transverse thermal expansion coefficient

VI.4.2 Temperature Dependent Thermal Expansion Coefficients

Read if ITLOAD.GT.1.

VI.4.2.1 Number of Temperatures for Thermal Expansion Coefficient Input (I5)

Note	Column	Variable	Description
	1-5	NTEMS	Number of temperatures for thermal expansion input, .GE.2 and .LE.10

VI.4.2.2 Variable Thermal Expansion Coefficient Cards (3F10.0) NTEMS cards are required, in order of ascending temperature.

Note	Column	Variable	Description
	1-10	ALP(1)	Longitudinal thermal expansion coefficient at TEMP
	11-20	ALP(2) =ALP(3)	Transverse thermal expansion coefficient at TEMP
	21-30	TEMP	Temperature

VI.5 FRACTION RETENTION OF ROOM TEMPERATURE PROPERTIES

If ITLOAD.GE.2, elastic coefficients are assumed to be variable
with temperature. This information is input as the fraction of room
temperature (RT) properties retained at a given temperature. Piecewise
linear curves of up to ten points are used.

VI.5.1 Number of Temperatures for Fraction Retention Input (I5)

Note	Column	Variable	Description
	1-5	NTEMS	Number of temperatures for fraction retention input, .GE.2 and .LE.10

VI.5.2 Fraction Retention Data (6F10.0)

Note	Column	Variable	Description
	1-10	TEMP	Temperature
	11-20	PE1	Fraction retention of E_{11} at TEMP
	21-30	PE2	Fraction retention of E_{22} at TEMP
	31-40	PG12	Fraction retention of G_{12} at TEMP
	41-50	PGNU12	Fraction retention of ν_{12} at TEMP
	51-60	PGNU23	Fraction retention of ν_{23} at TEMP

VI.6 ELEMENT CONNECTIVITY INFORMATION

Two cards are required for each element. Elements are numbered from ONE (1) to NUME within each element group, and must be input in increasing order.

VI.6.1 Element Card 1 (13I5)

Note	Column	Variable	Description
	1-5	N	Element number, .GE.1 and .LE.NUME
	6-10	NCON(I) I=1,12	First 12 node numbers of element N
	11-15		(See Figure A.1 for input order)
	16-20		
	etc.		

VI.6.2 Element Card 2 (5X,12I5)

Note	Column	Variable	Description
	1-5	---	Leave blank
	6-10	NCON(I) I=13,24	Last 12 node numbers for element N
			(See Figure A.1)

VII. LOAD CASE DATA

Data from this section must be present for each of the NLCASE load cases. Note that only one type of load increment (force, temperature change, or specified displacement) may be applied in a load case. Also note that specified displacements are incompatible with plasticity as implemented in NALCOM.

VII.1 Load Case Control (3I5)

Note	Column	Variable	Description
	1-5	LDTYP	Load type, =1, concentrated force =2, temperature change =4, specified displacement
	6-10	NSTP	Number of equal steps of this load type to be applied in this load case
	11-15	IPRINT(3)	Print flag, =0, print displacement, strain, and stress information for every load step of this load case =1, only print information for last load step of this load case

VII.2   Concentrated Force Load (LDTYP.EQ.1)

VII.2.1   Number of Loaded Degrees of Freedom (I5)

Note	Column	Variable	Description
	1-5	NLOAD	Number of loaded degrees of freedom

VII.2.2   Concentrated Force Card(s) (2I5,F10.0)
         NLOAD of these cards are required.

Note	Column	Variable	Description
	1-5	NOD	Node to which force is applied
	6-10	IDIRN	Direction in which force acts, =1, X-direction =2, Y-direction =3, Z-direction
	11-20	FLOAD	Increment of load to be applied for each of the NSTP steps of this load case

VII.3   Temperature Increment (LDTYP.EQ.2) (F10.0)

Note	Column	Variable	Description
(1)	1-10	DTEMP	Temperature increment to be applied for each of the NSTP steps of this load case

NOTE -

(1) Only uniform temperatures are currently implemented, so all
     temperatures are constant through the entire structure.

VII.4 Specified Displacement Loads (LDTYP.EQ.4)

VI.4.1 Number of Degrees of Freedom with Specified
        Displacements (I5)

Note	Column	Variable	Description
	1-5	NBC	Number of degrees of freedom with specified displacements

VII.4.2 Specified Displacement Card (2I5,F10.0)
         NBC of these cards are required.

Note	Column	Variable	Description
(1)	1-5	NOD	Node to which specified displacement is applied
(2)	6-10	IDIRN	Direction of displacement =1, X-direction =2, Y-direction =3, Z-direction
(3)	11-20	DISP	Incremental displacement to be applied for each of the NSTP steps of this load case

NOTES -

(1) Specified displacement loads are not compatible with plasticity

(2) ID(IDIRN,NOD) must be nonzero, i.e. an equation must exist for this degree of freedom

(3) The value of DISP may be zero

B.4 Program Output

Printed output consists of an echo of the input data as it is
read, Cartesian coordinates of the Gauss points (for IPRINT(2).EQ.0),
stiffness matrix bandwidth information, nodal displacements, and
stress and strain data at the Gauss points. The amount of output is
controlled by the values in the IPRINT array. Strain output consists
of total strains at the Gauss points of each element. Strains are
output in the global (XYZ) and material (123) coordinate systems.
Plasticity output includes the global plastic strain increment, value
of Hill's yield function (YF) at the end of the step, the maximum
value Hill's yield condition has achieved (YFMAX), the fraction of
the load step which was elastic (PCEL), and the loading parameter
(LAMBDA). Also printed is an indicator (NYC), which has the following
meanings:

NYC = -1   Gauss point unloading elastically or reloading
            elastically toward subsequent yield

NYC = 0   Gauss point is, and has always been, elastic

NYC = 1   New (first step) yield or subsequent yield. Part
            of the step may have been elastic

NYC = 2   Prior plastic, continuing plastic flow.

The dominant direction of the plastic flow is denoted by the variable
IDOM.

It should be noted that no postprocessing is currently available.
Scratch files IDISP, ISTRS, and ISTRN, as well as others, are available
at the end of the run, and could be read by a postprocessor. A

technique of this type was used for generation of some of the plots in the body of the report.

APPENDIX C

YIELD AND PLASTICITY RELATIONS FOR ISOTROPIC MATERIALS

APPENDIX C

YIELD AND PLASTICITY RELATIONS FOR ISOTROPIC MATERIALS

The purpose of this appendix is to show how Hill's orthotropic yield function (equs. 3.22 and 3.23), equivalent stress (equ. 3.24), and equivalent plastic strain increment (equ. 3.27) reduce to the familiar von Mises relationships for isotropic materials. If these can be shown, the relationships 3.56-3.60 follow, since the same heuristic arguments made for orthotropic materials can also be advanced for isotropic materials.

Consider Hill's orthotropic yield function,

$$f(s_i) = F(S_2-S_3)^2 + G(S_3-S_1)^2 + H(S_1-S_2)^2$$

$$+ 2LS_{23}^2 + 2MS_{13}^2 + 2NS_{12}^2 = 1, \qquad (C.1)$$

where

$$2F = \frac{1}{Y^2} + \frac{1}{Z^2} - \frac{1}{X^2}$$

$$2G = \frac{1}{X^2} + \frac{1}{Z^2} - \frac{1}{Y^2}$$

$$2H = \frac{1}{X^2} + \frac{1}{Y^2} - \frac{1}{Z^2}$$

$$2L = \frac{1}{R^2} \qquad (C.2)$$

$$2M = \frac{1}{S^2}$$

$$2N = \frac{1}{T^2}$$

159

and X, Y, Z, R, S, and T are the yield strengths in the principal material directions 1, 2, 3, 23, 13, and 12, respectively. For an isotropic material,

$$X = Y = Z \qquad\qquad\text{(C.3)}$$

and

$$R = S = T. \qquad\qquad\text{(C.4)}$$

Also, Mendelson [38] shows that for a distortion energy theory of yielding,

$$R = \frac{X}{\sqrt{3}}. \qquad\qquad\text{(C.5)}$$

Therefore,

$$F = G = H = \frac{1}{2X^2} \qquad\qquad\text{(C.6)}$$

and

$$2L = 2M = 2N = \frac{3}{X^2} \qquad\qquad\text{(C.7)}$$

Substituting C.6 and C.7 into C.1 results in

$$f(s_i) = \frac{1}{2X^2}\,[(S_2-S_3)^2 + (S_3-S_1)^2 + (S_1-S_2)^2]$$

$$+ \frac{3}{X^2}\,(S_{23}^2 + S_{13}^2 + S_{12}^2) = 1, \qquad\qquad\text{(C.8)}$$

thus

$$f(s_i) = \frac{1}{X^2}\,[(S_2-S_3)^2 + (S_3-S_1)^2 + (S_1-S_2)^2$$

$$+ 6S_{23}^2 + 6S_{13}^2 + 6S_{12}^2] = 1, \qquad\qquad\text{(C.9)}$$

where X is the yield stress in simple tension. Note that C.9 is the familiar von Mises yield criterion for an isotropic material.

Next consider the effective stress, S^2 of equ. 3.24,

$$S^2 = \frac{3}{2(F+G+H)} [F(S_2-S_3)^2 + G(S_3-S_1)^2 + H(S_1-S_2)^2$$

$$+ 2LS_{23}^2 + 2MS_{13}^2 + 2NS_{12}^2]. \tag{C.10}$$

Note that S^2 is related to $f(s_i)$ by

$$S^2 = \frac{3}{2(F+G+H)} f(s_i). \tag{C.11}$$

Using C.6 and C.9 in conjunction with C.11 yields

$$S^2 = \frac{3}{2} [\frac{1}{2X^2}] \frac{1}{X^2} [(S_2-S_3)^2 + (S_3-S_1)^2 + (S_1-S_2)^2$$

$$+ 6S_{23}^2 + 6S_{13}^2 + 6S_{12}^2], \tag{C.12}$$

and

$$S^2 = (S_2-S_3)^2 + (S_3-S_1)^2 + (S_1-S_2)^2 + 6S_{23}^2 + 6S_{13}^2 + 6S_{12}^2. \tag{C.13}$$

Equation C.13 is the von Mises or effective stress for an isotropic material. Finally, consider the equivalent plastic strain increment of equ. 3.27,

$$d\bar{e}^P = \frac{2}{3} (F+G+H) \frac{F(Gde_{22}^P-Hde_{33}^P)^2}{(FG+GH+HF)^2}$$

$$+ \frac{G(Hde_{33}^P-Fde_{11}^P)^2}{(FG+GH+HF)^2} + \frac{H(Fde_{11}^P-Gde_{22}^P)^2}{(FG+GH+HF)^2}$$

$$\left[\frac{(de_{23}^P)^2}{8L} + \frac{(de_{13}^P)^2}{8M} + \frac{(de_{12}^P)^2}{8N} \right]^{\frac{1}{2}} \tag{C.14}$$

where de_{ij}^P $i \neq j$ have been converted to engineering shear strain. Substituting C.6 and C.7 into C.14 results in

$$d\bar{e}^P = \frac{2}{3} \left(\frac{3}{2X^2}\right) \left[\frac{\frac{1}{2X^2} [\frac{1}{2X^2}]^2 [(de_{22}^P - de_{33}^P)^2 + (de_{33}^P - de_{11}^P)^2 + (de_{11}^P - de_{22}^P)^2]}{(\frac{3}{4X^4})^2} \right.$$

$$\left. + \frac{4X^2}{3} [(de_{23}^P)^2 + (de_{13}^P)^2 + (de_{12}^P)^2] \right]^{\frac{1}{2}} \tag{C.15}$$

$$d\bar{e}^P = \frac{1}{X} \frac{2X^2}{9} \left[(de_{22}^P - de_{33}^P)^2 + (de_{33}^P - de_{11}^P)^2 + (de_{11}^P - de_{22}^P)^2 \right.$$

$$\left. + \frac{4X^2}{3} [(de_{23}^P)^2 + (de_{13}^P)^2 + (de_{12}^P)^2] \right]^{\frac{1}{2}} \tag{C.16}$$

$$d\bar{e}^P = \left[(de_{22}^P - de_{33}^P)^2 + (de_{33}^P - de_{11}^P)^2 + (de_{11}^P - de_{22}^P)^2 \right.$$

$$\left. + 6(de_{23}^P)^2 + 6(de_{13}^P)^2 + 6(de_{12}^P)^2 \right]^{\frac{1}{2}} \tag{C.17}$$

which is the same form of the equivalent plastic strain increment for an isotropic material, where the shear strains are engineering shear strains.

The relationships between Hill's orthotropic plasticity model and the von Mises (or distortion energy) theory for isotropic materials have been shown. The model developed in Chapter 3 can

be used for isotropic as well as orthotropic materials. Results from isotropic material analyses exhibit good experimental/analytical correlation, as shown in Figure 5.1.

Prof. Donald F. Adams
Dept. Of Mechanical Engineering
University Of Wyoming
Laramie, WY 82070

Dr. N. R. Adsit
General Dynamics Convair
P.O. Box 80837
San Diego, CA. 92138

Dr. Clifford J. Astill
Solid Mechanics Program
National Science Foundation
1800 G St. N.W.
Washington, D.C.

AVCO, Systems Division
Subsystems & Meth. Structures
201 Lowell Street
Wilmington, MA. 01887

Dr. J. A. Bailie
D81-12 Bldg. 154
Lockheed Missiles & Space Co,Inc
1111 Lockheed Way
Sunnyvale, CA. 94088

Dr. Charles W. Bert, Director
School Of Aerospace, Mechanical
  & Nuclear Engineering
The University Of Oklahoma
Norman, Oklahoma 73069

Dr. C. M. Blackmon
NSWC, Code K21
Dahlgren, VA 22448

Mr. Richard Boitnott
Mail Stop 190
Nasa-Langley Research Center
Hampton, VA. 23665

Mr. David Bowles
Mail Stop 188B
NASA-Langley Research Center
Hampton, Va. 23665

Dr. H. F. Brinson
ESM Dept.
Virginia Tech
Blacksburg, VA. 24061

Mr. Ernie Brooks
ESM Dept.
Virginia Tech
Blacksburg, VA. 24061

Dr. Micharl F. Card
Mail Stop 190
NASA-Langley Research Center
Hampton, VA 23665

Dr. C. Chamis
NASA-Lewis Research Center
2100 Brook Park Rd.
Cleveland, Ohio 44135

Dr. Paul A. Cooper
Mail Stop 190
NASA-Langley Research Center
Hampton, Va. 23665

Dr. Frank Crossman
Lockheed Research Lab
Org. 52-41, Bldg. 204
3251 Hanover Street
Palo Alto, CA. 94304

Dr. I. M. Daniel, Manager
IIT Research Institute
10 West 35 Street
Chicago, IL. 60616

Dr. John R. Davidson
Mail Code 188E
MD-Structural Integrity Branch
Langley Research Center
Hampton, VA. 23665

Dr. John G. Davis, Jr.
Mail Stop 188A
Langley Research Center
Hampton, VA. 23665

Mr. Jerry W. Deaton
Mail Stop 188A
NASA-Langley Research Center
Hampton, VA. 23665

Mr. H. Benson Dexter
Mail Stop 188A
NASA-Langley Research Center
Hampton, VA. 23665

Mr. O. Earl Dhonau
Section 2-53400
Vought Corp.
P.O. Box 5907
Dallas, TX. 75222

Dr. M. P. Duggan
52-33/205/2
Lockheed Palo Alto Lab.
3251 Hanover St.
Palo Alto, Ca. 94304

Prof. John C. Duke, Jr.
ESM Dept.
Virginia Tech
Blacksburg, VA. 24061

Prof. George J. Dvorak
Civil Engineering
University of Utah
Salt Lake City, UT. 84112

Dr. Wolf Elber
Mail Stop 188E
NASA-Langley Research Center
Hampton, VA. 23665

Mr. Dave Erb
Aero & Ocean Engr. Dept.
Virginia Tech
Blacksburg, VA. 24061

Mr. Gary L. Farley
Mail Stop 188A
NASA-Langley Research Center
Hampton, VA. 23665

Mr. Larry Fogg
Lockheed-California
Dept. 7572, Bldg. 63, Plant A1
P.O. Box 551
Burbank, CA. 91520

Dr. R. L. Foye
USAMRDL
SAUDLAS (207-5)
Moffet Field, CA. 94035

Dr. D. Frederick
ESM Dept.
Virginia Tech
Blacksburg, VA. 24061

Mr. Samuel P. Garbo
McDonnell Aircraft Co.
Bldg. 34, Post 350
St. Louis, MO. 63166

Mr. Ramon Garica
Mail Stop 190
NASA-Langley Research Center
Hampton, VA. 23665

Prof. Jim Goree
Dept. of Mechanical Engr.
Clemson University
Clemson, S.C. 29631

Dr. Login B. Greszczuk
McDonnell Douglas Astr. Co.
5301 Bolas Avenue
Huntington Beach, CA. 92647

Dr. Hayden O. Griffin, Jr.
B .F. Goodrich
500 South Main St.
D/6145, B/10E
Akron, Ohio 44318

Mr. Glen C. Grimes
Dept. 3852/82
Northrop Corp., Aircraft Div.
3901 West Broadway
Hawthorne, CA. 90250

Dr. H. T. Hahn
Washington University
St. Louis, MO. 63130

Dr. J. C. Halpin
Flight Dynamics Lab
Wright-Patterson AFB
Ohio 45433

Professor Z. Hashin
School of Engineering
Solid Mech. Materials & Struc.
Tel Aviv University
Tel Aviv, Israel

Dr. R. A. Heller
ESM Dept.
Virginia Tech
Blacksburg, VA. 24061

Dr. E. G. Henneke
ESM Dept.
Virginia Tech
Blacksburg, VA. 24061

Prof. Carl T. Herakovich
Laboratoire de Mecanique
  des Solides
Ecole Polytechnique
91128 Palaiseau cedex, FRANCE

Professor Phil Hodge
107 Aeronautical Engr. Bldg.
University of Minnesota
Minneapolis, MN 55455

Dr. K. E. Hofer
IIT Research Institute
10 West 35 Street
Chicago, Illinois 60616

Mr. Edward A. Humphreys
Materials Science Corporation
Blue Bell Office Campus
Blue Bell, PA. 19422

Dr. Michael W. Hyer
ESM Dept.
Virginia Tech
Blacksburg, VA. 24061

Dr. Eric R. Johnson
ESM Dept.
Virginia Tech
Blacksburg, VA. 24061

Dr. N. J. Johnson
Mail Stop 226
NASA-Langley Research Center
Hampton, VA. 23665

Dr. M. P. Kamat
ESM Dept.
Virginia Tech
Blacksburg, VA. 24061

Dr. Keith T. Kedward
1768 Granite Hills Dr.
El Cajon, CA. 92021

Mr. John M. Kennedy
Mail Stop 188E
NASA-Langley Research Center
Hampton, VA. 23665

Mr. Eric Klang
ESM Dept.
Virginia Tech
Blacksburg, VA. 24061

Mr. James P. Knauss
Northrop Corporation
3901 West Broadway
Dept. 3852/82
Hawthorne, CA. 90250

Dr. Ronald D. Kriz
Dept. Com. NBS Bldg. 2
Boulder, CO. 80302

Dr. S. V. Kulkarni
L342 Lawrence Livermore Lab
P. O. Box 808
Livermore, Ca. 94550

Dr. Trent R. Logan
Mgr. Structures, Design, Dev.
Boeing Commercial Airplane Co.
P.O. Box 3707 - M.S. 3M-23
Seattle, WA. 98124

Dr. M. R. Louthan
Materials Engineering
Virginia Tech
Blacksburg, VA. 24061

Mr. Vic Mazzio
General Electric Co.
P.O. Box 8555
Bldg. 100, Rm. M4018
Philadelphia, PA. 19101

Dr. Martin M. Mikulas
Mail Stop 190
NASA-Langley Research Center
Hampton, VA. 23665

Mr. J. Steve Mills
A3-220 13-3 McDonald Douglas
5301 Bolsa Avenue
Huntington Beach, CA 96247

Dr. D. H. Morris
ESM Dept.
Virginia Tech
Blacksburg, VA. 24061

Mr. Anya Nagarkar
Material Sciences Corp.
Blue Bell Office Campus
Blue Bell, PA. 19422

NASA Scientific & Technical
Information Facility
P.O. Box 8757
Baltimore/Washington Inter. Air.
Baltimore, MD. 21240

Mr. Michael Nemeth
ESM Dept.
Virginia Tech
Blacksburg, VA. 24061

Newman Library - Virginia Tech

Mr. David A. O'Brien
5902 Kingsford Pl.
Bethesda, MD 20034

Dr. Donald W. Oplinger
Army Materials & Mechanics
  Research Center
Department of the Army
Watertown, MA. 02171

Dr. Nicholas J. Payano
WPAFB/MBM
Wright Patterson AFB
Ohio 45433

Mr. Michael Parin
3M Co., 3M Center
Bldg. 230-1P
St. Paul, MN. 55101

Dr. Nicholas Perrone, Director
Structural Mechanics Program
Department of the Navy
Office of Naval Research
Arlington, VA. 22217

Prof. T. H. H. Pian
Mass. Inst. of Tech.
Dept. of Aero. & Astr.
Cambridge, MA. 02139

Mr. Marek-Jerzy Pindera
ESM Dept.
Virginia Tech
Blacksburg, VA. 24061

Dr. R. Byron Pipes
Dept. of Mech. & Aero. Engr.
107 Evans Hall
University of Delaware
Newark, DE. 19711

Prof. Robert Plunkett
Dept. Aero & Eng. Mech.
Aero 107
University of Minnesota
Minneapolis, MN. 55455

Dr. K. L. Reifsnider
ESM Dept.
Virginia Tech
Blacksburg, VA. 24061

Dr. Gary D. Renieri
McDonnell Douglas Astro. Co-East
P.O. Box 516
Bldg. 106, Level 4, Post C-5
St. Louis, MO. 63166

Dr. Michael W. Renieri
McDonnell Aircraft Co.
Bldg. 34, Post 350
St. Louis, MO. 63166

Dr. Larry Roderick
Mail Stop 188E
NASA-Langley Research Center
Hampton, VA. 23665

Dr. B. W. Rosen
Materials Science Corporation
Blue Bell Office Campus
Blue Bell, PA. 19422

Dr. R. E. Rowlands
Dept. of Engineering Mechanics
University of Wisconsin
Madison, WI. 53706

Dr. Edmund F. Rybicki
Mechanical Engineering Dept.
The Univ. of Tulsa
Tulsa, OK. 74104

Mr. Harminder Saluja
Boeing Vertol Company
Structural Technology
P.O. Box 16858
Philadelphia, PA. 19142

Dr. J. Wayne Sawyer
Mail Stop 190
NASA-Langley Research Center
Hampton, VA. 23665

Dr. George P. Sendeckyj
Structures Division
Air Force Flight Dynamics Lab.
Wright-Patterson AFB
Ohio 45433

Mr. Steven M. Serabian
28 Berkeley Drive
Chelmsford, MA. 01824

Mr. John S. Short, Jr.
ESM Dept.
Virginia Tech
Blacksburg, VA. 24061

Mr. Mark J. Shuart
Mail Stop 188
NASA-Langley Research Center
Hampton, VA. 23665

Dr. J. R. Stafford
B.F. Goodrich
500 S. Main St.
D/6145, B/10-E
Akron, Ohio 44318

Dr. James H. Starnes, Jr.
Mail Stop 190
NASA-Langley Research Center
Hampton, VA. 23665

Prof. Yehuda Stavsky
Gerard Swope Prof. of Mech.
Technion-Israel Inst. of Tech.
Technion City, Haifa, Israel

Dr. W. W. Stinchcomb
ESM Dept.
Virginia Tech
Blacksburg, VA. 24061

Dr. Darrel R. Tenney
Mail Code 188B
MD-Materials Research Branch
Langley Research Center
Hampton, VA. 23665

Dr. S. W. Tsai
Nonmetallic Materials Division
Air Force Materials Laboratory
Wright-Patterson AFB
Ohio   45433

Dr. J. R. Vinson
Dept. of Mech. & Aero. Engr.
107 Evans Hall
University of Delaware
Newark, DE. 19711

MR. M. E. WADDOUPS
General Dynamic Corp.
Fort Worth, TX   76101

Prof. A. S. Wang
Mechanical Engineering
Drexel University
Philadelphia, PA. 19104

Prof. S. S. Wang
Dept. Theoretical & Applied
   Mechanics
University of Illinois
Urbana, IL. 61801

Dr. T. A. Weisshaar
School of Aero. & Astro.
331 Grissom Hall
Purdue Univ.
West Lafayette, IN. 47907

Dr. J. M. Whitney
Nonmetallic Materials Division
Air Force Materials Laboratory
Wright-Patterson AFB
Ohio   45433

Dr. Ernest G. Wolff
The Aerospace Corp.
P.O. Box 92957
Los Angeles, CA.   90009

Dr. Edward Wu
Lawrence Livermore Lab.
University of California
Box 808, L-338
Livermore, CA. 94550

Mr. Thomas A. Zeiler
School of Aero. & Asro.
c/o Dr. T. A. Weisshaar
Purdue Univ.
West Lafayette, IN.   47907

Dr. Carl H. Zweben
General Electric Co.
Space Division
P.O. Box 8555
Philadelphia, PA.   19101